

MODELLING AND SIMULATION OF ZINC-AIR BATTERIES

**A Thesis Submitted to
the Graduate School of Engineering and Sciences of
İzmir Institute of Technology
in Partial Fulfillment of the Requirements for the Degree of**

MASTER OF SCIENCE

in Chemical Engineering

**by
Ege DURAK**

**July 2024
İZMİR**

We approve the thesis of **Ege DURAK**

Examining Committee Members:

Prof. Dr. Özgeç EBİL

Department of Chemical Engineering, İzmir Institute of Technology

Asst. Prof. Dr. Başar ÇAĞLAR

Department of Energy Systems Engineering, İzmir Institute of Technology

Assoc. Prof. Dr. Güler NARİN

Department of Chemical Engineering, Uşak University

5 July 2024

Prof. Dr. Özgeç EBİL

Supervisor, Department of Chemical
Engineering, İzmir Institute of Technology

Prof. Dr. Aysun SOFUOĞLU

Head of the Department of
Chemical Engineering

Prof. Dr. Mehtap EANES

Dean of the Graduate School of
Engineering and Sciences

ACKNOWLEDGEMENTS

First and foremost, I would like to express my deepest gratitude to my thesis advisor Prof. Dr. Özgeç EBİL for his never-ending guidance, encouragement and support throughout this thesis journey. His insights, feedback have been crucial in shaping the thesis and I am profoundly grateful for his mentorship.

I would also like to extend my sincere thanks to my colleagues at TÜPRAŞ for their encouragement and support throughout this journey. Special thanks to my Production Manager Kürşad KAVDIR, Production Specialist Özgür ODABAŞI and my colleague Yasir ARSLAN for their never-ending support to help me keeping the balance between the work and thesis.

Lastly, I would like to thank my family, my mother Pınar DURAK my father Hakan DURAK and friends for their unwavering support and understanding throughout this challenging journey.

ABSTRACT

MODELLING AND SIMULATION OF ZINC-AIR BATTERIES

Renewable energy sources are key components of a sustainable future. However, most of the renewable energy sources have intermittent natures, that can significantly affect the stability of grids. Thus, Energy Storage Systems (ESS) are introduced to store the energy produced for later use. Even though there are various ESS candidates, batteries are superior candidates due to technological readiness. Batteries still suffer from disadvantages that prevent their mass adoption as ESS for grid-scale applications. As an ESS, a battery that can last long cycles, have high power densities, and material availability should be designed and commercialized. Commercial batteries such as lead-acid and Li-ion batteries still suffer from material availability, environmental friendliness, or feasibility. Therefore metal-air batteries, especially zinc-air batteries (ZAB), have significant potential due to their high-power densities, material abundance, and technological readiness. However, ZABs are not ready enough to be commercialized as grid-scale ESS due to their low cycle lives due to aging mechanisms. Therefore, more research should be conducted to improve the rechargeability of a ZAB.

However, experimental procedures are time and resource-consuming. To tackle this, accurate mathematical models and simulations should be implemented. In this study, the electrochemical behavior of zinc-air batteries was simulated with Finite Element Analysis (FEM) method. The motivation of the work was to demonstrate the feasibility of a simple 1-D zinc-air battery model to investigate the effect of various phenomena on the battery capacity and charge-discharge cycles. The results were compared to literature and experimental values to evaluate the model's accuracy.

ÖZET

ÇİNKO-HAVA BATARYALARIN MODELLENMESİ VE SİMÜLASYONU

Yenilenebilir enerji kaynakları sürdürülebilir bir geleceğin temelini oluşturmaktadır. Ancak, çoğu yenilenebilir enerji kaynağı dengesiz bir yapıya sahip olduğu için, şebekelerin stabilitesi önemli ölçüde etkilenme riski ile karşı karşıyadır. Bu nedenle, üretilen enerjinin depolanması adına Enerji Depolama Sistemleri (EDS) ortaya çıkmıştır. Her ne kadar süperkapasitörler plug-in elektrikli araçlar gibi EDS adayları olsa da bataryalar aralarındaki en umut vadedenidir.

Yine de bataryalar, şebeke ölçeğinde EDS olarak benimsenmek için hazır değildir. Yüksek şarj-deşarj ömrü, fizibilite, yüksek güç yoğunluğu ve malzeme bulunabilirliği bataryalar için ana kriterlerdir. Bu nedenle, uzun şarj-deşarj ömrüne sahip, yüksek güç yoğunluklu ve malzeme bulunabilirliği yüksek bir batarya tasarlanmalı ve ticarileştirilmelidir. Kurşun-asit ve lityum-iyon piller gibi yaygın olarak kullanılan ticari batarya teknolojileri olmasına rağmen, bu bataryalar hala malzeme bulunabilirliği, çevre dostu olmama veya fizibilite gibi sorunlarla karşı karşıyadır. Bu nedenle, yüksek güç yoğunlukları, malzeme bolluğu ve teknolojik olarak hazır olmaları nedeniyle metal-hava bataryaları, özellikle çinko-hava bataryaları (ÇHB) önemli bir potansiyele sahiptir. Ancak, ÇHB'ler yıpranma mekanizmaları nedeniyle düşük şarj-deşarj ömrüne sahip olduklarından, şebeke ölçekli EDS olarak ticarileştirilmeye yeterince hazır değildir. Bu nedenle, bir ÇHB'nin yeniden şarj edilebilirliğini artırmak için daha fazla araştırma ve çalışma yapılmalıdır. Fakat, deneysel prosedürler zaman ve kaynak açısından maliyetlidir. Bu unsurlardan tasarruf sağlamak için, doğru matematiksel modeller ve simülasyonlar uygulanmalıdır. Bu çalışmada, çinko-hava pillerinin elektrokimyasal davranışı Sonlu Elemanlar Analizi (SEA) metodu ile simüle edilmiştir. Çalışmanın motivasyonu, batarya kapasitesi ve şarj-deşarj döngü sayısı üzerinde çeşitli fenomenlerin etkisini araştırmak için basit bir 1-D çinko-hava pil modelinin uygulanabilirliğini göstermektir. Elde edilen sonuçlar literatürdeki veriler ile karşılaştırılarak modelin tutarlılığı değerlendirilmiştir.

TABLE OF CONTENTS

LIST OF FIGURES	viii
CHAPTER 1. INTRODUCTION	1
1.1 Energy Storage Systems (ESS).....	2
1.2 Battery Terminology.....	3
1.2.1 Electrolytes	3
1.2.2 Separators.....	4
1.2.3 Electrodes.....	4
1.2.4 Current collectors.....	5
1.2.5 Cut-off voltage and Discharge Time	5
1.2.6 Theoretical and Volumetric Theoretical Capacity, Discharge Rate ..	6
1.2.7 SOC, Depth of Charge, Depth of Discharge.....	6
1.2.8 Energy Density	6
1.2.9 Overpotential	7
1.2.10 Open Circuit Voltage, Nominal Voltage, Terminal Voltage	7
1.2.11 Self-Discharge and Cycle Life.....	7
CHAPTER 2. BATTERIES AS ESS.....	8
2.1 Primary Batteries	8
2.2 Secondary Batteries	8
2.3 Flow Batteries (Redox Flow Batteries: RFBs)	8
2.4 Battery Types with Respect to Materials.....	9
2.4.1 Conventional Batteries: Zinc-carbon & Alkaline	9
2.4.2 Lead-acid Batteries	10
2.4.3 Lithium-ion Batteries	11
2.4.4 Nickel-Based Batteries	11
2.4.5 ZEBRA Batteries	12
2.5 Metal-air Batteries (MABs).....	13
2.5.1 MAB Components	13
2.5.2 Magnesium-air (Mg-Air) Batteries	14
2.5.3 Aluminium-air (Al-Air) Batteries	15
2.5.4 Sodium-air (Na-Air) Batteries	15
2.5.5 Iron-air (Fe-Air) Batteries.....	16
2.5.6 Silicon-air (Si-Air) Batteries.....	16
2.5.7 Lithium-air Batteries (LAB)	17
2.5.8 Zinc-air (Zn-air) Batteries (ZAB)	18
2.5.8.1 Zinc-Electrode	20

2.5.8.2 Electrolyte	21
2.5.8.3 Separators.....	23
2.5.8.4 Air Electrode.....	23
CHAPTER 3. MODELLING OF ZABs.....	28
3.1 Previous Models of ZABs.....	28
3.2 Battery of the Model.....	32
3.2.1 Theory and the Physics Used Within the Model	33
3.2.1.1 Electrochemical Physics Used within the Model	34
3.2.1.2 Mass Transport Phenomena in the Model	51
3.2.1.3 Model Definitions, Parameters, and Variables	53
3.2.1.4 Boundary, Initial Conditions.....	57
3.2.1.5 Meshing of the Model.....	58
3.2.2 Aging Mechanisms Implemented in the Model.....	59
3.2.2.1 Aging Mechanisms: Anode	60
3.2.2.2 Aging Mechanisms: Gas Diffusion Electrode (GDE)	64
3.2.2.3 Aging Mechanism: Electrolyte	64
3.2.2.4 Effect of Temperature on Battery Degradation	65
CHAPTER 4. RESULTS AND DISCUSSION.....	67
4.1 Zinc Dendrite Growth Simulation Results.....	67
4.2 Anode Film Resistance Simulation Results.....	69
4.3 GDE Catalyst Layer (CL) Activity Loss Simulation Results	70
4.4 Electrolyte Loss Simulation Results	71
4.5 Combined Aging Simulation Results	72
CHAPTER 5. CONCLUSION	77
REFERENCES	79
APPENDICES	
APPENDIX A. PARAMETERS, VARIABLES AND POST-PROCESSING.....	102

LIST OF FIGURES

<u>Figure</u>	<u>Page</u>
Figure 1.1. Overall battery scheme with components	3
Figure 3.1. The 1-D representation of the battery of the model.....	33
Figure 3.2. Points (boundaries) and domains for the ZAB model geometry.....	57
Figure 3.3. ZAB simulation with a model without aging mechanisms.	59
Figure 4.1. ZAB with stand-alone anodic dendrite growth aging.....	68
Figure 4.2. ZAB with stand-alone anodic film resistance aging.	69
Figure 4.3. ZAB with stand-alone GDE aging due to catalytic activity loss.....	70
Figure 4.4. Stand-alone aging due to electrolyte loss on the overall battery.....	72
Figure 4.5. Complete ZAB simulation with aging mechanisms combined.	73
Figure 4.6. Electric potential vs Time for combined aging mechanisms in a ZAB.....	74
Figure 4.7. Specific charge discharge curves for the combined aging model.	74
Figure 4.8. Specific charge discharge cycle mode behavior for 1 mA/cm ²	75
Figure 4.9. Specific charge discharge cycle mode behavior for 5 mA/cm ²	76

CHAPTER 1

INTRODUCTION

Energy is an indispensable part of humanity and civilization as it is necessary for heating, cooling, electricity, and lighting to support fundamental aspects of society. Besides, it is essential for industries, vehicles for transportation, electronic products, and technology to make lives easier, achieve progress, and help humanity adapt to every condition. Energy utilization played a critical role in civilization from the past to the present. With the first industrial revolution and the introduction of the steam engine by James Watt (Haradhan and Kumar Mohajan 2019) in the late 18th century, humanity changed forever. New methods with machinery within factories were introduced, increasing the efficiency and capacity of production. These changes in efficiency and capacity resulted in significant economic and population-wise growth (Haradhan and Kumar Mohajan 2019). However, this population growth has also introduced many challenges in terms of energy demand.

The conventional resources used for energy, such as fossil fuels, have created major problems for humanity. Even with high energy densities, fossil fuels such as coal, oil, and gas are finite resources and have significant environmental impacts. Using fossil fuels has environmental degradation effects such as air and water pollution and climate change due to Greenhouse Gas emissions (Kalair et al. 2021; Khan et al. 2019). One of the very first examples of air pollution caused by fossil fuel usage can be given as the Great Smog of London in 1952, where an excessive amount of coal combustion within London caused a massive smoke where hundreds, even thousands of people were affected by the air pollution, locked in their houses, harmed by the polluted air and some even lost their lives (Polivka 2018). Environmental pollution significantly affects not just humans but all living things in the world.

Besides the environmental impacts, many conflicts between countries have been occurring due to the scarcity and centralized nature of fossil fuels. Oil wars resulted in catastrophe in the Middle East and demolished the region's stability (Kaldor, Karl, and Said 2007). Organization of the Petroleum Exporting Countries (OPEC), which consists of countries Venezuela, Saudi Arabia, Iran, Iraq, United Arab Emirates, Kuwait, Libya,

Nigeria, Algeria, Angola, Gabon, Congo, and Equatorial Guinea, corresponds to 80.4% present of the crude oil reserves of the world (Behrouzifar, Siami Araghi, and Emami Meibodi 2019). In the past, many economic and energy-related crisis, such as the OPEC crisis (Hancock and Vivoda 2014) affected millions of lives, resulting in poverty and social inequalities. Therefore, re-evaluating energy sources to generate the necessary energy is critical.

Re-evaluation of alternative energy sources has led to new concepts such as renewable energy and sustainability. Renewable energy sources such as wind, solar, and geothermal are being used to generate the required electricity to drive the fundamental needs of humanity. However, due to the intermittent nature of these sources, especially the wind and solar energies due to weather conditions prevents/slows down the transition from fossil fuels to renewable energy sources. Efficient and stable energy generation can only be done if this instability is resolved. Therefore, Energy Storage Systems (ESS) are being considered to tackle this issue and help the transition process with a stabilized grid (Kalair et al. 2021).

1.1 Energy Storage Systems (ESS)

With ESS, the energy produced can be saved for later use, and the gap between energy production and consumption can be narrowed. Therefore, better utilization of renewables while stabilizing the grid can help humanity achieve a better and sustainable future with a renewable energy grid that can scale. ESS consists of different methods to conduct energy storage. ESS can be done through durable batteries, supercapacitors, superconducting magnetic energy storage (SMES), and plug-in electric vehicles. However, due to technological readiness and effectiveness, batteries are considered the best possible way to stabilize renewable energy (Kalair et al. 2021; May, Davidson, and Monahov 2018). Batteries, such as ESS, also differ within themselves in many aspects.

1.2 Battery Terminology

Figure 1.1 below represents the basic structure of a battery. Batteries consist of components such as electrodes, electrolyte, current collectors and separator. Each component has its own specific functionality to maintain battery operations in terms of electrochemical reaction kinetics, electrical properties and mass transfer phenomena. Within this section, components of batteries, battery types and materials will be discussed.

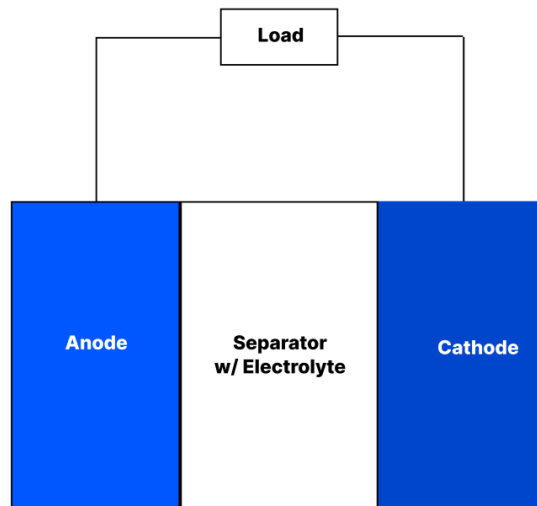


Figure 1.1 Overall battery scheme with components.

1.2.1 Electrolytes

Electrolyte is a critical component of batteries. The electrolyte is responsible for the ionic charge transport within the battery. Electrolytes are usually in form of aqueous solutions of salts. However, these salts can be in different liquid solvents, or solids that can also have ionic conductivity. Electrolyte's conductivity is orders of magnitude smaller than an electrode's electrical conductivity (Comsol 2020).

1.2.2 Separators

Separators are key components of batteries that provide necessary safety measurements while promoting efficient operations. These materials provide the necessary separation of the positive and negative electrodes to keep ionic gradients at the required levels. These isolating materials help batteries to safely and effectively operate. Separators can prevent short-circuits due to abnormal ionic gradients. Separators also promote structural durability of the battery against different formations such as dendrites and deposition which is also a critical role to prevent short circuit of a battery (Y. Li and Dai 2014).

1.2.3 Electrodes

Electrodes are the most essential parts of batteries, providing necessary electrical and electrochemical properties. These domains of batteries conduct the current transport which is in form of electrons. These materials are conventionally metals with decent electrical conductivities. At the interface between electrode-electrolyte, the electrical current generated within the electrode is transformed into ionic current in the electrolyte.

These currents generated must balance each other in order to fulfill overall charge conservation (Comsol 2020). To increase the electrode-electrolyte interface, batteries usually contain porous electrodes.

Batteries must complete their circuits with electrochemical cell configuration where two or more electrodes are used to conduct current transport. Within two electrode configuration, one electrode is referred as the anode, and the other one is referred as the cathode.

At these electrodes, reduction-oxidation reactions occur simultaneously. These reactions are usually referred as the redox reactions. Commonly in these reactions, oxygen, hydrogen or electrons are transferred from one electrode to another. Reduction is the process where the species gain electrons, while the oxidation process the species lose electrons (Shehu, 2015).

The simplified representation of redox reactions can be described as (Comsol 2020):



At the anode side, oxidation process is conducted, while on the cathode side, the reduction process is being conducted. These electrodes may also refer as negative and positive electrodes respectively within the discharge mode. However, these references and reactions are reversed during the charging mode (Dell et al. 2001).

1.2.4 Current collectors

Current collectors are components to conduct electrical charges obtained from the redox reactions occurred within electrodes. Therefore, these components play a critical role in full-circuit maintenance of a battery by connecting it to source or load (Haverkort 2024).

1.2.5 Cut-off voltage and Discharge Time

Cut-off voltage is the potential at which the battery is assumed fully discharged or not. Voltages below this determined voltage means that the battery is empty. Further discharging within safe conditions cannot be achieved below this point. The time passed until the battery reaches the cut-off voltage is defined as the discharge time (Haverkort 2024).

1.2.6 Theoretical and Volumetric Theoretical Capacity, Discharge Rate

It is the theoretical indication of the maximum charge that can be utilized from a battery during its redox reactions. Units are mostly mAh and Ah. Volumetric theoretical capacity means the maximum charge can be obtained from a battery per its volume. The term discharge rate is a representation of the time it takes to fully discharge a battery when compared to its theoretical capacity. This term is usually noted by a rate notation “C” rate. The battery of interest is discharged in 1 hour at C rate, in the C/3 rate, the battery will reach this full discharge limit in 3 hours, or 3C means it will reach this limit in 20 minutes (Haverkort 2024).

1.2.7 SOC, Depth of Charge, Depth of Discharge

State-of-charge (SoC) is the fractional representation of the battery’s full capacity that can left to be utilized within discharge operations. The depth-of-charge (DoC) and depth-of-discharge (DoD) are the rational representations of the battery’s charged and discharged capacity with respect to full capacity (Dell et al. 2001).

1.2.8 Energy Density

Energy density represents maximum energy that is available, usually described in per unit mass or volume of a battery. Units of measure are usually Wh/kg or Wh/L (Haverkort 2024).

1.2.9 Overpotential

The term overpotential is used to define the potential difference between the theoretical potential and the practical potential within the operation of the battery (Comsol 2020).

1.2.10 Open Circuit Voltage, Nominal Voltage, Terminal Voltage

If there is no load or a source between the battery's anode and cathode, the voltage obtained is referred as the open circuit voltage (OCV). However, if there is a load between anode and cathode terminals of a battery, the voltage obtained is often referred as the terminal voltage. If there is a single electrochemical cell or cells in parallel configuration, this voltage is the potential difference between these terminals. If there are multiple cells in series, this voltage is the multiplication of the cells in series (MIT Electric Vehicle Team 2008; Haverkort 2024).

1.2.11 Self-Discharge and Cycle Life

As the name implied, self-discharge is a phenomenon where the electrical potential of a battery is lost regardless of batteries use (Gates Energy Products 1998). This mechanism occurs due to battery's internal chemical interactions. Therefore, the self-discharge phenomena can occur due to chemical or thermodynamical changes in the environment (Pop et al. 2008). Charging and discharging the battery can be referred as the battery cycle. The cycle life of a battery is determined via the number of cycles until the battery failure (Dell et al. 2001).

CHAPTER 2

BATTERIES AS ESS

2.1 Primary Batteries

Primary batteries cannot be charged after usage and are usually used for portable electronic devices. Despite being unable to charge, these batteries are simple, handy, and have almost no maintenance issues (Linden and Reddy 2002).

2.2 Secondary Batteries

These types of rechargeable batteries make them highly suitable for a wide range of applications. From powering portable electronic devices to powering a Battery Electric Vehicle (BEV) and hybrid vehicles (Deng and Aifantis 2023). Secondary batteries are commercialized by developing electrodes that can endure many charge-discharge cycles. This durability makes them favorable within ESS, especially in domestic usage with the wide adoption of renewable energy generation in households (Vincent 2000; Hoppmann et al. 2014). Commercially used/available secondary batteries are lithium-ion, lead-acid, nickel metal hydride, and nickel-cadmium batteries (C. Liu et al. 2010), which will be discussed later in the following sections.

2.3 Flow Batteries (Redox Flow Batteries: RFBs)

Flow batteries inherit different design features where the electrochemical reactions occur in a reaction chamber and electrolytes are stored in external tanks. Within these systems, electrochemically active materials are dissolved into liquid electrolytes where energy is produced with the reduction-oxidation reactions occurring in distinct

half-cells (Taylor et al. 2012; Nguyen and Savinell 2010). Distinct half-cells conduct reduction and oxidation reactions where electrons and ions are extracted from one electrolyte and recombined in another. The interconnection of these distinct half-cells is provided by an external storage tank (Alotto, Guarnieri, and Moro 2014). Due to this modular design, these types of batteries have the capability to separate power and energy. Separated reactants handle the energy storage, whereas the cell stack handles the power generation. This gives flow batteries high design capabilities and flexibility, such as easy monitoring, easy cell-temperature control, scalability, quick response time, and good stability with no self-discharge. However, due to low power and energy densities, pump management to control flow and power, and expensive materials usage such as Vanadium to obtain decent performances make these types of batteries hard to adapt on a much bigger scale (Alotto, Guarnieri, and Moro 2014; Weber et al. 2011). Besides, they conflict with the Circular Economy philosophy due to complex product designs (De Schoenmakere and Gillabel 2017).

2.4 Battery Types with Respect to Materials

Batteries also vary significantly depending on the materials used. Different materials cause variations in electrochemical, chemical, physical, and thermal properties in batteries and vary the electrochemical reaction kinetics. Each battery type has various advantages, disadvantages, and environmental and public health impact due to their design selections (Dehghani-Sanij et al. 2019). This part will briefly cover battery types, advantages, and disadvantages while considering the raw materials used in production, recycling, and environmental and public health impacts within life cycles except metal-air batteries which will be covered in a separate section.

2.4.1 Conventional Batteries: Zinc-carbon & Alkaline

Zinc-carbon batteries (Zn-C) have Zn as anode, a carbon-based cathode with MnO₂ catalyst as a paste, and acid as an electrolyte. These batteries were one of the most

commercially accepted and widely used batteries due to the wide range of shapes, sizes, and capabilities that make them applicable to a wide range of applications while having a decent shelf life (Abdul-Zehra 1999). However, these batteries have low energy densities, low leakage resistance, and voltage drop within discharge problems. Besides, due to material selection, such as acid as electrolytes, manganese as a paste, and zinc as an anode, these materials must be recovered appropriately or securely landfilled (Linden and Reddy 2002; Avraamides, Senanayake, and Clegg 2006; Panero et al. 1995).

Alkaline batteries inherit similar specs compared to Zn-C batteries since Zn is used as an anode and manganese dioxide is used as the cathode. However, for electrolyte, instead of acids, potassium hydroxide (KOH) is used in alkaline batteries (Martha De Souza, Corrêa De Oliveira, and Tenório 2001). Alkaline batteries show superior properties when compared to Zn-C batteries, at least two times higher rate performance. These batteries also have good low-temperature performances, low cost, and good shelf lives compared to Zn-C batteries (Abdul-Zehra 1999; Linden and Reddy 2002).

2.4.2 Lead-acid Batteries

As the name implies, lead acid batteries consist of lead as a negative and lead oxide as a positive electrode, while sulfuric acid is used as electrolyte (May, Davidson, and Monahov 2018). With low production costs, great high-rate performances, durability in a wide range of temperatures, high voltage, and great charge retentions, lead-acid batteries have the largest market share within secondary batteries in terms of sales and MWh of production (May, Davidson, and Monahov 2018; Linden and Reddy 2002). These batteries have various applications, from automotive to data networks (May, Davidson, and Monahov 2018).

However, despite being widely accepted and used, these batteries suffer from low cycle lives, limited energy densities, and acidic electrolyte. Besides, the production process for lead is another concern for our environment. To tackle environmental impact, the recycling of lead acid batteries is mandatory (Davidson, Binks, and Gediga 2016).

2.4.3 Lithium-ion Batteries

Since 1990, the development of lithium-based cells has dominated the battery industry due to their high performance (Linden and Reddy 2002). Lithium batteries today are accepted as the power source of sustainable transport with their high storage efficiencies (83%), long cycle lives, rapid charging times, and high energy densities. Thus, Li-ion batteries are the most popular batteries recently with a wide range of, ESS applications, especially Battery Electric Vehicles (BEVs) (Ahmadi et al. 2017). Besides, Li-ion batteries can inherit flexible designs with a selection of various electrolyte salts. Commercial Li-ion batteries have lithium hexafluorophosphate (LiPF_6) as electrolyte that limits batteries concerning thermal stability, moisture sensitivity, and toxicity (Linden and Reddy 2002; Goodenough and Kim 2010; Mauger et al. 2018). Alternative electrolyte salts or solid-state electrolytes are considered solutions to tackle these issues. However, solid-state electrolytes are expensive, and alternative salts still require further development to make these commercially accepted and usable (Mauger et al. 2018; Gao et al. 2018). Therefore, it prevents/aggravates safe and reliable battery operation (D. Shen et al. 2021).

2.4.4 Nickel-Based Batteries

In these batteries, a Ni-based positive electrode, and a negative electrode which is based on a variety of material are used. In a Ni-Cd battery, nickel and cadmium (Ni-Cd) are used for positive and negative electrodes (Ding et al. 2015). These batteries have long cycle lives, durable structures to high temperatures, and great charge retentions, making them suitable for long-term storage (Linden and Reddy 2002; Ding et al. 2015). Besides, with flat discharge behaviors and low maintenance requirements, Ni-Cd batteries can be integrated easily into a wide range of usage, such as portable electronic devices and uninterrupted power supply (UPS) (Ding et al. 2015). Despite these advantages, Ni-Cd suffers from low energy density and higher costs compared to other commercial batteries such as lead-acid, and significantly from memory effects. Memory effect can be described as an aging mechanism if the battery is charged in extended periods.

During this extension of charging, the nickel electrode's metallic structure changes and results as the cell's capacity loss with no possible recovery (Copeaand and Podrazhanskyb 1999). Due to Cadmium's toxicity levels, handling batteries and their waste is risky, and it is the largest contributor of Cd in municipal solid wastes. Cadmium exposure in low levels in air, food, or water may lead to catastrophic consequences such as kidney failure, bone fragility, and cancer (Genchi et al. 2020).

Like Ni-Cd batteries, nickel-zinc (Ni-Zn) batteries are generally used for portable electronic devices. These batteries also provide a high discharge rate for these types of devices. In addition, Ni-Zn batteries are much more cost-effective with lower initial costs while having high specific power and efficiency when compared to Ni-Cd ones (Linden and Reddy 2002). Environmental impacts are much lower due to the design selection of a negative electrode, which uses Zinc instead of Cadmium as the negative electrode material (Yanzhen Liu, Yang, and Yan 2016). On the other hand, these types of batteries tend to dry out and self-corrode, especially due to the nature of zinc in negative electrodes. Therefore, after some usage, within cycles, low discharge is observed (Yanzhen Liu, Yang, and Yan 2016; Linden and Reddy 2002).

Nickel-metal hydride (Ni-MH) batteries contain nickel hydroxyl oxide as the cathodic material, while metal hydrides are the anodic materials (Dhar et al. 1997)

These batteries were initially used in automotive industry for use in electric and hybrid vehicles since they show much higher energy densities and specific energies when compared to conventional lead-acid batteries. Besides higher performance, these batteries show long-term shelf lives, rapid charging times, long-cycle lives, and decent temperature capabilities. However, these batteries have higher costs when compared to lead-acid batteries and show low performances at low temperatures (Linden and Reddy 2002).

2.4.5 ZEBRA Batteries

Na-NiCl₂ batteries, also known as ZEBRA (Zeolite Battery Research Africa Project), are among the most popular batteries due to their long cycle lives, operational safety, and reliability. They can operate in low temperatures with good performance, endure thousands of charge cycles, and have a decent energy density. Big companies such as Mercedes use to work on prototypes to integrate these batteries (Trilochana and

Sangeetha 2021) However, despite the developments, these batteries are not mature and adapted enough to be technologically ready. Besides, the power density is not high enough compared to alternatives (Trilochana and Sangeetha 2021).

2.5 Metal-air Batteries (MABs)

Metal air batteries, also known as MABs, are promising batteries for use in ESS. They have significant advantages, such as high safety measures and low costs, due to using oxygen from ambient air as a cathode (Olabi et al. 2021). This utilization unlocks a development pathway and interest in adopting further lightweight but higher energy-density batteries to compete with and surpass the existing market leader, the Li-ion (Clark, Latz, and Horstmann 2018a).

2.5.1 MAB Components

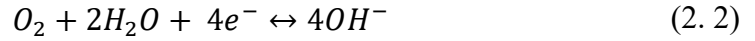
Like all batteries, metal-air batteries consist of elements such as the anode, cathode, separator, and current collectors. This section will briefly describe a metal-air battery's common materials and structures.

In these types of batteries, negative electrodes (anodes) consist of metals such as zinc, lithium, magnesium, aluminum, sodium, and iron. Various electrolytes, such as aqueous, non-aqueous, solid-state, and hybrids, have been used/tested to produce efficient and durable MABs (Amendola 2010).

The positive electrode consists of two main sections besides the current collector. These sections are the gas diffusion layer (GDL) and the catalyst layer (CL). The gas diffusion layer is the component where the oxygen from the ambient air diffuses through its channels and is transferred to the CL, where electrochemically active catalysts facilitate the electrochemical reactions (J. Pan, Xu, et al. 2018).

In general, MAB redox reactions are metal oxidation on the negative electrode side and Oxygen Reduction Reaction (ORR) on the positive electrode side (porous CL) in discharge mode. However, in charge mode, the metal oxide is reduced to metal where

the positive electrode handles the Oxygen Evolution Reaction (OER) simultaneously (Cheng and Chen 2012). These reactions of the air electrode are conducted in the three-phase or two-phase reaction zones within aqueous and non-aqueous electrolytes, respectively. The three-phase boundary is the contact zone of oxygen (gas phase), the aqueous electrolyte (liquid phase), and the cathode's catalyst (solid phase). This contact provides the necessary zone to generate OH^- or HO_2^- ions in ORR depending on the type of MAB and generate O_2 in charge modes, respectively (Choi et al. 2021). General reactions occurring within MABs are summarized in equations (2.1 and (2. 2 below.



2.5.2 Magnesium-air (Mg-Air) Batteries

Mg-air batteries have advantages such as uniform Mg deposition, material abundance, and high theoretical volumetric density of 3832 A h L^{-1} (Olabi et al. 2021; C. S. Li et al. 2017a). Utilizing such metal on the anode side has high potential in sustainability and cost-effective production compared to conventional batteries (Han et al. 2023). Additionally, when compared to Li-ion batteries, Mg-air has a lower tendency to overheat and ignite, just like other MABs (T. Li et al. 2023). However, to produce durable and rechargeable Mg-air batteries on a large scale, challenges due to their thermodynamics and kinetics should be resolved.

Magnesium is highly corrosive in air electrodes, and this can significantly affect the lifetime and performance of Mg-air batteries (Huang et al. 2024) MgO or MgO_2 creates an insulating film on the air cathode during the initial discharge (C. S. Li et al. 2017a). These deposited products during the discharge cause capacity fading of Mg-air batteries and result in poor cycling performance. Regardless of the electrolytes suggested

and tested, Mg-air batteries are still electrochemically unstable (C. S. Li et al. 2017b). More research is required to further improve Mg-air batteries.

2.5.3 Aluminium-air (Al-Air) Batteries

Al-air batteries have important features such as good recyclability, high energy density, and light-weightness (Dincer 2018). Al-air batteries have much higher energy density when compared to Li-ion batteries. They also have a 4.30 kWh/kg of practical energy density which is almost as high as the Li-air batteries (5.20 kWh/kg) (J. S. Lee et al. 2011a; Rahman, Wang, and Wen 2013). Aluminum as anode is a perfect material for light-weight batteries since it can be effectively reduced into a wire mesh. Aluminum has also good energy storage capacity and recyclability. However, Al-air batteries face many problems. There is a high rate of self-corrosion of aluminum when alkaline solutions are used as electrolytes. Also, Al_2O_3 and $\text{Al}(\text{OH})_3$ are by-products that can accumulate at the anode and cathode parts of the Al-air batteries or trivalent Al^{3+} intercalation in the cathode can lead to the degradation of electrochemical kinetics. Additionally, the formation of hydrated alumina is a major problem since it is irreversible (Goel, Dobhal, and Sharma 2020).

2.5.4 Sodium-air (Na-Air) Batteries

Due to the abundance of sodium and similar electrochemical properties to lithium, sodium-air batteries have gained attention in recent years. Besides, the safety of sodium as a material is another advantage that made this topic of research interesting (Bi et al. 2020; Adelhelm et al. 2015). Sodium-air batteries have a significantly high practical energy density, 1600 Wh/Kg which makes it a solid candidate for ESS (Chawla 2019). However, despite the advantage, sodium air batteries have low cycling qualities and round-trip efficiencies due to sodium superoxide compounds formed during the discharge operation (Enterría et al. 2022).

Additionally, high temperatures are required for Na-air batteries to operate properly due to the cell configuration, therefore alternative electrolytes and more effective positive electrode catalysts are necessary to tackle this problem (Peled et al. 2013; Ellis and Nazar 2012; Sun, Yang, and Fu 2012). Therefore, more research is needed to understand and evaluate the sodium-air batteries and parasitic effects during the operation.

2.5.5 Iron-air (Fe-Air) Batteries

These batteries have significant potential, especially for availability for large-scale adoption due to their low cost, environmentally friendliness, and material abundance. Fe-air batteries have moderate energy densities ranging between 50-75 Wh/kg and low cost per kWh produced, which is lower than \$100/kWh (Narayanan et al. 2012). However, two important performance issues of Fe-air batteries need to be resolved to achieve mass adoption. Firstly, Fe-air batteries have low round-trip efficiency and low cycle life. Interactions of the iron electrode and the electrolyte during the self-discharge result in a hydrogen evolution reaction which causes low round-trip efficiency (Narayanan et al. 2012). Therefore, more research on aging mechanisms, parasitic reactions of Fe-air batteries, and alternative electrolytes should be worked out to fully utilize Fe-air's advantages.

2.5.6 Silicon-air (Si-Air) Batteries

With high theoretical energy densities (8470 Wh kg^{-1}) and decent stability in electrolytes, Si-air batteries gained significant attention recently to be worked on (Bansal, Menon, and Sharma 2020). Besides its high potential, silicon is one of the most abundant materials on earth and it is environmentally friendly. Despite being a good candidate for mass adoption due to material abundance and high theoretical energy density, Si-air battery systems still face serious challenges. Most of the anode materials in Si-air systems have pure silicon wafer structures. This structure brings a critical problem of high rates

of corrosion. To overcome these aging problems, different structured silicon anodes should be worked on, such as nano-structured and doped. Therefore, the overall performance and durability of Si-air systems can be enhanced. Additionally, the use of additives is also considered a good solution to improve battery performance. However, more research on the corrosion and passivation mechanisms such as solid discharge product reversibility, pore blockage, and precipitation in Si-air systems is required to find a suitable solution (Bansal, Menon, and Sharma 2020).

2.5.7 Lithium-air Batteries (LAB)

As also mentioned in the previous parts; with the significant development of Li-ion batteries and the widespread adoption of it in various applications such as mobile electronic devices, EVs, and more, Lithium has become one of the most popular and promising materials in the battery industry. Therefore, the development of Li-air batteries has been one of the most focused MABs in the research field within past decades (Blurton and Sammells 1979). Li-air batteries have characteristics such as high theoretical specific energy and working voltages thus being a promising candidate to be integrated as ESS (J. S. Lee et al. 2011a; Jörisen 2006; Q. Li and Bjerrum 2002). However, there are major bottlenecks within these batteries that need to be issued. Firstly, the selection and utilization of electrolytes is a major problem. Various types of electrolytes such as non-aqueous, aqueous, solid-state, hybrid electrolytes were used (J. S. Lee et al. 2011a). Non-aqueous systems in LABs such as LiPF_6 in ethylene carbonate, showed the instability of the carbonate solvents (Abraham and Jiang 1996; McCloskey et al. 2012). Besides, the product of ORR, which is Li_2O_2 , can precipitate and this precipitation can lead to pore clogging, and electrode passivation due to electron transfer reduction and activity degradation (Olabi et al. 2021). Additionally, utilizing aqueous electrolytes is a tedious task where integration of additional glass-ceramic layers over the anode is required since Lithium metal aggressively interacts with the water (Horstmann, Danner, and Bessler 2013). Dendrite formation within the Li-electrode side is a problem that degrades batteries' cycling abilities and performance.

Additional use of materials such as additives in electrolytes should be used to help Li-electrode to build up a stable solid electrolyte interface to minimize performance

degradations (J. S. Lee et al. 2011b). New additives, electrolyte materials, or electrode structures are required to tackle the problems of LABs. More research should be done to improve LABs and increase their technological readiness.

2.5.8 Zinc-air (Zn-air) Batteries (ZAB)

ZABs are the oldest batteries in the metal-air battery category. Smee introduced the concept behind them in 1840, and the first commercial primary ZAB was released to the battery market in 1932. Since then, primary ZABs have been in our lives within medical aids and small communication devices (J. Zhang et al. 2019). Besides, within metal-air batteries, ZABs have the highest patent numbers and studies (C. T. Lu et al. 2022). Therefore, due to the high amount of research, ZABs are the most technically ready metal-air batteries in the battery industry.

In addition to small-scale applications, large-scale but low-rate ZABs are also used within systems such as railroad signaling, seismic telemetry, remote communication, and navigational buoys (Caramia and Bozzini 2014).

Similar to other MABs, ZABs share common components: a metal anode, which is zinc in this case, and an electrolyte, which is usually preferred as alkaline and is usually potassium hydroxide (KOH) for compatibility purposes. Finally, an air electrode consists of a GDL and CL where oxygen diffusion from the ambient air and electrochemical reactions occurs, respectively (Caramia and Bozzini 2014; Olabi et al. 2021). ZABs have an OCV of 1.65 V, and the theoretical capacity density is 820 mAh/g (Niu et al. 2021).

ZAB have several advantages when compared to other MABs. Additionally, these batteries even show advantages that can make ZABs potential alternatives for the commercial batteries such as Li-ion. These advantages make ZABs attractive for wide range of applications and research. The ZAB exhibit high energy densities. While the theoretical energy density is 1.3 kWh/kg, the practical energy density varies between 0.7-0.9 kWh/kg (Gilligan and Qu 2015; J. S. Lee et al. 2011a; Y. Li et al. 2013a; Jörissen 2006). ZABs having much higher energy densities when compared to commercial batteries, even the Li-ion (0.5 kWh/kg theoretical) is a major advantage. Besides high energy densities, zinc is an abundant resource which makes it more accessible and available when compared to precious metals, materials such as lithium (Shimizu et al.

1990). ZABs also have relatively cost-effective production processes with lower environmental impact. Unlike Li-ion batteries, ZABs utilize aqueous electrolytes that prevents complex cell chemistry and handling difficulties in terms of stability risks and safety due to atmospheric exposure. These mentioned advantages in terms of material safety, abundance and energy storage capability of ZABs makes them suitable candidates for ESS (Olabi et al. 2021; Gilligan and Qu 2015).

However, ZABs still face critical challenges that limit its mass adoption. Overall, ZABs suffer from aging mechanisms that prevent high cycle lives of the battery for rechargeable battery applications. These aging mechanisms occur within overall battery or in specific domains of a ZAB (Gilligan and Qu 2015).

For zinc-electrode side, anodic dendrite growth and film resistance due to ZnO deposition are critical. Additionally, parasitic reaction on the zinc-electrode side, which is the hydrogen evolution reaction (HER) is another aging mechanism that prevents the occurrence of desired electrochemical reactions on the battery (K. Wang et al. 2015; Harting, Kunz, and Turek 2012; Pei, Wang, and Ma 2014).

For air-electrode, due to openness of the system, carbonation of the battery is a significant problem which is caused by the CO₂ content in the ambient air surrounding the system. Due to carbonation of the system, battery pores can get clogged, or electrolytes lose their electrical activities due to complex species formation. Additionally, air-electrode's catalyst layer (CL) may lose its catalytic activity due to oxygen scratching or due to bi-functional activity during recharge. This bifunctional activity deactivates catalysts due to working in different overpotentials within different reactions such as ORR and OER (Schröder and Krewer 2014; Radenahmad et al. 2021; K. Wang and Yu 2020).

For overall battery, electrolyte loss due to open system conditions where the concentration gradient between the water concentration within the battery and the ambient air. Therefore, electrolyte loss due to evaporation may occur and lead to battery failure. Besides the evaporation, if the gradient is significantly high, flooding on the air electrode's pores may occur and degrade battery's performances (X. Liu et al. 2021; Schröder and Krewer 2014).

These aging mechanisms hinder the adoption of ZABs on a wider scale by preventing high cyclability. Therefore, for further adoption, rechargeability of ZABs must be improved by preventing these aging mechanisms. Hence, detailed studies to investigate and prevent aging mechanisms are needed. A more detailed explanation of

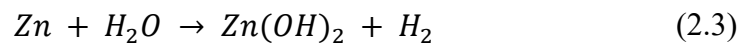
electrochemical reactions kinetics and mass transfer phenomena for ZABs will be given in the “MODELLING OF ZABs” chapter.

2.5.8.1 Zinc-Electrode

Within ZABs, the negative electrode, also known as the anode, is the zinc electrode. Various forms of zinc can be used within this electrode. Zinc can be powder or fiber form, depending on the design choices (Caramia and Bozzini 2014). In the literature, there are various structures of zinc in zinc electrodes, such as rolled sheet, atomized powder, dendritic powder, cash ribbons, threads, and pellets (X. G. Zhang 2009; C. C. Yang and Lin 2002; X. Gregory Zhang 2006). As a result of these design changes, the electrode's porosity varies, significantly altering the electrode's performance, stability, and durability. Common porosity values range between 60% to 80%, which is critical for a ZAB to operate, especially in large current densities during the operation, which minimizes voltage drops and increases durability. Each configuration of zinc used within these electrodes has different reasons to be selected. For example, configurations such as atomized zinc powder or fibers have much better electrical performances than others. However, these require additional agents such as gels and binders to increase its porosity to the ideal range that has been mentioned for long-term stability and performance (Othman et al. 2001; Mohamad 2006). Binders and gels such as polytetrafluoroethylene (PTFE), sago, carbopol, and tapioca are the agents that enhance electrode specs and minimize zinc corrosion (Mohamad 2006; C. W. Lee et al. 2006; Müller, Holzer, and Haas 1998; G. M. Wu, Lin, and Yang 2006; M. N. Masri and Mohamad 2009; Mohamad Najmi Masri et al. 2015). Despite the addition of these agents improving the battery's performance, these are additional costs for battery manufacturing, increasing the electrolyte resistance.

On the discharge mode of a zinc electrode, the zinc oxidizes. However, this oxidation reaction is not a one-step reaction. With the oxidation of the zinc ions on the surface, the ion's solvation and diffusion are followed by its precipitation if the solubility limit is reached (Caramia and Bozzini 2014). Mentioned reactions will be given and described in the following “MODELLING of ZABs” section.

During the discharge mode, the parasitic Hydrogen Evolution Reaction (HER) occurs on the anodic side, limiting the battery's performance, efficiency, and capabilities (Beverkog and Puigdomenech 1997). Therefore, powder or fiber forms of mercury are usually added to the zinc electrode to tackle HER and improve the battery's capabilities to limit or prevent hydrogen evolution (Devyatkina, Gun'ko, and Mikhalenko 2001). HER described at the Equation (2.3 below):



Recently, efforts have been made for alloying zinc with other metals such as Pb, Cd, or Ni to increase its HER overpotential (C. Zhang et al. 2001; Lan et al. 2006; El-Sayed, Mohran, and Abd El-Lateef 2012) or addition of materials such as Al_2O_3 , Li_2O - $2\text{B}_2\text{O}_3$ coatings to zinc particles to prevent its direct contact with the alkaline electrolyte. These coatings can inhibit corrosive side reactions and improve the battery's durability (S. M. Lee et al. 2013). However, these methods are tedious and have significant costs. Other novel solutions, such as adding organic materials such as polyethylene glycol, are also being studied to inhibit the corrosion mechanisms within the zinc electrode (Auinat and Ein-Eli 2005).

2.5.8.2 Electrolyte

ZABs have different electrolyte type selections in the design procedures. Various types, such as alkaline, room-temperature ionic liquids, polymer, solid-state, and hybrid electrolytes, have been used and investigated. Aqueous electrolytes such as KOH and NaOH are the most common, while KOH is the most typical due to its safe handling and efficiency. KOH has higher oxygen diffusion, lower viscosity, and higher ionic conductivity (See and White 1997). Besides these superiorities, KOH electrolytes show much better performance in terms of solubility of the reaction products with CO_2 - K_2CO_3 and KHCO_3 when compared to the ones within NaOH electrolytes. Hence, utilization of the KOH electrolytes is superior due to the minimization of carbonate precipitation, a

major aging mechanism for zinc-air batteries compared to other alkaline mediums as the electrolyte (Y. Li and Dai 2014).

Typically, for optimal utilization, the electrolyte conductivity of KOH is the one with 30%wt and 6-7 M of concentration (Toussaint et al. 2010; Z. Chen et al. 2012; Du et al. 2013; Prabu, Ramakrishnan, and Shanmugam 2014). Even though there is a minimization, alkaline electrolytes still mostly suffer from the absorption of CO₂ from the GDE, which results in the battery's carbonation. Thus, it reduces the battery's durability, stability, and performance (P. Chen et al. 2020). Additionally, alkaline electrolytes face problems such as water loss, a major aging mechanism, due to the system's openness within zinc-air batteries (Y. Li and Dai 2014b).

Solid-state electrolytes are different approaches to battery design. These designs improve electrolyte safety and handling by preventing electrolyte leakage. Additionally, these types of electrolytes are more stable in a wide range of temperatures. However, the main problem of these electrolytes is their low ionic conductivities and higher manufacturing costs than liquid electrolytes (Thomas Goh et al. 2014).

For non-volatility and electrochemical stability, room-temperature ionic liquids (RTILs) are more favorable for non-aqueous electrolyte selections. These electrolytes have higher thermal stabilities and wider electrochemical windows. The main drawbacks of these electrolytes are their higher costs and lower ionic conductivities concerning aqueous electrolytes (P. Chen et al. 2020).

Polymer electrolytes are also being researched due to their enhanced stability at the electrode-electrolyte interface. While these electrolyte applications show decent results in preventing electrolyte leakage, their complex manufacturing processes and lower ionic conductivities compared to liquid electrolytes are the main drawbacks (Q. Liu et al. 2022).

Additionally, alternative and mixed solutions such as hybrid electrolytes are novel applications studied to holistically tackle problems occurring with individual electrolyte types with combined configurations. With these configurations, the aim is to improve battery performance while minimizing the stability trade-offs.

For example, quasi-solid and flexible electrolytes possess properties of aqueous electrolytes with high ionic conductivity, and polymer electrolytes have enhanced stability. However, due to complex structure, compatibility, and cost are the main drawbacks of these types of electrolytes (Mainar et al. 2018).

2.5.8.3 Separators

Similar to other batteries, separators are the critical components of ZABs that ensure battery safety while promoting efficient operation. As the name implies, using separators maintains the separation of positive and negative electrodes. This isolation of counterparts helps batteries maintain their operation safely and efficiently by preventing short circuits and providing the ionic gradient across the battery. Additionally, separators with structural strength against zinc deposition and dendritic growth play a crucial role in preventing potential battery short circuits due to the puncturing of the separator and the loss of the ionic gradient (Y. Li and Dai 2014a).

The separators commonly used in metal-air batteries are the ones that have been commercially used in alkaline and lithium-ion batteries. Polymeric separators such as polyethylene (PE) and polypropylene (PP) and those made of polyvinyl alcohol performed well in various applications in metal-air batteries (Arora and Zhang 2004; Kritzer and Cook 2007). Especially in the production of zinc-air batteries, commercial applications of separators are usually Celgrad® 550-based separators, which consist of tri-layer structured PP/PE/PP separators that maintain safe operations with overheating protection and mechanical durability. The fibrous structure of these materials can go up to 75% and ensure high electrolyte retention with low ionic resistances.

The main disadvantage of these types of separators is the open structures that may allow soluble zincate ions to permeate readily. Hence, it may significantly increase the polarization within the battery, which can degrade its cycling performance as an aging mechanism (Y. Li and Dai 2014a).

2.5.8.4 Air Electrode

The structure of conventional ZABs air electrodes (GDE) consists of three sections. These are the GDL, CL, and the current collector. As mentioned in the previous parts, GDL is the layer that handles the transportation of O₂ from ambient air. At the same time, the diffused oxygen is reduced to OH⁻ ions in ORR in the discharge mode at the CL's electrochemically active sites. In the charge mode, OH⁻ ions are oxidized into O₂

(OER), and the produced O_2 diffuses from CL to ambient air via GDL channels (J. Pan, Xu, et al. 2018).

Metal meshes with conductive properties are commonly selected for current collectors. Nickel foam and stainless steel are also being selected for this purpose, both conventionally and commercially (Y. C. Lu et al. 2011; Park and Park 2012). The material selected for GDL should have certain properties. The GDL must have effective surface areas sufficient for gas transfer and a hydrophobic structure to prevent electrolyte leakage from the hydrophilic CL (Wei et al. 2000). Commonly, materials for this purpose are porous carbonic materials and PTFE with water-resistant and chemically stable properties (Eom et al. 2006; J. Pan, Yang Xu, et al. 2018). The CL is the most significant part of an air electrode, determining its electrochemical activity and performance capabilities since ORR/OER are being conducted within this layer's triple-phase boundary (Viculis, Mack, and Kaner 2003). Therefore, the porous form of an air electrode is much favored (Lin and Van Nguyen 2005). The classical configurations of the air electrodes are the CLs, which are porous and in contact with the electrolyte. This active CL is usually covered on the surface of the current collector, while the GDL is on the opposite side, exposed to ambient air without any connection to the electrolyte (J. Pan, Yang Xu, et al. 2018). The current collector metal mesh is sandwiched between the GDL and the CL (Wassei and Kaner 2013).

Due to O_2 having low solubilities and diffusivities in electrolytes, O_2 is usually in the gaseous phase while ORR reactions are conducted. Thus, the CL's triple-phase with effective and high surface areas is critical to conduct these reactions efficiently (Stamenkovic et al. 2016). Therefore, just like the GDL, the porous architecture is required for the CL (Lin and Van Nguyen 2005). With its porous structure, the CL provides the required contact with the oxygen, electrolyte, and catalyst at the triple-boundary (Zhu et al. 2011). Catalyst utilization is highly dependent on the use of supporting materials, which significantly determines the catalyst's durability and activity. Therefore, using supporting materials provides the porous structures with a high specific surface area to facilitate effective oxygen interaction in the electrolyte at the catalyst surface (P. C. Li et al. 2017). Supporting materials also promote the corrosion resistance of the air electrode while having great conductivity properties (Gu et al. 2017). Usually, porous carbon nano-carbons are used as supporting materials with overall physical and chemical advantages while being abundant and low-cost sources such as graphene-based composites (Y. Zhang et al. 2005; Maja et al. 2000). Since the catalysts must be embedded

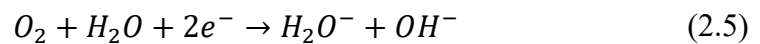
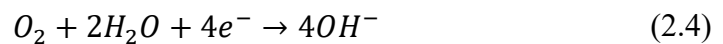
with these supporting materials, polymer binders are used for this purpose (Xiao et al. 2010; Prabu, Ramakrishnan, and Shanmugam 2014).

ZABs air-electrodes are highly sensitive to relative humidity, therefore a fine-tuned balance between hydrophilicity and hydrophobicity is needed. Since the CL is the layer where triple-phase contact occurs with the electrolyte, it must have a hydrophilic structure and effective wettability. In contrast, the GDL that facilitates O₂ gas transfer from the ambient has a hydrophobic structure. Hence, this well-balanced structure can prevent or minimize evaporation loss or flooding of electrolytes regardless of the relative humidity (Y. Shen et al. 2013).

The electrocatalyst where ORR/OER reactions occur is the core of a ZAB's functionality (Strasser 2016). Therefore, to tackle any limits due to sluggish kinetics within ORR/OER, electrocatalysts with high active site densities, effective porous structures, high surface areas, and uniform distribution are required in ZABs to prevent performance degradation (Y. Shen et al. 2013; Z. Chen et al. 2011; Li Zhu et al. 2010). Hence, any limiting conditions due to electrode kinetics and mass transfers will be minimized (Nam et al. 2015; Ang et al. 2016). The electrocatalyst must have the required mechanical and chemical stability for durable architecture while being an abundant and feasible resource (Qiang Wu et al. 2017). Thus, electrocatalyst selection in ZABs requires detailed design selections based on the criteria mentioned.

During material selection, trade-offs should be considered delicately. Depending on the type of ZABs, primary or secondary electrocatalysts change and vary in structure and contents (J. Pan, Yang Xu, et al. 2018).

For primary ZABs, uni-functional catalysts that only conduct ORR on the triple phase are used for discharge purposes (Y. Li and Dai 2014a). Two main pathways occur during the ORR: the 2-electron and 4-electron pathways. Equation (2.4) represents the 4-electron direct pathway, while the Equation (2.5) and Equation (2.6) represent the 2-electron pathway respectively.





A ZAB's efficiency and stability highly depend on these pathways and their dominance. The 2-electron pathway is the indirect way of ORR, while the 4-electron pathway is the direct ORR. Therefore, electrocatalysts that favor the 4-electron pathway improve the battery's performance, making them much preferable (Cao et al. 2011; G. Li et al. 2016). For this purpose, electrocatalysts commonly use transition metal oxides, noble metals, alloys, and carbon-based materials (J. Pan, Yang Xu, et al. 2018). The “MODELLING OF ZABs” chapter will give more information about ORR pathways.

Transition metal oxides are cost-effective materials suitable for electrocatalytic activity for ORR on primary ZABs. Manganese dioxide (MnO_2) is a commonly used electrocatalyst and has been commercially used, such as Duracell®'s γ - MnO_2 used hearing aid batteries with 400 Wh kg⁻¹ energy densities (Qiumei Wu et al. 2014; Dong and Li 2014; Y. Li and Dai 2014a). Noble metals and alloys of noble metals are also known for their excellent catalytic activities. However, their high cost and scarcity are the limiting factors for their mass adoption and commercialization (J. W. Zhang et al. 2009). Carbon-based materials are usually N-doped carbon nanotubes (CNTs) and/or graphene composites. These materials show decent ORR activities. Additionally, porous doped carbon materials produced from MOFs show decent ORR activity. N-doped mesoporous carbon polyhedrons are specially produced with Cu-doped ZIF-8 materials, which are potential candidates for applications with 132 mW cm⁻² power densities (Barkholtz and Liu 2017; H. Zhang et al. 2017).

There are two existing pathways for a battery to be rechargeable. One is mechanical, and the other is electrical rechargeability (Neburchilov et al. 2010). Mechanical recharge is the process where the discharge products, such as zinc oxides and zincates, are removed. However, during the electrical recharge process, charge/discharge cycles are used to provide the necessary conversion of materials and sustain the required gradients among the battery (H. Kim et al. 2013). Due to applicability and feasibility, electrical rechargeable is much more preferred for rechargeable ZABs (J. Pan, Yang Xu, et al. 2018). At these secondary batteries' triple-phase boundary, the active sites' reaction changes depending on the battery's mode. ORR and OER are being conducted at this region in discharge and charge modes (H. F. Wang et al. 2017). Therefore, bifunctional catalysts are required instead of using a uni-functional electrocatalyst for rechargeability.

Commonly used materials are mixed metal oxides, perovskite oxides, and carbon-based materials (J. Pan, Yang Xu, et al. 2018).

Mixed metal oxides are usually materials that contain Co_3O_4 or MnO_x -based materials that combine OER and ORR functionality in material for rechargeability. Some examples for these types of materials can be given as $\text{Co}_3\text{O}_4/\text{MnO}_2$ or $\text{Ni}@\text{MnO}_x/\text{C}$ composites, which show high durabilities, efficiencies, and power densities even up to 543 charge/discharge cycles (J. Pan, Yang Xu, et al. 2018; Qiumei Wu et al. 2014). Besides mixed metal oxides, NiFe layered double hydroxides, and CoO/CNT hybrid materials have also demonstrated potential stability and activities (Y. Li et al. 2013b; P. C. Li, Chien, and Hu 2016). Additionally, perovskite oxide materials such as $\text{La}_{0.8}\text{Sr}_{0.2}\text{Co}_{0.6}\text{Mn}_{0.4}\text{O}_3$ showed promising results with balanced bifunctional activity and performances along the charge/discharge cycling (Q. Wang et al. 2017).

Even though two-electrode configurations for secondary ZABs are the most common, they are not the only ones. Despite being effective, two-electrode configurations face problems like the ORR catalyst's deactivation during the charge mode, where OER with high voltages occurs. Therefore, this high voltage can reach 2.0 V in charge mode while the OCV is 1.2 V in the discharge mode (Y. Li and Dai 2014a).

High voltages in charge operation may affect the catalyst's structure due to oxidation and corrosion, resulting in catastrophic results such as catalyst loss and mechanical damage that short-circuiting the battery (Y. Li et al. 2013b). Thus, the tri-electrode configuration is proposed where one electrode is only loaded with a catalyst dedicated to ORR, and the other is devoted to OER. The position of the Zn electrode is between these ORR and OER electrodes. Hence, this discrete execution of reactions reduces the catalyst loss or structural damage significantly (P. C. Li, Chien, and Hu 2016).

Despite increasing the stabilities of ZABs, which result in higher cycling performances, tri-electrode configurations increase the volume and weight of the batteries. Therefore, it reduces the volumetric energy and power densities of ZABs while adding additional production costs. Thus, researchers focus on two-electrode configurations with durable and efficient bifunctional catalysts (J. Pan, Yang Xu, et al. 2018).

CHAPTER 3

MODELLING OF ZABs

As mentioned in the previous parts, ESS is necessary to integrate renewable energy sources into our lives. Batteries are one of the most promising components in ESS research. Within batteries, due to high specific energy densities and lightweight properties, MABs demonstrate a great potential. When compared to other MABs, ZABs are the most promising and technologically ready ones. Even though these batteries show technological readiness, and decent performances, there are still problems to be resolved. Therefore, experimental procedures and steps are required during the research and development of these batteries. However, these procedures are/can be time and money-consuming (Clark, Latz, and Horstmann 2018a). Therefore, modeling these batteries with the help of theory and empirical data is crucial to reduce development time and cost. Modeling also gives researchers the flexibility to investigate the desired mechanisms separately for further understanding of that respective mechanism's contribution to battery operation and aging. Since these mechanisms co-occur in experimental conditions, the stand-alone effect of a mechanism cannot be investigated easily.

Within this section, previous models of ZAB will be discussed in detail. In the following sections, the theory behind the thesis's model will be explained in terms of electrochemical reactions, mass transfer phenomena, and multiphysics-coupled modeling.

Detailed explanations of this work's modeling will be given, such as the physics used, model definitions, variables, parameters, mesh selection, boundary, and initial conditions.

3.1 Previous Models of ZABs

Prior to the discussion of the ZAB model, the modeling of ZABs should be mentioned briefly in conjunction with previous models. Every model differs from the others in various approaches. Some of these models work on different dimensions (0-D,

1-D, 2-D, 3D), some of them are based on different gas diffusion electrodes, zinc electrode structures, electrolytes, and materials, and some of them involve different boundary conditions, such as current applied, initial electrolyte concentration, and more. Modeling of ZABs requires a multiphysics approach since the battery operation involves multiple phenomena. Thus, modeling these battery types is tedious and needs to be holistically designed to work properly.

Cell-level modeling is based on a continuum model, an effective and common strategy for analyzing metal-air batteries. Within continuum models, use of charge and mass continuity equations helps researchers capture the dynamic behaviors of systems segmented into discrete parts (Tan et al. 2017; Neidhardt et al. 2012). These continuum models are derived from non-equilibrium thermodynamics, and complete derivations can be found in the literature (Stamm et al. 2017; Clark, Latz, and Horstmann 2017; Xue et al. 2015). Most models are 1-D (Clark, Latz, and Horstmann 2018a) and can effectively interpret phenomena occurring inside the battery. Further analysis of batteries can also be conducted with the help of 2-D and 3-D models.

ZAB modeling has a decent background in research. Models within these batteries have been developed since the 1980s (Clark, Latz, and Horstmann 2018b). Some of these models focused on the specific parts of the cell, such as the zinc electrode, gas diffusion electrode, or electrolyte within the battery. Some of these models focused on the overall battery mechanics and kinetics. In these models, for electrolyte transport modeling, two different approaches were used concerning the ionic strength of the electrolytes. If the ionic strength is low, Dilute Solution Theory (DST) is used, and if it is high, Concentrated Solution Theory (CST) is used to model solute diffusion and migration (Newman and Balsara 2021). The equations (3.1 and (3.2 below represents the DST and CST respectively.

$$N_i^D = -D_i \nabla c_i, N_i^M = \frac{D_i c_i z_i F}{RT} \nabla \phi_e \quad (3.1)$$

$$N_i^{D,M} = -D_i \nabla c_i - \frac{t_i}{z_i F} j, \quad j = -K \nabla \phi_e + \frac{K}{F} \sum_i \frac{t_i}{z_i} \frac{\partial \mu_i}{\partial c_i} \nabla c_i \quad (3.2)$$

At these equations given above, the term D_i represents the diffusion coefficient, T represents the temperature, ∇c_i represents the concentration gradient, N_i^M represents the flux due to migration, z_i represents the charge of the ionic species. The $\nabla \phi_e$ term represents the electrical potential gradient, and the terms F , R are the constants that are commonly used in electrochemical reaction kinetics, which are the Faraday's constant and the gas constant respectively.

On the CST equation, the term t_i represents the transference number, the term j is to represent the electrical current density, K represents the electrolyte conductivity, and the term μ_i represents the chemical potential of the ionic species.

In 1980, Sunu and Bennion developed a 1-D continuum model to predict concentrated transport. This model utilizes CST in porous electrodes to examine Zn and ZnO shape changes within the anode. The model's shape changes were observed in the battery's charge-discharge cycling state. Simulations in this work showed the inhomogeneous precipitation of ZnO and its effect on the zinc electrode's shape change while cycling the battery (Sunu and Bennion 1980a).

In 1992, Mao and White (Mao and White 1992) developed a mathematical model to extend Sunu and Bennion's model where constraints such as the separator domain, precipitation of solid ZnO and $K_2Zn(OH)_4$, and the air electrode domain are included. Increased constraints in this model helped researchers analyze overall battery design features more accurately. Model results showed the effects of separator thickness, electrode thickness, hydroxide ions depletion, and material loading per unit volume on the anodic material utilization (Mao and White 1992) It has been predicted and observed that the material utilization on the anode is mostly limited due to the depletion of the hydroxide ions concentration; a thicker separator increases the utilization; however, it reduces the cell voltage, and the electrode thickness is insignificant.

In 2002, Deiss et al. (Deiss, Holzer, and Haas 2002; Clark, Latz, and Horstmann 2018b) developed a rechargeable alkaline ZAB model to predict the charge-discharge profiles of the rechargeable ZABs. As domains, porous Zn/ZnO electrodes, and porous air electrodes are negative and positive electrodes, respectively. 1-D model's predictions were compared to empirical values of galvanostatic experiments of a ZAB. Results showed that the model's output was close to the experimental values of electrode potentials within both anode and cathode parts.

Besides the electrode potentials, the model also showed decent results regarding Zn redistribution and the concentration gradients within the cell compared to experimental results (Clark, Latz, and Horstmann 2018b) and concluded that this model could be useful when optimizing the cell.

In 2016, Vasile et al. (Vasile et al. 2016) developed a 3-D multi-physics multi-component model to investigate the GDE within non-isothermal conditions. This work utilized the multi-physics platform to predict the effects of catalyst structures, activity, and porosity on the GDE of a ZAB. The model utilizes the widely used Butler-Volmer, Stokes-Brinkman, and Maxwell-Stefan equations for electrochemical reactions, mass, and heat transfer respectively. Results indicated that the model was valid concerning experimental data and could be a useful tool to simulate GDE configurations with different electrocatalysts, porosity, and other properties to optimize it.

In 2014, Schröder and Krewer (Schröder and Krewer 2014) developed a 0-D model to investigate the effects of the air composition on rechargeable ZABs. The proposed model can flexibly predict/simulate the secondary ZAB operation for the surrounding air's varying relative humidity, CO₂, and O₂ composition. Therefore, the model can be used to investigate the effect of air composition on overall battery performance, especially the GDE. The results of this model proved that the air composition is one of the most critical aspects of battery performance while operating. The model also suggested that intermediate relative humidity values (approx. 65%) and CO₂ concentrations lower than 10 ppm are necessary for ZABs operating at 298 K and 6 M KOH electrolytes for long-term stability and high performance. The proposed model is a useful method when working on different operating conditions and can be adapted to be used within different MABs.

In 2022, Lu et al. (C. T. Lu et al. 2022) investigated the effects of parameters in cell design on ZAB performance. The proposed model was developed to analyze and optimize overall battery performance. This work used four different cell configurations, close-proximity electrode, equal-area electrode, large-zinc electrode, and air channel flow, as structural parametrization. Other factors were also analyzed, such as the effect of the carbon paste addition to GDE, natural/forced convection, anode/cathode area ratio, and the distance between anode and cathode. This work showed that the proposed model can be useful for model-based cell engineering.

Even though ZABs are the most focused ones within the MABs, for technological readiness, there are still more modeling work to perform. Despite having models since

1980, quite a few are based on overall battery performance concerning overall battery aging mechanisms, battery domains, and holistic properties. As mentioned in the previous parts, prior models usually focus on one domain, such as zinc-electrode performance.

However, there is little work on the GDE side of ZABs; only significant progress has been made by Schröder and Krewer's work in 2018, which is a 0-D model that focuses on air composition.

Therefore, it is necessary to develop such a model that considers GDE parameters, aging in addition to zinc-electrode aging, and parameters to develop such a model that can be applied much more flexibly. This thesis aims to develop a multi-physics model of overall ZAB, especially including the GDE, where mass transport of O₂ within the surrounding air is considered. In the following parts, details of the model will be explained.

3.2 Battery of the Model

The battery model consists of three main sections: A zinc electrode as anode, a separator domain, and an air electrode as cathode. However, in this model, the air electrode's GDL is just represented as a boundary condition. Thus, the air electrode domain focuses on the porous electrode where CL exists with the electrocatalyst. For this modeling problem, the ZAB of interest is simplified into the 1-D structure. As mentioned in the previous part, the 1-D models can effectively interpret phenomena inside the battery. Further thermal and structural durability analysis of batteries can also be conducted with the help of 2-D and 3-D models (Clark, Latz, and Horstmann 2018b) Since this thesis focuses on overall ZAB with electrochemical and mass transfer phenomena specific, 1-D modeling is sufficient to model this battery of interest. At the Figure 3.1 below, the 1-D geometry is indicated.

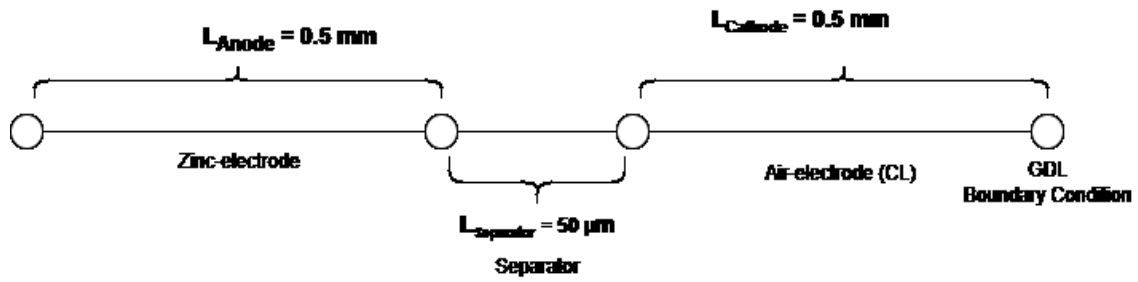


Figure 3.1 The 1-D representation of the battery of the model.

3.2.1 Theory and the Physics Used Within the Model

As mentioned in the previous parts, electrochemical reactions and mass transfer phenomena co-occur within ZABs. Due to this complex system with coupled interactions in an open system, multiphysics approach is required to model properly. For this purpose, various numerical methods are being used. Methods such as Finite Element Method (FEM), Finite Difference Method (FDM), and Finite Volume Method (FVM) are robust numerical methods that can handle these types of multi-physics interactions (Bathe 1996; Zienkiewicz, Taylor, and Zhu 2005; Versteeg 2007; Moukalled et al. 2016).

FEM is ideal for many applications, from structural and electrical, to thermal analysis of multi-physics systems, while FVM is mostly preferred for fluid flow and mass transport problems. Additionally, FDM is a method mostly applied to solve simpler problems on simple geometries and systems (Bathe 1996; Zienkiewicz, Taylor, and Zhu 2005; Versteeg 2007; LeVeque 2007; Moukalled et al. 2016) Utilization of these methods, a holistic and comprehensive analysis of zinc-air batteries can be done.

- i) FEM is a numerical method that solves Partial Differential Equations (PDEs) that are faced in engineering and physical sciences problems. FEM discretizes a continuous domain into a finite number of sub-domains which are also known as finite elements. Elements of subdomains can be in different shapes, such as triangles, tetrahedra, etc., depending on the problem dimensionality. This method solves PDEs by approximating these sub-domains with piecewise polynomial functions (Bathe 1996). The process of applying FEM

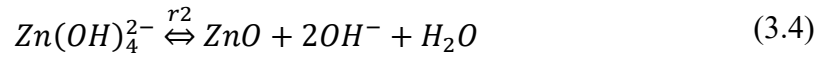
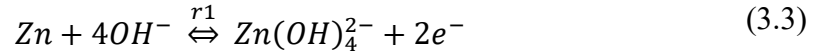
to a numerical problem can be summarized as following. Firstly, the physical domain is discretized into finite elements; suitable polynomial functions are then selected to achieve the best approximations for each element. With these approximations, the PDEs of elements are transformed into algebraic equations. Then, with these element equations, global system equations are assembled to represent the entire domain. Finally, these global systems of equations are solved with numerical methods to obtain an approximate overall solution (Zienkiewicz, Taylor, and Zhu 2005). FEM is known for its high capability and compatibility. The method can accurately and flexibly handle problems within complex geometries and boundary conditions. From structure, thermal to electrical field or magnetic field analysis, multi-physics problems FEM is the most used method (Zienkiewicz, Taylor, and Zhu 2005; Bathe 1996). There are various programming languages, such as Python or C++ with suitable libraries, or MATLAB suite with built-in functionalities for FEM (Walker 2018). Software such as ANSYS or COMSOL present detailed capabilities. Especially COMSOL is the software of choice when multi-physics modeling is desired with minimal requirements for coding (Pepper and Heinrich 2017).

The following sections will provide the physics behind ZAB, including the electrochemical reactions and mass transfer phenomena with their governing equations, aging mechanisms, model definitions, variables, parameters, boundary, and initial conditions with the simple meshing information. For solutions of these physics, FEM is being used. Within the electrochemical physics used and mass transfer parts, physics equations were obtained from various modelling sources, including the reference manuals of the well-known FEM software COMSOL Multiphysics (Comsol 2020).

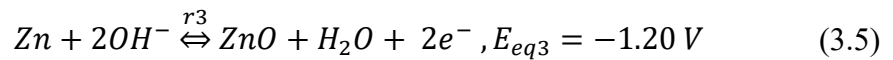
3.2.1.1 Electrochemical Physics Used within the Model

As mentioned in the previous parts, secondary batteries operate in two modes: charge and discharge. During discharge mode, electrochemical reactions on the zinc electrodes in alkaline electrolytes involve several steps. First, solid zinc ions and OH-

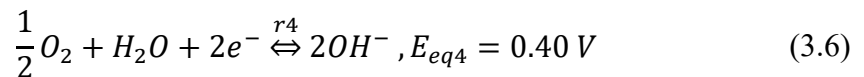
ions form zincate ions. These zincate ions are precipitated into solid ZnO when the solubility limit is reached. During the charge mode, the deposited ZnO species are converted back into zinc at the zinc electrode via reduction (Caramia and Bozzini 2014; Schröder and Krewer 2014). The equations (3.3 and (3.4 below summarize the half-cell reactions on the zinc electrode side.



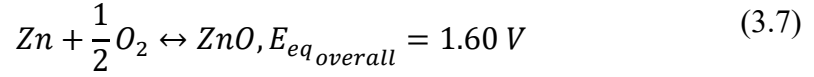
Overall, reactions on the anode side where surface Zn atoms are converted and deposited into ZnO solid particles can be obtained via a combination of reactions r_1 and r_2 . Therefore, the resulting reaction of dissolving-depositing species, Zn to ZnO in discharge, and ZnO to Zn in charge electrochemical conversion can be obtained. The equation is summarized in Equation (3.5 below:



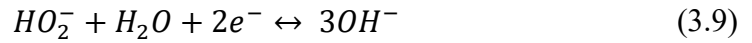
On the cathode side, ORR occurs at CL's triple phase boundary with O_2 and water, forming OH^- ions. During the charge mode, the OH^- ions are oxidized into O_2 , and oxygen evolves (OER) on the air electrode side. Cathode reactions summarized at the Equation (3.6 below.



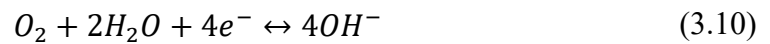
The combination of the r_3 and r_4 half-cell reactions and full-cell reactions is obtained and can be seen in Equation (3.7 below:



The ORR reaction at the air electrode may occur via two different pathways: the 2-electron and the 4-electron pathway. In the 2-electron pathway, O_2 diffused from the GDL is reduced to hydrogen peroxide (H_2O_2) as an intermediate before the OH^- production (Xia et al. 2016). Overall, O_2 reduction into OH^- occurs within 2-step reactions and is summarized in the 2-electron pathway's reaction equations (3.8 and (3.9 below:



As can be seen from the equations above, initially, O_2 is reduced into hydroperoxide (HO_2^-) ions, which can easily poison the electrocatalyst and lead to corrosion in the air electrode which is not desired (Xia et al. 2016; J. Pan, Yang Xu, et al. 2018) In the further step, HO_2^- ions are reduced into hydroxide ions. Therefore, the overall reduction can be summarized in the Equation (3.10 below:



The 4-electron pathway directly reduces O_2 into OH^- ions, as summarized in equation (3.10) above. The 4-electron pathway for ORR is the more efficient pathway for ZABs since the direct conversion of O_2 is obtained. Thus, this direct conversion without intermediate products prevents/minimizes any corrosive or inhibiting materials for the ZAB's air electrode, resulting in high efficiency and stability (W. Zhang, Lai, and Cao 2017). Other side reactions and by-products that may lead to the battery's aging with activity and stability degradation will be discussed in detail in the "Aging Mechanisms" section of the thesis.

The model for electrochemical reaction utilizes FEM to compute values of potential and current distribution throughout the entire ZAB model. The electrodes' charge transport is described using Ohm's law, while the concentrated electrolyte theory describes the mass and charge transport in the KOH electrolyte. Since KOH contains K^+ and OH^- as cations and anions, the electrolyte is recalled as a binary electrolyte (Haverkort 2024).

Within the model, FEM solves PDEs for five dependent variables. These are the electric potential Φ_s , the electrolyte potential Φ_l , species that are intercalating can be denoted as c_s , $\Delta\Phi_{s,film}$ represents the potential drop if the porous electrode particles produce a film resistance while c_l represents the electrolyte's salt concentration. Since the electrolyte is binary and the electroneutrality holds, the cation and anion concentration of the electrolyte can both be represented by the term c_l . The charge and mass conservation of the electrolyte salt can be represented with the following equations:

$$\nabla \cdot i_l = i_{tot} + Q_l \quad (3.11)$$

$$i_l = -\sigma_l \nabla \varphi_l - \left(\frac{2\sigma_l RT}{F} \right) \left(1 + \frac{\partial \ln f}{\partial \ln c_l} \right) \left(t_+ + \frac{c_l}{c_0} \right) \nabla \ln c_l \quad (3.12)$$

$$\frac{\partial \varepsilon_l c_l}{\partial t} + \nabla \cdot N_l = R_l \quad (3.13)$$

$$N_l = -D_l \nabla c_l + \left(\frac{i_l t_+}{F}\right) \quad (3.14)$$

Where:

- i_l is the current density of the electrolyte.
- σ_l is the conductivity of the electrolyte.
- f is the activity coefficient for electrolyte salt.
- t_+ is the transport number for the cation.
- i_{tot} is the total current due to electrochemical processes.
- c_0 is the solvent concentration.
- N_l is the cation flux.
- ε_l is the volume fraction of the electrolyte depending on the porosity of the domain.
- D_l is the electrolyte salt's diffusivity constant.
- R_l is the total source term of the cation in the electrolyte.

On porous electrodes and separators with certain porosity values, terms such as porosity and tortuosity play a crucial role while determining effective conductivities, diffusivities. To measure these effects, Bruggeman correction is the most used approach (Newman and Balsara 2021; Lai and Ciucci 2011). With Bruggeman correction, effective conductivities and chemical diffusivities can be represented as:

$$\sigma = \sigma_0 \varepsilon^{Br} \quad (3.15)$$

$$D = D_0 \varepsilon^{Br} \quad (3.16)$$

The constant “Br” is Bruggeman's constant, and it is commonly 1.5 in the literature (Comsol 2020).

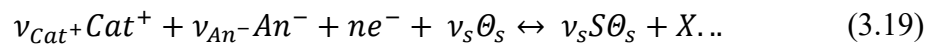
On the electrode side, the current density can be noted as the i_s term is related with the electrical potential (Φ_s) and conductivity of the electrode (σ_s) and can be described as the following Equation (3.17):

$$i_s = -\sigma_s \nabla \Phi_s \quad (3.17)$$

The electrode domains current conservation equations can be described with the total current sources with addition of arbitrary current source term Q_s :

$$i_s = -i_{tot} + Q_s \quad (3.18)$$

As mentioned at the previous parts of this thesis, reactions occur on the surface of the electrodes. Various reactions can occur on the surface of these electrodes, from electrochemical to chemical adsorption/desorption reactions. Occasionally, electrochemical reactions contain cations and anions since redox reactions are in process. Even though adsorption/desorption reactions are chemical reactions that do not involve any electrons, these reactions should be also considered inside the electrochemical reactions as an effecting aspect since these reactions may occur the free reaction sites; θ_s . When these sites are occupied due to these reactions, it can be denoted such as $S\theta_s$. These reactions can be summarized as in the Equation (3.19):



In this equation Cat^+ and An^- represent cations and anions respectively, while the term X is denoted to represent product species that are not in the scope of this physics model. Additionally, the ν_i represents the stoichiometric coefficient for species i. As can be understood from the equation, free and occupied sites relation in this equation

represents the absorption/desorption reactions on the electrode. So, if these terms are isolated from the electrochemical reactions, the absorption/desorption reactions can be expressed as:



These chemical reactions depend on a reaction rate constant, k (mol / (s. m²) in SI units). Concentration of free sites c_{θ_s} can be assumed as constant if the total reaction sites; $c_{s,max}$ is assumed to be constant. The relationship between these two parameters can be summarized as:

$$c_{\theta_s} = c_{s,max} - c_s \quad (3.21)$$

Recall that the term c_s is the concentration of intercalating particles. If there are no intercalating particles, the concentration of free sites is equal to the concentration of total reaction sites. However, if there is an intercalation on the electrode, the free sites concentration varies with respect to intercalation kinetics. Intercalation kinetics is also an important aspect that determines the SOC of the battery significantly. Also, in batteries that have intercalation, equilibrium potentials, E_{eq} becomes a function of SOC. The relation between state of charge and intercalating species concentration can be summarized as:

$$SOC = \frac{c_s}{c_{s,max}} \quad (3.22)$$

Even though the reactions are conducted on the particles surface, if there are intercalating species, these can transfer due to diffusion. This phenomenon can be described as:

$$\frac{\partial c_s}{\partial t} = -D_s \nabla c_s \quad (3.23)$$

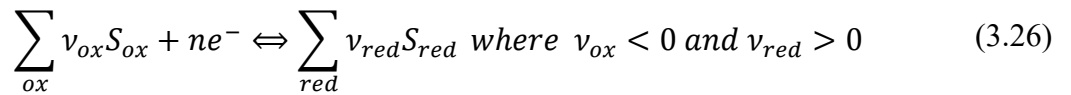
With respect to particle type, spherical, cylindrical or flake, the divergence and gradient operators in this equation can vary. For these types of particles, spherical, cylindrical or cartesian coordinates were used respectively. Boundary conditions can be summarized as:

$$\frac{\partial c_s}{\partial t} = 0|_{r=0} \quad (3.24)$$

$$-D_s \frac{\partial c_s}{\partial t} = R_{s,tot}|_{r=r_p} \quad (3.25)$$

The term $R_{s,tot}$ represents the intercalating species total molar flux because of electrochemical and chemical reactions.

Overall electrochemical reactions can be expressed as the equations below. The terms ν_{red} , S_{red} , and ν_{ox} , S_{ox} represents the stoichiometric coefficients of reducing and oxidizing species respectively.



In this equation it can be understood that n is the number of electrons that are included in the electrochemical reaction. This number can be easily expressed as function of charge of species z_i and its stoichiometric coefficients.

$$n = - \sum_i \nu_i z_i \quad (3.27)$$

With respect to the porous electrode theory, the i_{tot} represents the total current densities due to charge transfer. This can be described as:

$$i_{tot} = \sum_i A_{v,m} i_{loc,m} \quad (3.28)$$

The term A_v represents the specific surface. The term m is to indicate the index of the electrode reactions. Within the porous electrode, the mass balance source term can be expressed as the following equations.

$$R_{l,p} = \sum_m A_{v,m} \frac{\nu_{cat} i_{loc,m}}{n_m F} \quad (3.29)$$

$$R_l = R_{l,p} + R_{l,src} \quad (3.30)$$

$R_{l,src}$ is the source term if there are additional sources of reaction that affect the total species. Surface of the solids, the electrochemical reaction source term can be expressed as:

$$R_{s,electrochem} = \sum_m \frac{A_{v,m}}{\frac{N_{shape} \epsilon_s}{r_p}} \frac{\nu_{s\theta,m} i_{loc,m}}{n_m F} \quad (3.31)$$

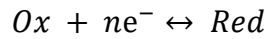
Where $A_{v,m}$ represents the surface area which has been derived by using particle size, shape as shape factor and the volume fraction of the electrode. As the name implies,

the shape factor varies with the shape of the particles. If the particles demonstrate flake shape $N_{shape} = 1$, if it demonstrates a cylindrical shape, $N_{shape} = 2$, or if it is spherical $N_{shape} = 3$. The surface area can be formalized as:

$$A_{v,m} = \frac{N_{shape}\epsilon_s}{d_p} \quad (3.32)$$

Therefore, within the electrochemical source term total, the left side of the product equals 1. However, it is a useful scaling factor that checks and corrects the differences between the surface area used to calculate the volumetric current density and the surface area of the particles in the solid diffusion model of lithium.

Since the concentrations at the electrode surface change on the anode side with dissolving and depositing species (due to Zn and ZnO conversion) and on the cathode side due to ORR/OER and mass transfer, the electrochemical reactions are concentration dependent. To generalize redox reactions occurring inside a battery, Equation (1.1) can be recalled:



Therefore, from the reaction kinetics perspective this redox reaction with forward and backward reaction kinetics can be shown as:

$$r = \frac{i_{loc}}{nF} = k_{fwd}C_R \exp \exp \left(\frac{\alpha_a FE}{RT} \right) - k_{bwd}C_o \exp \left(-\frac{\alpha_c FE}{RT} \right) \quad (3.33)$$

Where the n is the number of electrons in the electrochemical reaction, and F is the Faraday constant. The terms k_{fwd} and k_{bwd} are the forward and backward reaction rates respectively. On the other hand, the terms C_R and C_O represent reducing and

oxidating species expressions and their activities respectively. Additionally, the terms E , α_a and α_c are potential, anodic, and cathodic transfer coefficients respectively. Transfer coefficients α_a and α_c were originally described by Butler, Erdey-Gruz and Volmer (Guidelli et al. 2014). These definitions represent the fractional electrical energy that contributes to anodic and cathodic reactions on the anode and cathode side respectively. These components are the crucial aspects of Butler-Volmer equations which is one of the most used and accepted models to relate current-potential in an electrochemical reaction system (Guidelli et al. 2014; Bard, Faulkner, and White 2022). With these constants and models of electrochemical systems, many insights about what fractions of the total energy change impact the activation energy for anodic and cathodic reactions respectively. (Bard, Faulkner, and White 2022). Additionally, these transfer coefficients summation is equal to total electrons (n) used in the electrochemical reactions:

$$n = \alpha_a + \alpha_c \quad (3.34)$$

Therefore, the total of anodic and cathodic transfer coefficients cannot surpass the total number of electrons contributed to electrochemical reactions. The potential on the other hand depends on the difference between the electric and electrolyte potentials. This can be represented as:

$$E = \Phi_s - \Phi_l \quad (3.35)$$

Reaction rate equation with forward and backward rate constants can be represented by Butler-Volmer equation. This representation can be achieved by introducing equilibrium potential, where the forward and backward reaction rates are equal. Therefore, the electrochemical reaction can be represented as:

$$i_{loc} = i_0 \left(\exp\left(\frac{\alpha_a FE}{RT}\right) - \exp\left(-\frac{\alpha_c FE}{RT}\right) \right) \quad (3.36)$$

Where i_0 is the exchange current density and it is derived from electrode current density at standard conditions ($i_{0,0}$), number of electrons contributing (n) and charge transfer coefficients (α_a and α_{ac}):

$$i_0 = i_{0,0} C_R^{\frac{\alpha_a}{n}} C_O^{\frac{\alpha_c}{n}} \quad (3.37)$$

Overpotential can be described as:

$$\eta = E - E_{eq} \quad (3.38)$$

The term E_{eq} represents the equilibrium potential and it can be derived from reference equilibrium potential at standard conditions $E_{eq,0}$ with Nernst equation:

$$E_{eq} = E_{eq,0} - \frac{RT}{nF} \ln \frac{C_R}{C_O} \quad (3.39)$$

Since within the Butler-Volmer equation, terms i_0 and E_{eq} are concentration dependent, they vary with the changes in activity of reducing and oxidizing species. This electrochemical equation needs to be written to consider while modelling batteries with mass transport. If the concentration of reducing or oxidizing species becomes low, the term $\ln \frac{C_R}{C_O}$ may result as undefined and corrupt the solution process since these terms will tend to go to zero. Therefore, to tackle this problem, the Butler-Volmer equation can be rewritten by introducing fixed reference state activities of reducing and oxidizing species concentrations to define the overpotential.

$$i_{loc} = i_{0,ref} \left(\frac{C_R}{C_{R,ref}} \exp\left(\frac{\alpha_a F \eta_{ref}}{RT}\right) - \frac{C_O}{C_{O,ref}} \exp\left(-\frac{\alpha_c F \eta_{ref}}{RT}\right) \right) \quad (3.40)$$

Thus, the representations of exchange current, overpotential and the equilibrium potential can be rewritten as follows:

$$i_{0,ref} = i_{0,0} C_{R,ref}^{\frac{\alpha_a}{n}} C_{O,ref}^{\frac{\alpha_c}{n}} \quad (3.41)$$

$$\eta_{ref} = E - E_{eq,ref} \quad (3.42)$$

Therefore:

$$\eta_{ref} = \Phi_s - \Phi_l - E_{eq,ref} \quad (3.43)$$

Where:

$$E_{eq,ref} = E_{eq,0} - \frac{RT}{nF} \ln \frac{C_{R,ref}}{C_{O,ref}} \quad (3.44)$$

It should be noted that the terms reference activity of reducing and oxidizing species concentrations $C_{R,ref}$ and $C_{O,ref}$, are the initial concentrations of the species. Thus, with these equations, modelling of air-electrode and zinc-electrode reactions can be modeled with the following steps.

Firstly, in the zinc-electrode electrochemical reactions are simplified into conversion between Zn and ZnO since the reaction is only assumed to be in the

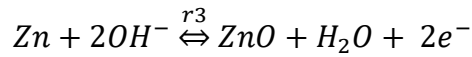
dissolving-depositing species scope. To model this depositing-dissolving species rates on the surface can be represented as:

$$\frac{\partial c_{s,i}}{\partial t} = \sum_m \frac{v_{i,m} i_{loc,m}}{n_m F} \quad (3.45)$$

Where:

- $c_{s,i}$ is the concentration of dissolving-depositing species at the surface.
- m , is the indicator of the respective electrochemical reaction.
- i , is the indicator of the respective species. In this case these are Zn and ZnO since these are the dissolving-depositing species. >
- n , is the number of electrons involved in the electrochemical reactions.
- $v_{i,m}$ is the stoichiometric coefficient for the respective species.

Recall, reaction r_3 from the Equation (3.5 :



Therefore, the surface concentrations for Zn-ZnO dissolving depositing can be expressed as:

$$\frac{\partial c_{Zn}}{\partial t} = -\frac{1}{2F} \alpha i_{loc,3} \quad (3.46)$$

$$\frac{\partial c_{ZnO}}{\partial t} = \frac{1}{2F} \alpha i_{loc,3} \quad (3.47)$$

In porous electrodes, porosity varies and the effective conductivity changes during battery operation. Therefore, in addition to the Bruggeman correction, effective conductivity and diffusivity values should be expressed as:

$$\sigma_{l,eff} = \frac{\varepsilon_e F^2}{RT} (D_{K^+} + D_{OH^-}) c_l \quad (3.48)$$

Where:

- $\sigma_{l,eff}$ is the effective electrolyte conductivity.
- D_{K^+} and D_{OH^-} are the diffusivity coefficients for electrolyte ions.
- c_l is the electrolyte salt concentration.
- ε_e is the porosity of the porous electrode or the separator.

This effective electrolyte constant is applied to Zn-electrode domain. The porosity changes within Zn electrode due to dissolving depositing species is calculated via:

$$\Delta\varepsilon_e = (c_{Zn} - c_{Zn,0}) \frac{MW_{Zn}}{\rho_{Zn}} + (c_{ZnO} - c_{ZnO,0}) \frac{MW_{ZnO}}{\rho_{ZnO}} \quad (3.49)$$

On the zinc-electrode side, since Zn-ZnO dissolution deposition occurs and these components have significant differences in terms of conductivity, greatly affecting the conductivity of the porous electrode regarding to the electrochemical reactions and the concentrations. The effective solid particles conductivity can be written as:

$$\Delta\varepsilon_e = (c_{Zn} - c_{Zn,0}) \frac{MW_{Zn}}{\rho_{Zn}} + (c_{ZnO} - c_{ZnO,0}) \frac{MW_{ZnO}}{\rho_{ZnO}} \quad (3.50)$$

Where the terms m and $\sigma_{s,k}$ represents mass fraction and electrical conductivities of the solid particles within the porous electrode. Mass fraction of these particles Zn and ZnO is calculated simply by the following equations Equation (3.51 and (3.52:

$$m_{Zn} = \frac{c_{Zn}MW_{Zn}}{c_{Zn}MW_{Zn} + c_{ZnO}MW_{ZnO}} \quad (3.51)$$

$$m_{ZnO} = \frac{c_{ZnO}MW_{ZnO}}{c_{Zn}MW_{Zn} + c_{ZnO}MW_{ZnO}} \quad (3.52)$$

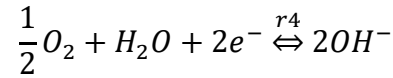
With a time-dependent concentration relation, concentration change of these particles can be monitored, while the change in effective conductivity change on the porous zinc electrode can also be examined. Additionally, the electrochemical reactions of these dissolving-depositing species can now be integrated into concentration-dependent Butler-Volmer kinetics to investigate the electrochemical reactions on the zinc-electrode side and calculating the overpotential. Final form can be expressed as in the Equation (3.53 below:

$$i_{loc,3} = i_{0,3} \left(\exp\left(\frac{C_{OH^-}}{C_{OH_{ref}^-}}\right)^2 \frac{C_{Zn}}{C_{Zn_{ref}}} \exp\left(\frac{\alpha_{a3}F\eta_3}{RT}\right) - \left(\frac{C_{ZnO}}{C_{ZnO,ref}}\right) \exp\left(-\frac{\alpha_{c3}F\eta_3}{RT}\right) \right) \quad (3.53)$$

Where the number 3 represents the redox reactions on the zinc electrode, r_3 where electrochemical dissolution and deposition of Zn-ZnO occurs. The exponential numbers on the reducing and oxidizing species terms comes from the stoichiometric coefficients of the respective species within the electrochemical reaction (Comsol 2020; Sunu and Bennion 1980b; Deiss, Holzer, and Haas 2002; Mao and White 1992).

For the air-electrode side, the electrochemical reactions ORR and OER during the discharge and charge reactions are heavily dependent on the mass transfer of oxygen from

the GDL boundary to the CL domain. Therefore, these reactions also have concentration dependent kinetics, and multi-physics coupling is required to model an electrochemical reaction where constant diffusion of oxygen through and throughout the GDL and CL is assumed. In this section, only the electrochemical part of the air electrode will be discussed while the mass transfer part will be explained in the “Mass Transport Phenomena in the Model” section. Recalling the reaction r_4 in Equation (3.6) the electrochemical reactions on the air electrode side can be written as:



$$i_{loc,4} = i_{0,4} \left(\exp\left(\frac{C_{OH^-}}{C_{OH^-ref}}\right)^2 \exp\left(\frac{\alpha_{a4}F\eta_4}{RT}\right) - \left(\frac{C_{O_2}}{C_{O_2,init}}\right)^{\frac{1}{2}} \left(\exp\left(-\frac{\alpha_{c4}F\eta_4}{RT}\right)\right) \right) \quad (3.54)$$

Within this porous electrode reaction, particle-based area is implemented while the particle types are accepted as spheres. Therefore, the active specific surface area equation, Equation (3.32) for air electrode and zinc electrode can be written as:

$$A_{v,4} = \frac{3\varepsilon_s}{r_p} \quad (3.55)$$

Unlike the zinc-electrode, the concentrations within the air-electrode reaction are not just the CL related and a closed system, but also related to the open system where O_2 from ambient air is diffused. Therefore, porous electrode coupling will be applied to this CL domain and information will be given in the following part of this thesis. Eventually, both reactions on the anode and cathode sides overpotentials can be calculated from:

$$\eta = \Phi_s - \Phi_l - E_{eq} \quad (3.56)$$

3.2.1.2 Mass Transport Phenomena in the Model

As mentioned in the previous parts, the air-electrode of the ZAB is an open system where constant contact with the ambient air exists through the GDL boundary. Therefore, mass transfer physics within this boundary should be conducted besides mass transfer and electrochemical reaction coupling in the porous CL domain of the air electrode. For the electrolyte medium where the solvent's concentration is equal to or greater than 90 mol%, solute species are accepted as dilute species. Therefore, within the electrolyte, the properties of the solvent dominate. In this way, the electrolyte's properties can be accepted as the solvent's properties. A general mass transport equation is used to model the mass transport of these diluted species. General form is summarized at the Equation (3.57 below:

$$\frac{\partial c_i}{\partial t} = \nabla \cdot J_i + u \cdot \nabla c_i + R_i \quad (3.57)$$

Within the equation, c_i represents the species concentration. The species concentration is related to the diffusive mass flux vector J_i , mass averaged velocity due to convection, and the reaction rate if there are any reactions occurring. Since the model does not involve convection and migration mass transport, the only considerable aspects of this mass balance model are molecular diffusion and porous electrode reaction. The diffusive mass flux vector J_i can be written as:

$$J_i = -D \nabla c \quad (3.58)$$

The model focuses on the O₂ mass transport, and only diffusion is considered; the equation can be rewritten as:

$$\frac{\partial c_{O_2}}{\partial t} = -D \nabla c_{O_2} + R_{O_2} \quad (3.59)$$

Considering a 1-D geometry and cartesian coordinates, the gradient operator can be rewritten as:

$$\frac{\partial c_{O_2}}{\partial t} = -D \frac{\partial c_{O_2}}{\partial x} + R_{O_2} \quad (3.60)$$

The reaction term in this model is due to the porous electrode reaction where the electrochemical reactions ORR/OER occur. This term can be expressed further as:

$$N_j = -\frac{v_{jm} i_m}{n_m F} \quad (3.61)$$

Where the chemical species flux to the surface, N_j is related to the current density i_m with respect to reaction m which is the reaction index. n_m is the number of the electrons used in this porous electrode, and v_{jm} is the stoichiometric coefficient in electrochemical reaction while the term F is the Faraday constant. Due to the stoichiometry of the electrochemical reaction, flux of the chemical species can be related and coupled to the current density of the reaction. Therefore, for O₂, if we recall r_4 (ORR/OER) this Equation (3.61) can be rewritten as:

$$N_{O_2} = -\frac{v_{O_2,4} i_4}{n_4 F} \quad (3.62)$$

Therefore, the overall reaction can be rewritten as:

$$\frac{\partial c_{O_2}}{\partial t} = -D \frac{\partial c_{O_2}}{\partial x} - \frac{v_{O_2,4} i_4}{n_4 F} \quad (3.63)$$

Briefly, from mass transport to electrochemical reactions, these previous sections introduced the foundations of the model.

For solution of these equations, from electrochemical to mass transport, model definitions, parameters, variables, boundary, and initial conditions are required. These will be mentioned in the next section.

3.2.1.3 Model Definitions, Parameters, and Variables

Even though the foundations of the model are built, the governing equations require certain definitions, variables, and parameters for simulation. In this section, model definitions, parameters and variables will be discussed with their respective reasonings.

Firstly, general parameters that will be applied to overall battery regardless of the domain are required. Electrolyte properties that are required to be solved within electrochemical governing equations are applied to overall battery domains, including the molar mass of potassium ion, hydroxide ion, and their diffusivities respectively. Additionally, transport coefficient, electrical conductivity for the electrolyte is also defined. Besides the electrolyte salt, the molar mass and properties of the solvent which is water in this case are also defined. Lastly, the current density i_{app} applied to or collected from the battery is assumed to be constant and equal to 10 mA/cm². An experimental Zn-air battery was also fabricated for comparison of experimentally measured battery parameters with the modeling study. The surface area A_{cell} of the battery was 25 cm² and the current applied or drawn, I_{cell} was equal to 250 mA.

For the air electrode side, the required parameters are related to electrochemical and mass transport properties. This domain has contact with ambient air and an open

system. The solubility of oxygen in the electrolyte is also an important parameter. The solubility affects the oxygen concentration within the CL, it significantly alters the ORR/OER reaction mechanisms due to the concentration dependent electrochemical kinetics. Therefore, oxygen solubility in KOH reported in literature is used (Tromans 1998). Additionally, there is also a diffusive oxygen flux from the GDL boundary strongly affecting the reaction kinetics. Due to electrode's porous structure, the porosity of the air-electrode is also a model parameter. For electrochemical properties, the number of electrons contributing to ORR/OER, n_{CL} and $\alpha_{a,CL}$ are defined. Since the number of electrons contributing to the electrochemical reaction is equal to total of charge transfer coefficients, activity coefficient $\alpha_{c,CL}$ is also calculated. The activity coefficients are arbitrary numbers. However, $\alpha_{a,CL}$ value is selected from the literature value and usually this value varies between 0.5-1.5 (De Vidts and White, n.d.; Schröder and Krewer 2014).

The only important constraint is not exceeding the total number of electrons contributing to reactions. To calculate the overpotentials and the local current due to electrochemical reactions, equilibrium potentials are also defined as $E_{eq,pos}$. Besides the equilibrium potential, the exchange current density of the porous electrode is also defined to calculate concentration dependent Butler-Volmer kinetics. Additionally, initial concentrations of reactants such as OH^- due to the initial electrolyte salt concentration are also defined within this domain as reference. For electrical properties, the conductivity of CL is defined. Since the CL mostly contains Ni-mesh as a material for current conduction and the catalysts are embedded in it, conductivity of the Ni-mesh can be used.

For the separator domain, only the separator porosity and thickness are given. Electrolyte is assumed to fill the porosity of the separator.

For the zinc-electrode, electrochemical terms such as number of electrons in the electrochemical reaction n_{Zn} , transfer coefficients $\alpha_{a,Zn}$ and $\alpha_{c,Zn}$ are defined in the respective sections.

To recall, $\alpha_{a,Zn}$ is an arbitrary number that is selected within a range from the literature with a constraint that the total of $\alpha_{a,Zn}$ and $\alpha_{c,Zn}$ should not exceed the total number of electrons in the reactions, n_{Zn} . One of the main differences in zinc-electrode from the air-electrode is the dissolving-depositing species, Zn/ZnO .

Therefore, recalling the dissolution deposition equations, surface concentrations of these particles significantly affect the electrochemical reactions where concentrations of these particles also affect the reaction kinetics. Hence, the molecular weight,

conductivity, density of these Zn and ZnO particles are crucial and needed to be entered as fixed parameters.

To observe that if the battery modeled is consistent with the practical values, initial theoretical capacity of the battery is calculated. The theoretical specific capacity of ZAB is equal to 820 mAh g⁻¹ Zn (Niu et al. 2021).

In order to calculate theoretical specific capacity, the volume of the solids in zinc-electrode is determined. From this volume calculation, the weight of Zn material is evaluated to calculate the capacity. To calculate ZABs theoretical capacity, following equations, (3.64), (3.65), (3.66) were used:

$$cap_{Zn,theor} = scap_{Zn,theor} w_{zn} \quad (3.64)$$

Where $cap_{Zn,theor}$ is the theoretical capacity of the model which is calculated by the specific theoretical capacity and the weight of the Zn in the zinc electrode. To calculate Zn's weight in the battery, the following equations were used:

$$V_{zn} = A_{cell} L_{neg} (1 - \varepsilon_l) f_{Zn/ZnO} \quad (3.65)$$

$$w_{zn} = \rho_{zn} V_{zn} \quad (3.66)$$

As can be understood from the equations above, the term V_{zn} represents the volume of the zinc-electrode, which is calculated via the surface area of the cell, length of the zinc-electrode, the porosity of the zinc electrode and the fraction of Zn in the zinc electrode. Due to better battery performances, ZnO is also introduced in the zinc electrode. Therefore, a mixture of Zn & ZnO exists at the electrode (L. Li et al. 2022). The theoretical capacity of the battery modeled is 5532.8 mAh. Therefore, for the model's validation, the calculated practical capacity within simulations should not surpass this value.

The presented model is based on several assumptions for simplification of the complex processes:

- Isothermal operation condition is valid for entire battery.
- GDL domain is reduced to a boundary since the permeability of the layer is known as $6.78 \cdot 10^{-8} \text{ mol/m}^2\text{s}$ for oxygen mass transport.
- For electrochemical modelling at the zinc-electrode, the zincate formation and supersaturation are simplified into one overall reaction which is the Zn/ZnO dissolution/deposition.
- Due to battery's novel GDE design, porosity of CL does not change.
- CO₂ that is dissolved in GDE, cannot move through the separator to the zinc electrode domain.
- O₂ gas exhibits ideal gas behavior.
- Electrolyte diffusion properties does not change with respect to varying K⁺ and OH⁻ concentrations. Diffusion coefficients and transport properties remain constant.
- Any change in terms of the aqueous electrolyte in GDE domain, does not affect the electrode's porosity due to flooding.
- Parasitic reactions, HER in zinc-electrode is neglected.

All the mentioned parameters, variables and definitions will be summarized at Appendix A Table A.1 and Table A.2 with their respective references and/or reasonings.

3.2.1.4 Boundary, Initial Conditions

The boundary and initial conditions are implemented on several specific domains and points (boundaries). The Figure 3.2 illustrates these specific boundaries and domains to visualize mathematically implemented logic.



Figure 3.2 Points (boundaries) and domains for the ZAB model geometry.

The boundary and initial conditions are required to solve ODE and PDEs. In this section, these boundaries and initial conditions will be discussed. The Point-1 is the boundary of the zinc-electrode is grounded while the Point-4 is the boundary of the air-electrode is charge-discharge cycled with constant current density application or drawing. For this cycling, 10 mA/cm^2 of current density is applied to or withdrawn from this Point-4 during charging or discharging, respectively. The charging operation starts from the electric potential of 1.29 V and continues until 1.89 V . A rest period of 10 s takes place and then, the charging mode stops, and discharge starts. The discharge mode continues from 1.89 V to 1.29 V .

To solve electrochemical models with nonlinear electrode kinetics like Butler-Volmer, it is critical to assign suitable initial values to enhance the convergence of the solver. As a rule of thumb, if a boundary is grounded, the adjacent domains initial electric potentials should be equal to 0 V . While the current applied or drawn boundaries adjacent domain should have the electric potential of the overall electric potential as the initial potential. For electrolyte potentials in each domain, the common initial potential to assign is the equilibrium potential of the grounded electrode. Therefore, electrolyte potential is equal to equilibrium potential of the zinc electrode domain, $E_{eq,Zn}$ while the overall electric potential is at the air-electrode domain with $\Phi_s = E_{eq,Zn} + E_{eq,CL}$. Since at the

outermost parts of both electrodes, there are no electrolytes, these boundaries are also accepted as no electrical flux boundaries.

Since the zinc-electrode has dissolving/depositing species, the concentration changes of these Zn-ZnO species are crucial. Therefore, to solve concentration equation given at the physics section, initial concentrations for these species are set. For mass transport physics, no flux boundaries are determined. Within the model, only the zinc-electrode's Point-1 is the boundary where mass diffusion flux is zero. Therefore, for no flux boundaries it can be written as:

$$-n \cdot (-D\nabla c) = 0 \quad (3.67)$$

Where the term n is to denote normal of the boundary. On the other hand, the CL is in contact with the GDL boundary. There is a constant mass flux at this Point-4, and it is equal to permeability of the GDL which is equal to 10 barer. Additionally, the CL is connected to an open system with ambient air and diffusion of O_2 occurs in this domain. The initial concentration of O_2 inside the CL domain with respect to solubility in KOH is given. The concentration of the O_2 is also defined at the GDL boundary due to initial concentrations significance in the concentration gradient, which drives the mass transport.

The boundary and initial condition values mentioned are listed in Appendix A Table A.1. With these conditions, further iterations and solutions of the governing equations can be performed.

3.2.1.5 Meshing of the Model

For battery modeling, with respect to 1-D geometry, meshing is applied to 0.5 mm of Zinc electrode, 50 μm separator and 0.5 mm of GDE domains. Additionally, the battery of model's geometry contains a cross-sectional area of 25 cm^2 . With this information obtained from the battery of the model, meshing is applied. The applied mesh consists of 0.074 mm and 0.0105 mm maximum and minimum element sizes, respectively.

3.2.2 Aging Mechanisms Implemented in the Model

The model's foundations were set and described in the previous sections. As a bare model, charge-discharge cycling can be performed; however, the bare model does not have any aging mechanisms. Thus, there are no mechanisms that will degrade battery performance until a failure. This no aging mechanism simulation is represented in the Figure 3.3

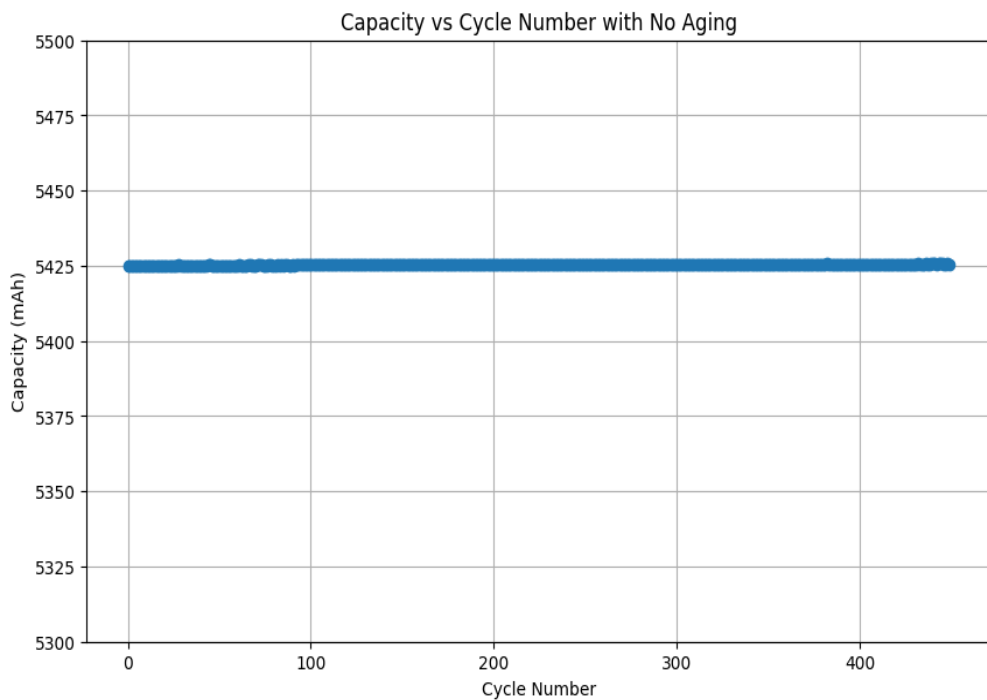


Figure 3.3 ZAB simulation with a model without aging mechanisms.

As seen in Figure 3.3 battery can easily be cycled up to 400 cycles with no aging and can handle further cycles with no capacity loss due to absence of any aging mechanisms. For realistic simulation of the battery, the model requires implementation of aging mechanisms. In this section, aging mechanisms implemented to the model will be described.

Additionally, each aging mechanisms will be investigated for further understanding of that respective mechanism's contribution to battery operation and aging.

After the separate examination of certain aging mechanisms, these degrading effects are coupled to model and simulate overall aging that can be encountered during practical battery operation. For this purpose, separate aging mechanisms on anode, cathode and overall battery are simulated.

3.2.2.1 Aging Mechanisms: Anode

As for the anode side aging mechanisms, dendrite growth and film resistance, and film resistance at the surface of the zinc-electrode are considered. These two mechanisms have significant effect on electrode and battery aging (K. Wang et al. 2015; Harting, Kunz, and Turek 2012; Pei, Wang, and Ma 2014; Zequan Zhao et al. 2019). Due to uneven deposition of zinc during the charging, formation of zinc dendrites occurs (Yi et al. 2018). The formation of zinc dendrites become a critical problem within alkaline solutions such as KOH. Zinc demonstrates significant electrochemical activity within these types of electrolytes and grows dendrites aggressively (Kundu et al. 2016; H. Pan et al. 2016; Bengoa et al. 2018). Zinc dendrites have sharp morphologies with high possibility of puncturing the separator of the ZAB. Due to separator damage, short circuit of the battery occurs and leads to battery failure (Cheng and Chen 2012; Y. Li and Dai 2014a). Besides these effects, an increase in the specific surface area of the electrode promotes zinc corrosion which leads to lower zinc utilization rate (K. Wang et al. 2015). Additionally, zinc dendrites with low adhesion have tendency to detach from the electrode surface, forming dead zones where zinc particles that cannot be recovered. Therefore, non-reversibility of these zinc particles/dendrites will result as a loss in the battery capacity (H. I. Kim and Shin 2015; Bae, Lee, and Kim 2019). This dendrite growth mechanism contains two main steps, initial nucleation and growth (Guoxing Li et al. 2018; K. Wang et al. 2015; Zequan Zhao et al. 2019). During the initial nucleation step, zinc ions near the electrode surface are migrated and absorbed at the nucleation sites due to electric field force (Guoxing Li et al. 2018). These ions gather electrons from the zinc electrode and the zinc atoms deposit at the nucleation sites. Once the overpotential on this electrode exceeds the energy barrier for zinc initial nucleation step, zinc atoms begin to diffuse freely on the electrode's surface. On this surface, zinc atoms are combined and forms the initial zinc core (McLarnon and Cairns 1991; Zhiming Zhao et al. 2019; Mitha

et al. 2018; Luan et al. 2019). At the growth step, zinc ions continue to build-up mostly on these initially formed zinc cores since at these core tips electrical field shows more strength when compared to free nucleation sites (Z. Wang et al. 2019; R. Zhang et al. 2017). As the cycling of the ZAB continues, zinc accumulation continues the electrode surface (Q. Zhang et al. 2020).

Due to zinc ion conversion into zinc metal, zinc ions concentration in the electrolyte becomes low which creates a significant concentration gradient (W. Lu et al. 2018; Xu et al. 2015). This gradient acts as a significant driving force which affects the electrode potential. Therefore, the deviation of electrode potential causes zinc ions to reduce more and accumulate more on these zinc core structures (Q. Yang et al. 2019).

For zinc dendrite growth, one of the most influential parameters is the exchange current density of the ZAB. At low current densities, less electrical field deviations on the surface of the electrode occurs in uniform deposition where sharp dendrite growths can be minimized and prevented. However, at the high current densities, zinc dendrites grow into sharp forms which can puncture the separator and significantly affect the batteries cyclability (Yangyang Liu et al. 2021; Ohmori et al. 1993; Zuo et al. 2021).

As mentioned in the previous parts, current density of the battery is fixed at 10 mA/cm². Even though it is known that at this current density dendrite height does not increase significantly due to uniform distribution of the zinc atoms (Zuo et al. 2021) in order to observe its effects on the battery capacity, dendrite formation was implemented to the model. Therefore, the relationship between the increasing dendrite height and capacity fade was observed. Additionally, to observe the growth in the respective current density is not limited, height of the dendrite continued to be increased until a point where the capacity fade of the battery is significant.

To implement this aging mechanism into the model, simple approach where the active specific surface area of the zinc-electrode changes is used. For this purpose, modification of the active specific surface area on the zinc-electrode is used and modified:

$$A_{v,Zn} = \frac{N_{shape} \epsilon_s}{d_p} \quad (3.68)$$

Reportedly at 10 mA/cm² current density, zinc dendrites show monolithic structures when growing (Pu et al. 2023). Therefore, during this aging mechanism's implementation, the shape factor N is changed to cylindrical from spherical, which $N_{shape} = 2$. For this purpose, particle size is also determined from the literature and given at the Appendix A Table A.1. To implement particle size growth on the electrode's specific surface area, the particle size parameter d_p is embedded in a variable where the d_p increases 5% within every cycles. The implementation can be formulated as:

$$d_{p,Zn,e} = d_{p,Zn} * 1.05^{cyc_{num}} \quad (3.69)$$

Where, $d_{p,e}$ is the effective particle size on the zinc-electrode that varies with respect to 5% dendritic growth per cycle, denoted by power of cycle number, cyc_{num} .

Film resistance is also one of the most important reasons that affect low zinc utilization which increases the gap between practical and theoretical energy density of batteries. In alkaline mediums such as KOH, zinc electrodes suffer from passivation (Zequan Zhao et al. 2019). The term passivation indicates that the product ZnO from the electrochemical reaction on the zinc electrode getting supersaturated in KOH. Therefore, this supersaturated ZnO particles deposit on the surface of the electrode.

These deposited particles create an insulating layer where the electrochemical reactions are hindered (Farmer and Webb 1972). This insulating film of ZnO, also hinders the discharge process and capacity loss occurs (Bockelmann et al. 2019; 2018). Hindering the discharge process also results as the batteries cycling capabilities since it also blocks the reverse conversion of metallic zinc (Zequan Zhao et al. 2019; Y. Wu et al. 2018). It has been reported that at low current densities the porous ZnO layers formed can avoid passivation until the hydroxide ions transfers through these porous ZnO layers hindered (M. Liu, Cook, and Yao 1981). Even though the current density in this model is not high and constant at 10 mA/cm², it is implemented to observe ZnO film's resistive effects on the electrochemical activity and electric potential. Within this aging mechanism model, for zinc-electrode passivation due to a film resistance caused by ZnO, film resistance physics are used:

$$\Delta\Phi_{s,film} = i_{tot}R_{film} \quad (3.70)$$

This equation represents a potential change in the electrode due to film resistance, R_{film} and it is related with the total current. R_{film} term can be calculated as:

$$R_{film} = \rho_{film}t_{film} \quad (3.71)$$

The film resistance equation is a variable that depends on the film thickness change, t_{film} . The thickness change is modeled by the resulting equation:

$$t_{film} = (if(t_{film} < 175 \text{ nm}, t_{film}1.08^{cyc_{num}}, t_{film,stop}) \quad (3.72)$$

Where the t_{film} is initially set at 1 nm and increases 8% by each charge-discharge cycle until it reaches the 100 nm of film thickness which is obtained from the literature.

Therefore, the overpotential equation Equation (3.56) can be rewritten as:

$$\eta = \Phi_s - \Delta\Phi_{s,film} - \Phi_l - E_{eq} \quad (3.73)$$

Where the surface resistance, R_{film} term is described with electrical resistivity ρ_{film} and the film thickness t_{film} of the material, which is ZnO in this case. From literature resistivity and film thickness of ZnO are obtained (Shariffudin et al. 2012) and given in the Appendix A Table A.1.

3.2.2.2 Aging Mechanisms: Gas Diffusion Electrode (GDE)

As mentioned previously, the air-electrode is one of the most important components of a ZAB, determining the capacity due to its sluggish ORR/OER kinetics. Therefore, catalytic activity within CL is a crucial part of the electrode which determines the performance and capacity of the ZAB. During the battery cycling operation, bifunctional catalyst material on the CL can lose its activity due to bifunctionality where two different reaction mechanisms ORR and OER takes place during cycling.

ORR and OER having significant differences in voltage during the discharge and charge processes limits the ZAB, resulting as the activity loss of the catalyst during the cycling process (Radenahmad et al. 2021). Additionally, during charge-discharge cycling of ZAB, catalysts at the air-electrode surface may get as a result of oxygen bubbles applying stress to the CL (K. Wang and Yu 2020).

In order to implement this aging mechanism to the model, model's electrochemical reaction kinetics on the air-electrode side is modified. Catalytic activity loss is associated with the anodic transfer coefficient within the ORR/OER electrochemical kinetics. To degrade air-electrode's electrochemical performance due to catalytic activity loss, the anodic transfer coefficient increased 1% to see how its aging effects on the ZAB. This aging mechanism can be formulated as:

$$\alpha_{a,CL,e} = \alpha_{a,CL} * 1.01^{cycnum} \quad (3.74)$$

Where $\alpha_{a,CL,e}$ represents the effective anodic transfer coefficient which varies within each cycle.

3.2.2.3 Aging Mechanism: Electrolyte

One of the most important aging mechanisms that effect the overall battery performance is the electrolyte loss. ZAB's are half open systems due to the openness of

air electrodes. This open-system where ambient air surrounds the air electrode affects the electrolyte due to evaporation. As a result of electrolyte evaporation, ionic conductivity and viscosity of the electrolyte decreases (X. Liu et al. 2021). Additionally, the carbonate formation due to the existence of CO₂ intake from the air may lead to loss of the electrolyte. Besides electrolyte leaks through the battery interfaces are also encountered during the battery operations due to gas evolution reactions occurring on the charge modes.

Therefore, to model this aging mechanism, the electrolyte concentration c_l is decreased within each cycle by 0.5% due to evaporation. The resulting aging mechanism can be formulated as:

$$c_l = c_l * 0.995^{cy_{cnum}} \quad (3.75)$$

After the stand-alone implementation and observation of these mentioned aging mechanisms, all of them are combined into one model to simulate more practical battery. With this way, results are aimed converge more to the practical values of ZABs.

In the following sections results of stand-alone and combined aging effects of these mechanisms will be discussed.

3.2.2.4 Effect of Temperature on Battery Degradation

Temperature has a significant influence on the battery performance by affecting electrochemical and physical processes within the cell. Increasing temperature promotes the electrochemical reaction kinetics and enhance batteries electrochemical properties. However, the increasing temperature will promote various aging mechanisms that will degrade the batteries performances (C.-X. Zhao et al. 2022; Vasile et al. 2016).

Aging mechanisms on the zinc-electrode side such as dendrite growth, ZnO passivation layer formation can be promoted if the temperature of the battery or surroundings is increased (Hosseini, Masoudi Soltani, and Li 2021).

For the air-electrode side of the battery, reaction kinetics may be hindered by the temperature due to O₂ diffusivity and solubility. Solubility of O₂ decreases when the temperature is increased. Therefore, increasing temperatures will hinder air-electrode's ORR since it depends on the O₂ oxygen diffusion and concentration (Vasile et al. 2016).

Additionally, high temperatures may lead to increased electrolyte evaporation, therefore the loss of ionic conductive material. Hence the ionic gradient across the battery may get corrupted and the battery fails (Hosseini, Masoudi Soltani, and Li 2021).

Even though temperature has various effects on the battery especially promoting the aging mechanisms, the temperature change of the battery is neglected, and system is accepted as isothermal for this thesis. This approach is selected since the current densities during the charge-discharge cycles are low enough and there are no thermal runaway reactions like Li-ion batteries (C.-X. Zhao et al. 2022). Hence the thermal effects are neglected, and the system is assumed to be isothermal.

CHAPTER 4

RESULTS AND DISCUSSION

During the simulation of the ZAB, each stand-alone aging mechanisms were firstly investigated within different cases. After the stand-alone observation of aging mechanisms these are combined into a single model to evaluate simultaneous effects on the aging of the battery. For this purpose, 10 mA/cm² current density charge-discharge cycling to the battery is applied. Charging process conducted until the battery reaches to 1.89 V. When the voltage reached to 1.89 V, battery enters 10 seconds resting period and starts the discharge mode. Discharge mode continues until it reaches to 1.29 V and begins the 10 seconds resting period. The cycling operation continued until the battery's failure or losses significant amount of capacity.

4.1 Zinc Dendrite Growth Simulation Results

Firstly, for the zinc electrode domain, the anodic dendrite growth is simulated. As can be seen from the Figure 4.1 which demonstrates the relationship between the capacity during the charge discharge cycles.

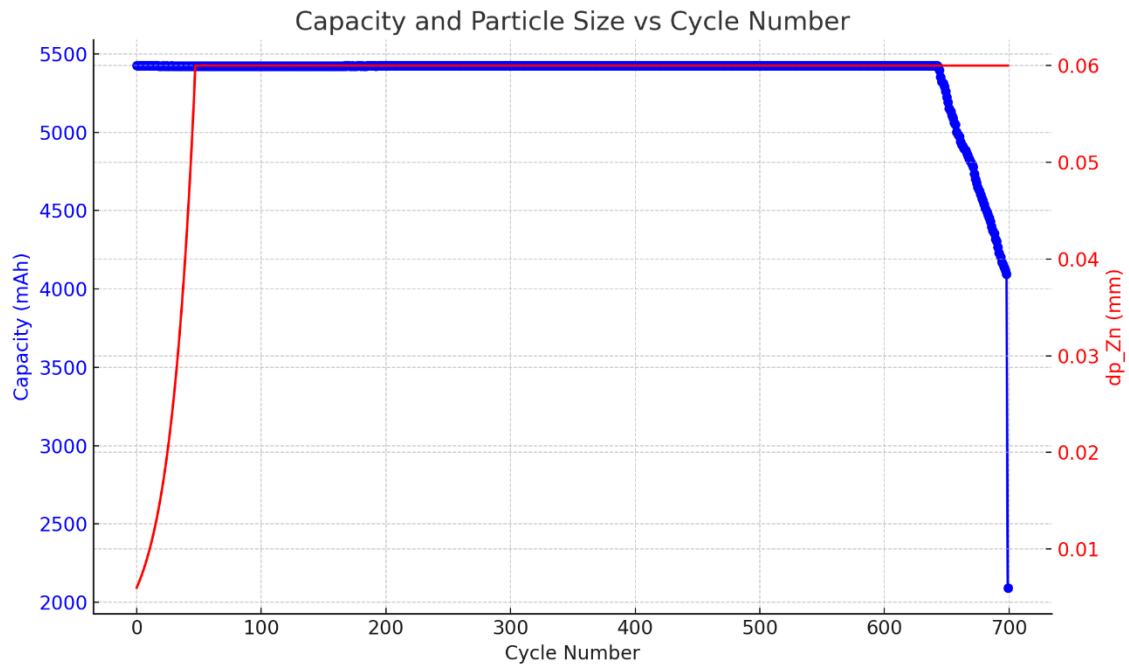


Figure 4.1 ZAB with stand-alone anodic dendrite growth aging.

Recalling Equation (3.68) for the representation of active specific surface area which depends on the particle size of the electrode. The particle size variation with respect to cycles can be referred from the respective Equation (3.69). As can be seen from these equations below, the active specific surface area decreases with an increase in the particle size in the zinc-electrode. The particle size is increased by 5% in each cycle to simulate the dendritic growth until it reaches the experimentally observed dendrite size, 60 microns. Therefore, the dendritic growth which leads to particle size increase in the electrode resulted as aging mechanism that reduces the capacity of the battery due to this active specific surface area reduction.

The dendritic growth's effect remains negligible for almost 650 cycles, after the 650th cycle, the capacity loss become significant, and it leads to large capacity drop at the 700th cycle which corresponds to 2000 mAh. This behavior is typically observed when the effect of particle size is isolated from other phenomena.

4.2 Anode Film Resistance Simulation Results

For film resistance at the zinc electrode domain due to ZnO deposition at the electrode surface, the change in the capacity was simulated by incorporating Equations (3.70), (3.71), and (3.72) respectively in the Zinc electrode domain. The simulation result can be seen in Figure 4.2. While the resistivity of ZnO is assumed to be constant during the simulation the film thickness of the ZnO deposited at the zinc electrode is increased from 1 nm to 175 nm which is the experimentally obtained limit for the ZnO films.

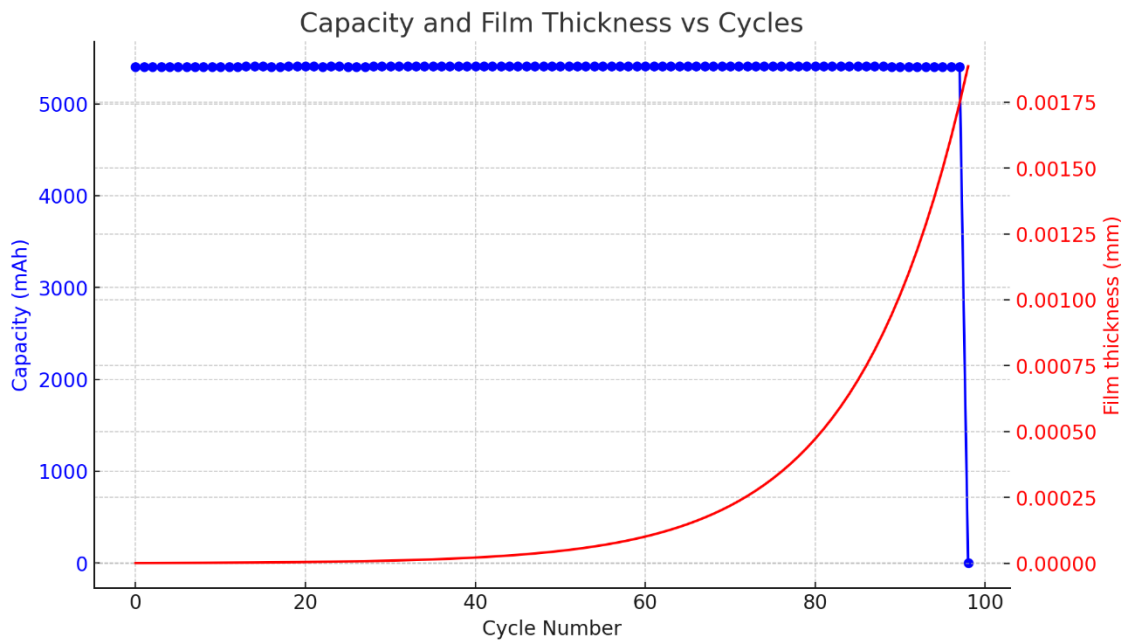


Figure 4.2 ZAB with stand-alone anodic film resistance aging.

For capacity loss examination, the same methodology is followed; capacity within each cycle is compared to each other. As can be seen from the graphics behavior, Battery's capacity did not change within almost 100 cycles where it drops significantly at the 90th cycle. After the film thickness reaches to 175 nm, battery begins to fail due to increased film resistance. This film resistance reduces the overpotential due to potential drop in the battery. Therefore, the resistivity of the deposited ZnO film will result as the battery's fail.

4.3 GDE Catalyst Layer (CL) Activity Loss Simulation Results

One of the most important aging mechanisms for ZABs is the catalytic activity degradation within CL domain. Based on Eq 3.73, the activity of the catalyst in that domain was reduced by increasing anodic transfer coefficient 1% in each charge-discharge cycle simulating approximately observed degradation rate in experimental lab-scale batteries. As seen in Figure Figure 4.3, the capacity values within 60 cycles can be seen for a ZAB with stand-alone GDE's CL catalytic activity loss. From the first cycle to 30th cycle, the capacity of GDE remains almost the same. After the 30th cycle, battery capacity suffers from a large drop and the battery fails when the cut-off potential is reached.

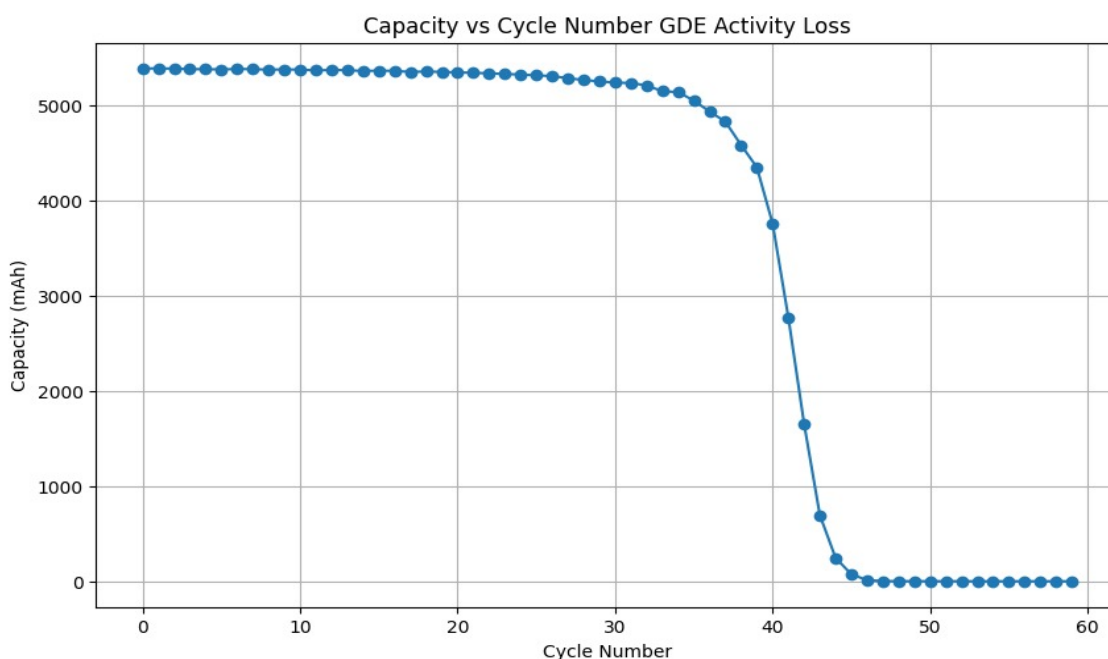


Figure 4.3 ZAB with stand-alone GDE aging due to catalytic activity loss.

The battery loses the significant part of the capacity due to the change of anodic transfer coefficient of the CL's active material. The increase in the anodic transfer coefficient of the battery result in imbalance between the anodic and cathodic activity within the battery. The increased anodic transfer coefficient determines the electrochemical reactions in favor of the anodic side activity; therefore, this will result as the decreased cathodic activity since the overall number of electrons in the electrochemical reactions is equal to total of anodic and cathodic transfer coefficients. This relation can be recalled from the Equation (3.34). Hence, the battery fails when the anodic activity is dominant and the activity of cathodic side that conducts ORR/OER degrades significantly.

4.4 Electrolyte Loss Simulation Results

Another important aging mechanisms that is responsible for low cycle life for AZBs is the loss of electrolyte due to several factors: Due to the openness of air electrodes electrolyte may evaporate. On addition, insoluble carbonate formation due to CO₂ intake from the air may lead to electrolyte loss. It is also common to have leaks through electrode interfaces due to gas evolution during charging. To simulate all these phenomena, the electrolyte concentration c_l is decreased by 0.5% each cycle. Figure 4.4 show the capacity fade of ZAB with overall electrolyte loss with increasing cycle count. As can be seen from the graphic, from 0th to 350th cycle, battery suffers from constant capacity downtrend due to electrolyte loss.

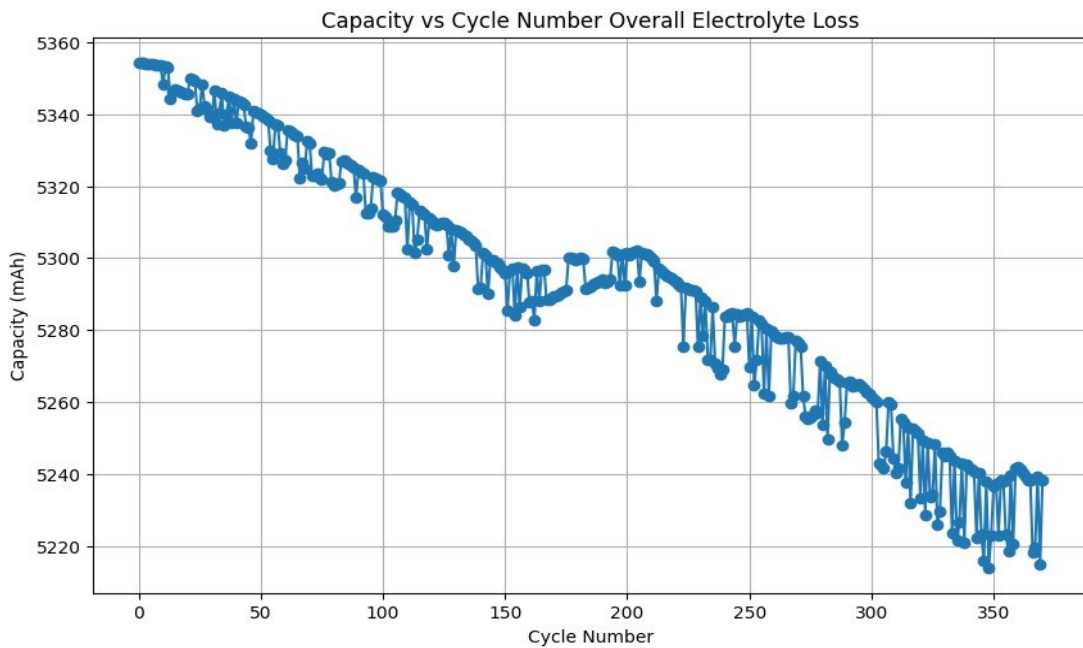


Figure 4.4 Stand-alone aging due to electrolyte loss on the overall battery.

Electrolyte loss significantly affects the battery since the ionic transport is conducted by the existence of this media. The electrolyte concentration decreases over this charge-discharge cycling simulation within 350 cycles. As can be seen from the Figure 4.4 above, the decreasing concentration of the electrolyte results as the degraded battery capacity. Degradation of the battery capacity is caused by the loss of conductive media that can handle the ionic transport through the battery which maintains the ionic gradient.

4.5 Combined Aging Simulation Results

In a zinc-air battery, all these individual aging mechanisms occur simultaneously. It is necessary to combine and simulate these mechanisms together in a single ZAB. Therefore, these mechanisms were combined into one model to simulate capacity fade of a ZAB in near real-life conditions. It is expected that simultaneous aging mechanisms will lead to a shorter cycle count with the same cut-off potential is used.

As can be seen from in Figure 4.5, the capacity remains stable until the 20th cycle. The capacity fade increases between the 20th and 42nd cycles and the cut-off potential of

1.29 V is reached. Simulation is conducted for 1500 hours, and it solved within 2 min 51 s.

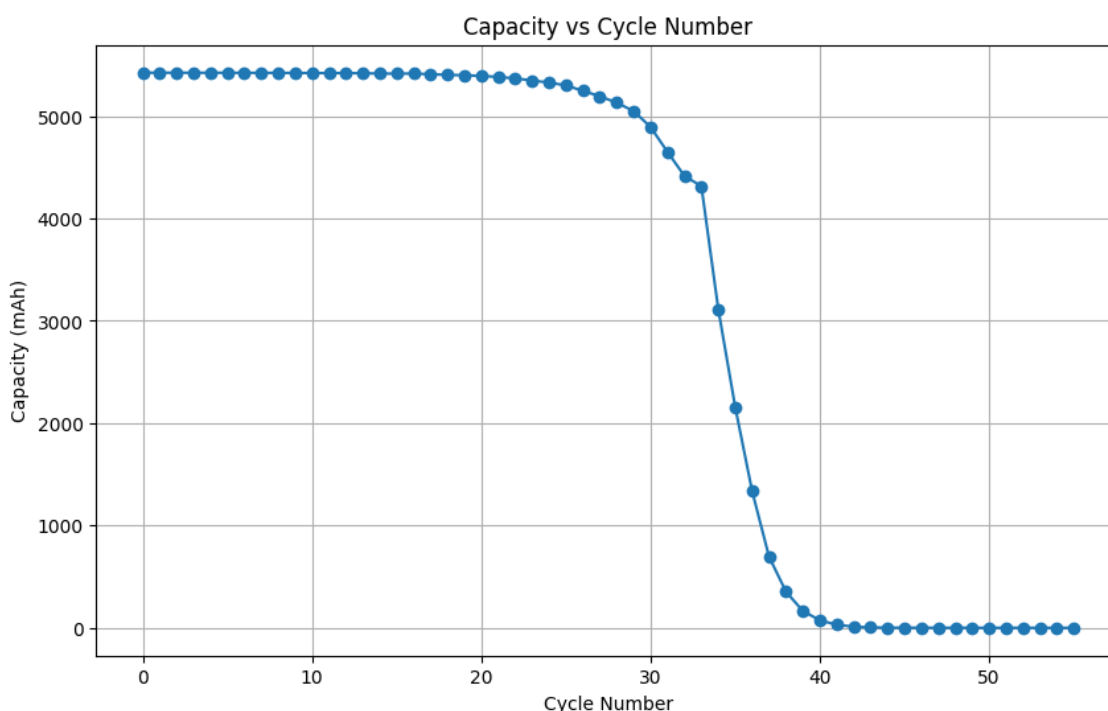


Figure 4.5 Complete ZAB simulation with aging mechanisms combined.

Combined aging mechanisms results in the capacity fade at the battery much shorter when compared to stand-alone aging mechanisms. Dendritic growth and film resistance on the zinc electrode domain, CL activity loss on the CL domain and the electrolyte loss at the overall battery domain degrades the battery significantly. The cycling performance of the battery is close to the stand-alone GDE CL aging mechanism. This result is expected since the battery's performance determining step is the GDE due to sluggish ORR/OER kinetics. The shorter lifespan of the combined aging mechanism when compared to GDE's CL aging mechanism is a result of the anode and electrolyte aging mechanisms combined within the model.

During the combined aging, the mechanisms have significant effects that can degrade the battery extremely during the cycling operation. As can be seen from the Figure 4.6, the "Electric Potential (V) vs Time (h)" graph, timespan of each cycle narrows down due to aging.

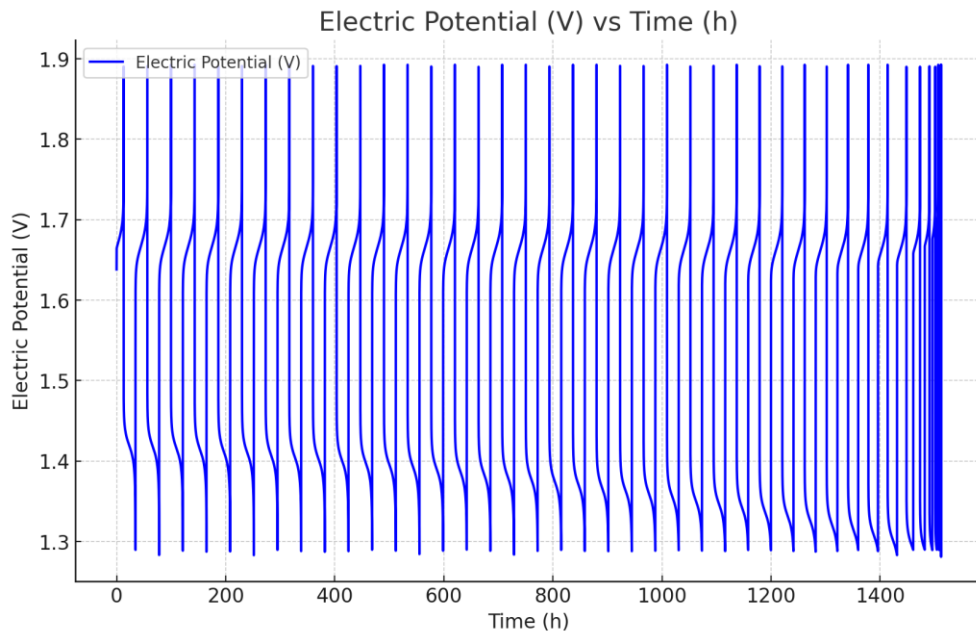


Figure 4.6 Electric potential vs Time for combined aging mechanisms in a ZAB.

The narrowed cycling timespans are investigated within specific cycles starting from the 1st cycle to the 41st cycle to observe the aging effects better. As can be seen from the Figure 4.7, the cycling time decreases within increasing cycle numbers due to shorter discharge and charge times at the battery.

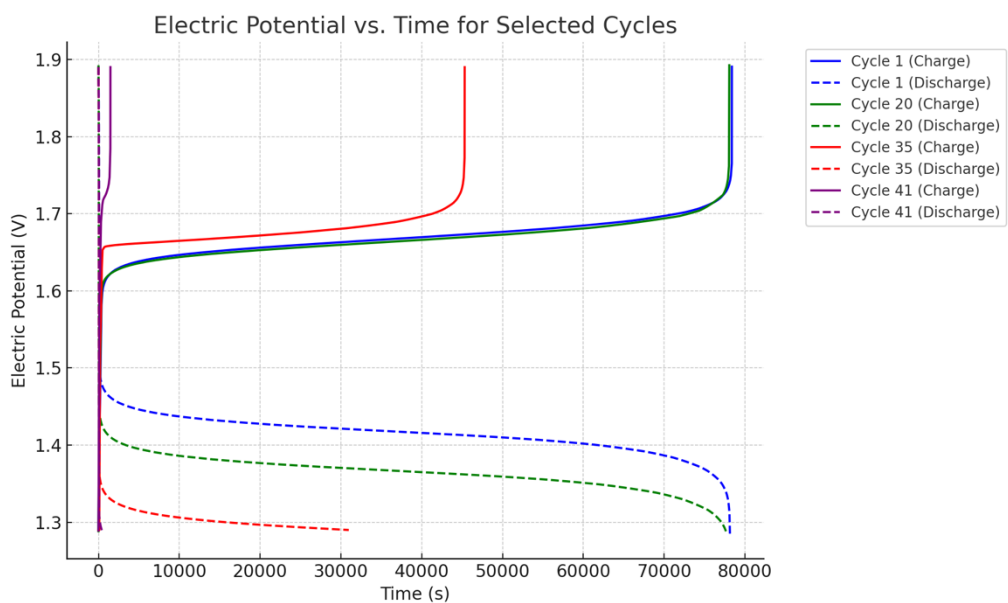


Figure 4.7 Specific charge discharge curves for the combined aging model.

After creating a holistic model with combined effects, for the justification of the model's motivation, simulations with different current densities, 1 mA/cm^2 and 5 mA/cm^2 were applied during the charge-discharge cycling to observe current density effects on the charge-discharge behaviors. Therefore, parametric study required during the experimental procedures can be shortened significantly with model's utilization.

The 1 mA/cm^2 current density simulation was conducted for the 11,370 hours and solved it in 10 min 4 s. The results were post-processed similar to 10 mA/cm^2 base case of combined aging where specific charge-discharge cycles were investigated to observe aging effects within the battery in detail. The obtained result can be seen at the Figure 4.8 below.

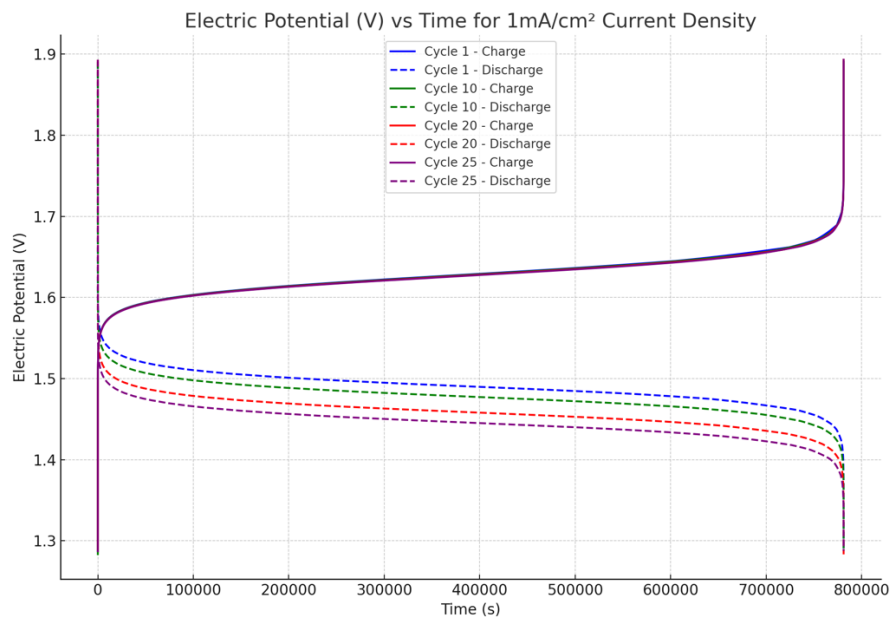


Figure 4.8 Specific charge discharge cycle mode behavior for 1 mA/cm^2 .

The 5 mA/cm^2 current density simulation was conducted for the 3430 hours and solved it in 3 min 17 s. The results were post-processed similar to 10 mA/cm^2 base case of combined aging where specific charge-discharge cycles were investigated to observe

aging effects within the battery in detail. The obtained result can be seen at the Figure 4.9.

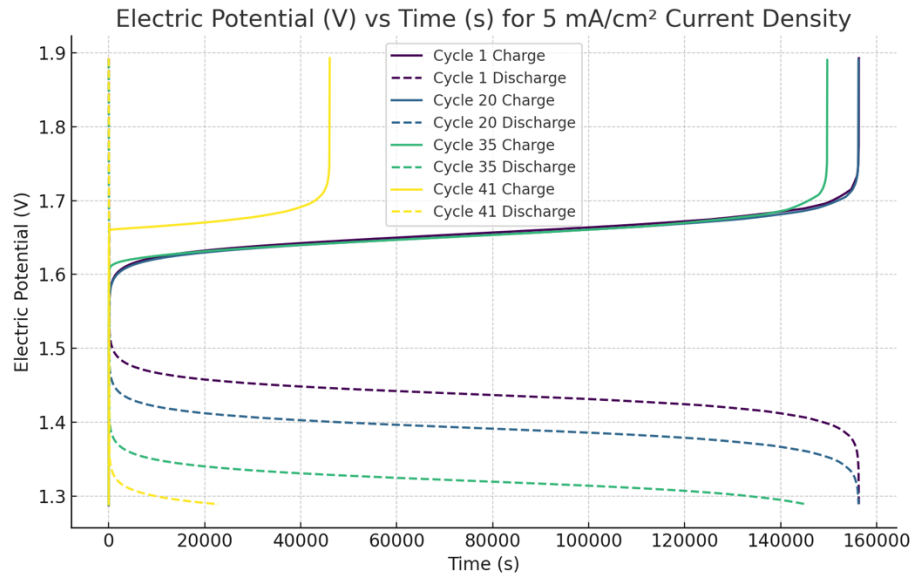


Figure 4.9 Specific charge discharge cycle mode behavior for 5 mA/cm²

As can be seen from the parametric study results, the model simulated different cases of current densities 1 mA/cm², 5 mA/cm² and 10 mA/cm². The model solved simulations for 11,337, 3430 and 1500 hours respectively for each case within 16 min 33 s total computation time. Each parametric study case lasted 26, 43 and 48 cycles respectively. Applying lower current densities resulted in higher cycle times and battery lives with lower cycle numbers, therefore proving the model’s feasibility and adaptability with the expected cycling behaviors. These results justify the model’s motivation where cost and time savings are aimed with the model’s utilization. If within experimental conditions, for a single ZAB, to conduct these cycling experiments would have taken 678 days. On the model side, the computational time took only 16 min 33 s which significantly lowered the time required to obtain results and investigate.

Additionally, simulations for optimizing the battery can be also conducted with utilization of this model, however due to limited time for the thesis, optimization works are not conducted. Besides, utilization of this 1-D model as a foundation and developing 2-D or 3-D models will be much more effective in terms of optimization purposes.

CHAPTER 5

CONCLUSION

In this study, the electrochemical behavior of zinc-air batteries was simulated. The motivation of the work was to demonstrate the feasibility of a simple 1-D zinc-air battery model to investigate the effect of various phenomena on the battery capacity and charge-discharge cycle count.

To model reactions kinetics and mass transport phenomena happening in anode, cathode and electrolyte during charging and discharging of a conventional zinc-air battery, Finite Element Analysis (FEA) method was chosen. A 1-D geometrical model based on an experimentally fabricated zinc-air battery was constructed. Although there are considerable number of physical and chemical phenomena occurs during battery operation, as described in detail in the previous chapters, only four important and easy-to-implement aging mechanisms were incorporated into the constructed battery model.

It has been shown that the model predicted the expected capacity fading behavior successfully with similar results reported studies in literature when the average particle size of particles in anode is increased at a certain rate with increasing cycle count.

The anodic film resistance simulations conducted as the stand-alone aging mechanism showed expected results. With increasing film thickness of ZnO the increased film resistance leads to potential drop and affected the overpotential significantly, which results to battery's depletion. Hence the ZnO deposition and film resistance with increasing cycle count at the anode demonstrated decent and similar results when compared to literature.

GDE of the ZAB determines the performance significantly. Therefore, aging mechanisms inside the GDE's CL domain is a critical phenomenon for cycle life of a ZAB. As can be seen from the results, CL aging has the shortest cycle-life when compared to other stand-alone aging mechanisms. Results showed the expected capacity fading behavior when compared to literature. Cycle life that is shorter than other stand-alone aging mechanisms, and longer than the combined aging mechanisms can also prove this accuracy.

The electrolyte loss aging stand-alone simulations showed the relationship between the capacity and the electrolyte concentration. As expected, the decreasing concentration of the ion transport conducting media resulted as the faded capacity within the ZAB.

These phenomena were later incorporated in a single model, to realistically simulate the battery operation. It has been shown that the final model incorporating these aging mechanisms successfully predicted the electrochemical performance of a zinc-air battery, including capacity fading with cycle count. Additionally, to emphasize the model's motivation that aims to save significant amount of time and costs, parametric study where different current densities such as 1 mA/cm² and 5 mA/cm² 10 mA/cm² were conducted. The model solved simulations for 11,337, 3430 and 1500 hours (678 days in total) respectively for each case within 16 min 33 s total of computation time. These results justify the model's motivation where cost and time savings are aimed with the model's utilization.

This study has demonstrated that a simple 1-D model incorporating electrochemical reactions and mass transport processes can successfully predict battery charge and discharge behavior, reducing both the cost of fabrication of a large number of batteries and the time required for charge-discharge cycling of those batteries to investigate the effect of various parameters. It should be noted that this work is by no means is a complete work, and it should on be seen as a starting point for more detailed 2-D and 3-D models incorporating all kinetics and transport related phenomena.

REFERENCES

- Abdul-Zehra, Hassan. 1999. "FUEL CELLS AND BATTERIES PRIMARY BATTERIES." https://www.uobabylon.edu.iq/eprints/paper_4_22941_736.pdf.
- Abraham, K. M., and Z. Jiang. 1996. "A Polymer Electrolyte-Based Rechargeable Lithium/Oxygen Battery." *Journal of The Electrochemical Society* 143 (1): 1–5. <https://doi.org/10.1149/1.1836378/XML>.
- Adelhelm, Philipp, Pascal Hartmann, Conrad L Bender, Martin Busche, Christine Eufinger, and Juergen Janek. 2015. "From Lithium to Sodium: Cell Chemistry of Room Temperature Sodium–Air and Sodium–Sulfur Batteries." *Beilstein Journal of Nanotechnology* 6:1016–55. <https://doi.org/10.3762/bjnano.6.105>.
- Ahmadi, Leila, Steven B. Young, Michael Fowler, Roydon A. Fraser, and Mohammad Ahmadi Achachlouei. 2017. "A Cascaded Life Cycle: Reuse of Electric Vehicle Lithium-Ion Battery Packs in Energy Storage Systems." *International Journal of Life Cycle Assessment* 22 (1): 111–24. <https://doi.org/10.1007/s11367-015-0959-7>.
- Alotto, Piergiorgio, Massimo Guarnieri, and Federico Moro. 2014. "Redox Flow Batteries for the Storage of Renewable Energy: A Review." *Renewable and Sustainable Energy Reviews* 29 (January):325–35. <https://doi.org/10.1016/J.RSER.2013.08.001>.
- Amendola, Steven. 2010. "Electrically Rechargeable, Metal-Air Battery Systems and Methods," no. 43 (July).
- Amunátegui, B., A. Ibáñez, M. Sierra, and M. Pérez. 2018. "Electrochemical Energy Storage for Renewable Energy Integration: Zinc-Air Flow Batteries." *Journal of Applied Electrochemistry* 48 (6): 627–37. <https://doi.org/10.1007/s10800-017-1133-7>.
- Ang, Jia Ming, Yonghua Du, Boon Ying Tay, Chenyang Zhao, Junhua Kong, Ludger Paul Stubbs, and Xuehong Lu. 2016. "One-Pot Synthesis of Fe(III)-Polydopamine Complex Nanospheres: Morphological Evolution, Mechanism, and Application of the Carbonized Hybrid Nanospheres in Catalysis and Zn-Air Battery." *Langmuir* 32 (36): 9265–75. <https://doi.org/https://doi.org/10.1021/acs.langmuir.6b02331>.
- Arora, Pankaj, and Zhengming Zhang. 2004. "Battery Separators." *Chemical Reviews* 104 (10): 4419–62.

- Auinat, Mahmud, and Yair Ein-Eli. 2005. "Enhanced Inhibition of Zinc Corrosion in Alkaline Solutions Containing Carboxylic Acid Modified PEG." *Journal of The Electrochemical Society* 152 (6): A1158. <https://doi.org/10.1149/1.1900963>.
- Avraamides, J., G. Senanayake, and R. Clegg. 2006. "Sulfur Dioxide Leaching of Spent Zinc–Carbon-Battery Scrap." *Journal of Power Sources* 159 (2): 1488–93. <https://doi.org/10.1016/J.JPOWSOUR.2005.11.081>.
- Bae, Suyeon, Jaehyuk Lee, and Dae Sik Kim. 2019. "The Effect of Cr³⁺-Functionalized Additive in Zinc-Bromine Flow Battery." *Journal of Power Sources* 413 (February):167–73. <https://doi.org/10.1016/J.JPOWSOUR.2018.12.038>.
- Bansal, Rishabh, Prajwal Menon, and R. C. Sharma. 2020. "Silicon–Air Batteries: Progress, Applications and Challenges." *SN Applied Sciences* 2 (6): 1–17. <https://doi.org/10.1007/S42452-020-2925-7/TABLES/1>.
- Bard, Allen J, Larry R Faulkner, and Henry S White. 2022. *Electrochemical Methods: Fundamentals and Applications*. John Wiley & Sons.
- Barkholtz, Heather M., and Di Jia Liu. 2017. "Advancements in Rationally Designed PGM-Free Fuel Cell Catalysts Derived from Metal–Organic Frameworks." *Materials Horizons* 4 (1): 20–37. <https://doi.org/10.1039/C6MH00344C>.
- Bathe, Klaus-Jurgen. 1996. "Finite Element Procedures Prentice-Hall." *New Jersey* 1037 (1).
- Behrouzifar, Morteza, Ebrahim Siami Araghi, and Ali Emami Meibodi. 2019. "OPEC Behavior: The Volume of Oil Reserves Announced." *Energy Policy* 127 (April):500–522. <https://doi.org/10.1016/j.enpol.2018.10.037>.
- Bengoa, Leandro N., Paola Pary, Pablo R. Seré, M. Susana Conconi, and Walter A. Egli. 2018. "Dendritic Zinc Growth in Acid Electrolyte: Effect of the PH." *Journal of Materials Engineering and Performance* 27 (3): 1103–8. <https://doi.org/10.1007/S11665-018-3139-7/METRICS>.
- Berverskog, B., and I. Puigdomenech. 1997. "Revised Pourbaix Diagrams for Zinc at 25–300 °C." *Corrosion Science* 39 (1): 107–14. [https://doi.org/10.1016/S0010-938X\(97\)89246-3](https://doi.org/10.1016/S0010-938X(97)89246-3).
- Bi, Xuanxuan, Rongyue Wang, Yifei Yuan, Dongzhou Zhang, Tao Zhang, Lu Ma, Tianpin Wu, Reza Shahbazian-Yassar, Khalil Amine, and Jun Lu. 2020. "From Sodium-Oxygen to Sodium-Air Battery: Enabled by Sodium Peroxide Dihydrate." *Nano Letters* 20 (6): 4681–86. <https://doi.org/https://doi.org/10.1021/acs.nanolett.0c01670>.

- Blurton, Keith F., and Anthony F. Sammells. 1979. "Metal/Air Batteries: Their Status and Potential — a Review." *Journal of Power Sources* 4 (4): 263–79. [https://doi.org/10.1016/0378-7753\(79\)80001-4](https://doi.org/10.1016/0378-7753(79)80001-4).
- Bockelmann, Marina, Maik Becker, Laurens Reining, Ulrich Kunz, and Thomas Turek. 2018. "Passivation of Zinc Anodes in Alkaline Electrolyte: Part I. Determination of the Starting Point of Passive Film Formation." *Journal of The Electrochemical Society* 165 (13): A3048–55. <https://doi.org/10.1149/2.0331813JES>.
- Bockelmann, Marina, Maik Becker, Laurens Reining, Ulrich Kunz, and Thomas Turek. 2019. "Passivation of Zinc Anodes in Alkaline Electrolyte: Part II. Influence of Operation Parameters." *Journal of The Electrochemical Society* 166 (6): A1132–39. <https://doi.org/10.1149/2.0791906JES>.
- Cao, R, J Lee, M Liu, and J Cho. 2011. "Adv. Energy Mater. 2012, 2, 816–829; d) G. Wu, KL More, CM Johnston, P. Zelenay." *Science* 332:443–47.
- Caramia, Vincenzo, and Benedetto Bozzini. 2014. "Materials Science Aspects of Zinc-Air Batteries: A Review." *Materials for Renewable and Sustainable Energy* 3 (2). <https://doi.org/10.1007/s40243-014-0028-3>.
- Chawla, N. 2019. "Recent Advances in Air-Battery Chemistries." *Materials Today Chemistry* 12 (June):324–31. <https://doi.org/10.1016/J.MTCHEM.2019.03.006>.
- Chen, Peng, Keyi Zhang, Dejian Tang, Weilin Liu, Fancheng Meng, Qiuwei Huang, and Jiehua Liu. 2020. "Recent Progress in Electrolytes for Zn–Air Batteries." *Frontiers in Chemistry* 8 (May):541689. <https://doi.org/https://doi.org/10.3389/fchem.2020.00372>.
- Chen, Zhu, Ja Yeon Choi, Haijiang Wang, Hui Li, and Zhongwei Chen. 2011. "Highly Durable and Active Non-Precious Air Cathode Catalyst for Zinc Air Battery." *Journal of Power Sources* 196 (7): 3673–77. <https://doi.org/10.1016/J.JPOWSOUR.2010.12.047>.
- Chen, Zhu, Aiping Yu, Raihan Ahmed, Haijiang Wang, Hui Li, and Zhongwei Chen. 2012. "Manganese Dioxide Nanotube and Nitrogen-Doped Carbon Nanotube Based Composite Bifunctional Catalyst for Rechargeable Zinc-Air Battery." *Electrochimica Acta* 69:295–300.
- Cheng, Fangyi, and Jun Chen. 2012. "Metal–Air Batteries: From Oxygen Reduction Electrochemistry to Cathode Catalysts." *Chemical Society Reviews* 41 (6): 2172–92. <https://doi.org/10.1039/c1cs15228a>.

- Choi, Sangjin, Hyung Wan Do, Dana Jin, Sungsoon Kim, Jeongyoub Lee, Aloysius Soon, Joocho Moon, and Wooyoung Shim. 2021. "Revisiting the Role of the Triple-Phase Boundary in Promoting the Oxygen Reduction Reaction in Aluminum–Air Batteries." *Advanced Functional Materials* 31 (41). <https://doi.org/10.1002/adfm.202101720>.
- Clark, Simon, Arnulf Latz, and Birger Horstmann. 2017. "Rational Development of Neutral Aqueous Electrolytes for Zinc–Air Batteries." *ChemSusChem* 10 (23): 4735–47. <https://doi.org/10.1002/CSSC.201701468>.
- Clark, Simon, Arnulf Latz, and Birger Horstmann. 2018a. "A Review of Model-Based Design Tools for Metal-Air Batteries." *Batteries*. MDPI. <https://doi.org/10.3390/batteries4010005>.
- Clark, Simon, Arnulf Latz, and Birger Horstmann. 2018b. "A Review of Model-Based Design Tools for Metal-Air Batteries." *Batteries 2018, Vol. 4, Page 5 4* (1): 5. <https://doi.org/10.3390/BATTERIES4010005>.
- Comsol. 2020. "The Battery Design Module User's Guide." www.comsol.com/blogs.
- Copeaand, Richard C, and Yury Podrazhanskyb. 1999. "The Art of Battery Charging."
- Davidson, Alistair J., Steve P. Binks, and Johannes Gediga. 2016. "Lead Industry Life Cycle Studies: Environmental Impact and Life Cycle Assessment of Lead Battery and Architectural Sheet Production." *International Journal of Life Cycle Assessment* 21 (11): 1624–36. <https://doi.org/10.1007/S11367-015-1021-5/TABLES/5>.
- Dehghani-Saniij, A. R., E. Tharumalingam, M. B. Dusseault, and R. Fraser. 2019. "Study of Energy Storage Systems and Environmental Challenges of Batteries." *Renewable and Sustainable Energy Reviews*. Elsevier Ltd. <https://doi.org/10.1016/j.rser.2019.01.023>.
- Deiss, Erich, F. Holzer, and O. Haas. 2002. "Modeling of an Electrically Rechargeable Alkaline Zn–Air Battery." *Electrochimica Acta* 47 (25): 3995–4010. [https://doi.org/10.1016/S0013-4686\(02\)00316-X](https://doi.org/10.1016/S0013-4686(02)00316-X).
- Dell, RM, Rand D A J, Pual Connor, and Robert (Bob) D Bailey. 2001. *Understanding Batteries*. RSC.
- Deng, Haokun, and Katerina E Aifantis. 2023. "Applications of Lithium Batteries." *Rechargeable Ion Batteries: Materials, Design and Applications of Li-Ion Cells and Beyond*, 83–103.

- Devyatkina, T. I., Yu L. Gun'ko, and M. G. Mikhalenko. 2001. "Development of Ways to Diminish Corrosion of Zinc Electrode." *Russian Journal of Applied Chemistry* 74 (7): 1122–25. <https://doi.org/10.1023/A:1013058615990/METRICS>.
- Dhar, S. K., S. R. Ovshinsky, P. R. Gifford, D. A. Corrigan, M. A. Fetcenko, and S. Venkatesan. 1997. "Nickel/Metal Hydride Technology for Consumer and Electric Vehicle Batteries—a Review and up-Date." *Journal of Power Sources* 65 (1–2): 1–7. [https://doi.org/10.1016/S0378-7753\(96\)02599-2](https://doi.org/10.1016/S0378-7753(96)02599-2).
- Dincer, Ibrahim. 2018. *Comprehensive Energy Systems*. Edited by Ibrahim Dincer. 1st ed. Elsevier.
- Ding, Yulong, Yongliang Li, Chuanping Liu, and Ze Sun. 2015. "Solar Electrical Energy Storage." In *Solar Energy Storage*, 7–25. Elsevier Inc. <https://doi.org/10.1016/B978-0-12-409540-3.00002-5>.
- Dong, Youzhen, and Jinghong Li. 2014. "Tungsten Nitride Nanocrystals on Nitrogen-Doped Carbon Black as Efficient Electrocatalysts for Oxygen Reduction Reactions." *Chemical Communications* 51 (3): 572–75. <https://doi.org/10.1039/C4CC07137A>.
- Du, Guojun, Xiaogang Liu, Yun Zong, T. S. Andy Hor, Aishui Yu, and Zhaolin Liu. 2013. "Co₃O₄ Nanoparticle-Modified MnO₂ Nanotube Bifunctional Oxygen Cathode Catalysts for Rechargeable Zinc–Air Batteries." *Nanoscale* 5 (11): 4657–61. <https://doi.org/10.1039/C3NR00300K>.
- Ellis, Brian L., and Linda F. Nazar. 2012. "Sodium and Sodium-Ion Energy Storage Batteries." *Current Opinion in Solid State and Materials Science* 16 (4): 168–77. <https://doi.org/10.1016/J.COSSMS.2012.04.002>.
- El-Sayed, Abdel Rahman, Hossnia S. Mohran, and Hany M. Abd El-Lateef. 2012. "Corrosion Study of Zinc, Nickel, and Zinc-Nickel Alloys in Alkaline Solutions by Tafel Plot and Impedance Techniques." *Metallurgical and Materials Transactions A: Physical Metallurgy and Materials Science* 43 (2): 619–32. <https://doi.org/10.1007/S11661-011-0908-4>.
- Enterria, Marina, Marine Reynaud, Juan Ignacio Paredes, Lidia Medinilla, Reza Younesi, and Nagore Ortiz-Vitoriano. 2022. "Driving the Sodium-Oxygen Battery Chemistry towards the Efficient Formation of Discharge Products: The Importance of Sodium Superoxide Quantification." *Journal of Energy Chemistry* 68 (May): 709–20. <https://doi.org/10.1016/j.jechem.2021.12.014>.
- Eom, Seung Wook, Chang Woo Lee, Mun Soo Yun, and Yang Kook Sun. 2006. "The Roles and Electrochemical Characterizations of Activated Carbon in Zinc Air

- Battery Cathodes.” *Electrochimica Acta* 52 (4): 1592–95.
<https://doi.org/10.1016/J.ELECTACTA.2006.02.067>.
- Farmer, E. D., and A. H. Webb. 1972. “Zinc Passivation and the Effect of Mass Transfer in Flowing Electrolyte.” *Journal of Applied Electrochemistry* 2 (2): 123–36.
<https://doi.org/10.1007/BF00609128/METRICS>.
- Gao, Zhonghui, Huabin Sun, Lin Fu, Fangliang Ye, Yi Zhang, Wei Luo, and Yunhui Huang. 2018. “Promises, Challenges, and Recent Progress of Inorganic Solid-State Electrolytes for All-Solid-State Lithium Batteries.” *Advanced Materials* 30 (17): 1705702. <https://doi.org/10.1002/ADMA.201705702>.
- Gates Energy Products, Inc. 1998. *Rechargeable Batteries Applications Handbook*. EDN Series for Design Engineers. Boston: Butterworth-Heinemann.
<http://site.ebrary.com/id/10276443>.
- Genchi, Giuseppe, Maria Stefania Sinicropi, Graziantonio Lauria, Alessia Carocci, and Alessia Catalano. 2020. “The Effects of Cadmium Toxicity.” *International Journal of Environmental Research and Public Health* 2020, Vol. 17, Page 3782 17 (11): 3782. <https://doi.org/10.3390/IJERPH17113782>.
- Gilligan, G. E., and D. Qu. 2015. “Zinc-Air and Other Types of Metal-Air Batteries.” In *Advances in Batteries for Medium and Large-Scale Energy Storage: Types and Applications*, 441–61. Elsevier. <https://doi.org/10.1016/B978-1-78242-013-2.00012-1>.
- Goel, P., D. Dobhal, and R. C. Sharma. 2020. “Aluminum–Air Batteries: A Viability Review.” *Journal of Energy Storage*. Elsevier Ltd.
<https://doi.org/10.1016/j.est.2020.101287>.
- Goodenough, John B., and Youngsik Kim. 2010. “Challenges for Rechargeable Li Batteries.” *Chemistry of Materials* 22 (3): 587–603.
https://doi.org/10.1021/CM901452Z/ASSET/IMAGES/MEDIUM/CM-2009-01452Z_0019.GIF.
- Gu, Peng, Mingbo Zheng, Qunxing Zhao, Xiao Xiao, Huaiguo Xue, and Huan Pang. 2017. “Rechargeable Zinc–Air Batteries: A Promising Way to Green Energy.” *Journal of Materials Chemistry A* 5 (17): 7651–66.
<https://doi.org/10.1039/C7TA01693J>.
- Guidelli, Rolando, Richard G. Compton, Juan M. Feliu, Eliezer Gileadi, Jacek Lipkowski, Wolfgang Schmickler, and Sergio Trasatti. 2014. “Defining the Transfer Coefficient in Electrochemistry: An Assessment (IUPAC Technical Report).” In *Pure and*

- Applied Chemistry*, 86:245–58. Walter de Gruyter GmbH.
<https://doi.org/10.1515/pac-2014-5026>.
- Han, Guang, Yangfan Lu, Hongxing Jia, Zhao Ding, Liang Wu, Yue Shi, Guoyu Wang, et al. 2023. “Magnesium-Based Energy Materials: Progress, Challenges, and Perspectives.” *Journal of Magnesium and Alloys*. KeAi Communications Co. <https://doi.org/10.1016/j.jma.2023.08.009>.
- Hancock, Kathleen J., and Vlado Vivoda. 2014. “International Political Economy: A Field Born of the OPEC Crisis Returns to Its Energy Roots.” *Energy Research and Social Science* 1:206–16. <https://doi.org/10.1016/j.erss.2014.03.017>.
- Haradhan, and Kumar Mohajan. 2019. “The First Industrial Revolution: Creation of a New Global Human Era.” *Journal of Social Sciences and Humanities*. Vol. 5.
- Harting, Katrin, Ulrich Kunz, and Thomas Turek. 2012. “Zinc-Air Batteries: Prospects and Challenges for Future Improvement.” *Zeitschrift Fur Physikalische Chemie* 226 (2): 151–66. <https://doi.org/https://doi.org/10.1524/zpch.2012.0152>.
- Haverkort, Willem. 2024. *Electrolysers, Fuel Cells and Batteries: Analytical Modelling*. TU Delft OPEN Publishing. <https://doi.org/10.59490/tb.93>.
- Hoppmann, Joern, Jonas Volland, Tobias S. Schmidt, and Volker H. Hoffmann. 2014. “The Economic Viability of Battery Storage for Residential Solar Photovoltaic Systems – A Review and a Simulation Model.” *Renewable and Sustainable Energy Reviews* 39 (November):1101–18. <https://doi.org/10.1016/J.RSER.2014.07.068>.
- Horstmann, Birger, Timo Danner, and Wolfgang G. Bessler. 2013. “Precipitation in Aqueous Lithium–Oxygen Batteries: A Model-Based Analysis.” *Energy & Environmental Science* 6 (4): 1299–1314. <https://doi.org/10.1039/C3EE24299D>.
- Hosseini, Soraya, Salman Masoudi Soltani, and Yuan Yao Li. 2021. “Current Status and Technical Challenges of Electrolytes in Zinc–Air Batteries: An in-Depth Review.” *Chemical Engineering Journal* 408 (March):127241. <https://doi.org/10.1016/J.CEJ.2020.127241>.
- Huang, Xu, Qingwei Dai, Qing Xiang, Na Yang, Gaopeng Zhang, Ao Shen, and Wanming Li. 2024. “Microstructure Design of Advanced Magnesium-Air Battery Anodes.” *Journal of Magnesium and Alloys*. KeAi Communications Co. <https://doi.org/10.1016/j.jma.2024.01.025>.
- Jörissen, Ludwig. 2006. “Bifunctional Oxygen/Air Electrodes.” *Journal of Power Sources* 155 (1): 23–32. <https://doi.org/10.1016/J.JPOWSOUR.2005.07.038>.

- Kalair, Anam, Naeem Abas, Muhammad Shoaib Saleem, Ali Raza Kalair, and Nasrullah Khan. 2021. "Role of Energy Storage Systems in Energy Transition from Fossil Fuels to Renewables." *Energy Storage* 3 (1). <https://doi.org/10.1002/est2.135>.
- Kaldor, Mary, Terry Lynn Karl, and Yahia Said. 2007. *Oil Wars*.
- Khan, N., E. Kalair, N. Abas, A. R. Kalair, and A. Kalair. 2019. "Energy Transition from Molecules to Atoms and Photons." *Engineering Science and Technology, an International Journal*. Elsevier B.V. <https://doi.org/10.1016/j.jestech.2018.05.002>.
- Kim, Hansu, Goojin Jeong, Young Ukg Kim, Jae Hun Kim, Cheol Min Park, and Hun Joon Sohn. 2013. "Metallic Anodes for next Generation Secondary Batteries." *Chemical Society Reviews* 42 (23): 9011–34. <https://doi.org/10.1039/C3CS60177C>.
- Kim, Hong Ik, and Heon Cheol Shin. 2015. "SnO Additive for Dendritic Growth Suppression of Electrolytic Zinc." *Journal of Alloys and Compounds* 645 (October):7–10. <https://doi.org/10.1016/J.JALLCOM.2015.04.208>.
- Kolhekar, Snehal, Michael Nyce, and Sanjoy Banerjee. 2021. "Reducing Zinc Redistribution and Extending Cycle Life Via Electrochemical Synthesis of Zinc/Zinc Oxide Anodes in Rechargeable Alkaline Batteries." *Journal of The Electrochemical Society* 168 (4): 040514. <https://doi.org/10.1149/1945-7111/ABF21C>.
- Kritzer, Peter, and John Anthony Cook. 2007. "Nonwovens as Separators for Alkaline Batteries." *Journal of The Electrochemical Society* 154 (5): A481. <https://doi.org/10.1149/1.2711064/XML>.
- Kundu, Dipan, Brian D. Adams, Victor Duffort, Shahrzad Hosseini Vajargah, and Linda F. Nazar. 2016. "A High-Capacity and Long-Life Aqueous Rechargeable Zinc Battery Using a Metal Oxide Intercalation Cathode." *Nature Energy* 2016 1:10 1 (10): 1–8. <https://doi.org/10.1038/nenergy.2016.119>.
- Lai, Wei, and Francesco Ciucci. 2011. "Mathematical Modeling of Porous Battery Electrodes—Revisit of Newman’s Model." *Electrochimica Acta* 56 (11): 4369–77.
- Lan, Chi-Jui, Tsung-Shune Chin, P Lin, and T Perng. 2006. "Zn-Al Alloy as a New Anode-Metal of a Zinc-Air Battery." *Journal of New Materials for Electrochemical Systems* 9 (January).
- Lee, Chang Woo, Seung Wook Eom, K. Sathiyarayanan, and Mun Soo Yun. 2006. "Preliminary Comparative Studies of Zinc and Zinc Oxide Electrodes on Corrosion Reaction and Reversible Reaction for Zinc/Air Fuel Cells." *Electrochimica Acta* 52 (4): 1588–91. <https://doi.org/10.1016/J.ELECTACTA.2006.02.063>.

- Lee, Jang Soo, Sun Tai Kim, Ruiguo Cao, Nam Soon Choi, Meilin Liu, Kyu Tae Lee, and Jaephil Cho. 2011a. "Metal–Air Batteries with High Energy Density: Li–Air versus Zn–Air." *Advanced Energy Materials* 1 (1): 34–50. <https://doi.org/10.1002/AENM.201000010>.
- Lee, Jang Soo, Sun Tai Kim, Ruiguo Cao, Nam Soon Choi, Meilin Liu, Kyu Tae Lee, and Jaephil Cho. 2011b. "Metal-Air Batteries with High Energy Density: Li-Air versus Zn-Air." *Advanced Energy Materials*. <https://doi.org/10.1002/aenm.201000010>.
- Lee, Sang Min, Yeon Joo Kim, Seung Wook Eom, Nam Soon Choi, Ki Won Kim, and Sung Baek Cho. 2013. "Improvement in Self-Discharge of Zn Anode by Applying Surface Modification for Zn–Air Batteries with High Energy Density." *Journal of Power Sources Complete* (227): 177–84. <https://doi.org/10.1016/J.JPOWSOUR.2012.11.046>.
- LeVeque, Randall J. 2007. *Finite Difference Methods for Ordinary and Partial Differential Equations: Steady-State and Time-Dependent Problems*. SIAM.
- Li, Chun Sheng, Yan Sun, Florian Gebert, and Shu Lei Chou. 2017a. "Current Progress on Rechargeable Magnesium–Air Battery." *Advanced Energy Materials* 7 (24). <https://doi.org/10.1002/aenm.201700869>.
- Li, Chun Sheng, Yan Sun, Florian Gebert, and Shu Lei Chou. 2017b. "Current Progress on Rechargeable Magnesium–Air Battery." *Advanced Energy Materials* 7 (24): 1700869. <https://doi.org/10.1002/AENM.201700869>.
- Li, G., M. A. Mezaal, R. Zhang, K. Zhang, and L. Lei. 2016. "Electrochemical Performance of MnO₂-Based Air Cathodes for Zinc-Air Batteries." *Fuel Cells* 16 (3): 395–400. <https://doi.org/10.1002/FUCE.201500077>.
- Li, Guoxing, Zhe Liu, Qingquan Huang, Yue Gao, Michael Regula, Daiwei Wang, Long Qing Chen, and Donghai Wang. 2018. "Stable Metal Battery Anodes Enabled by Polyethylenimine Sponge Hosts by Way of Electrokinetic Effects." *Nature Energy* 2018 3:12 3 (12): 1076–83. <https://doi.org/10.1038/s41560-018-0276-z>.
- Li, Liangyu, Yung Chak Anson Tsang, Diwen Xiao, Guoyin Zhu, Chunyi Zhi, and Qing Chen. 2022. "Phase-Transition Tailored Nanoporous Zinc Metal Electrodes for Rechargeable Alkaline Zinc-Nickel Oxide Hydroxide and Zinc-Air Batteries." *Nature Communications* 2022 13:1 13 (1): 1–9. <https://doi.org/10.1038/s41467-022-30616-w>.

- Li, Po Chieh, Yu Ju Chien, and Chi Chang Hu. 2016. "Novel Configuration of Bifunctional Air Electrodes for Rechargeable Zinc–Air Batteries." *Journal of Power Sources* 313 (May):37–45. <https://doi.org/10.1016/J.JPOWSOUR.2016.02.063>.
- Li, Po Chieh, Chi Chang Hu, Ting Hsuan You, and Po Yu Chen. 2017. "Development and Characterization of Bi-Functional Air Electrodes for Rechargeable Zinc-Air Batteries: Effects of Carbons." *Carbon* 111 (January):813–21. <https://doi.org/10.1016/J.CARBON.2016.10.057>.
- Li, Qingfeng, and Niels J. Bjerrum. 2002. "Aluminum as Anode for Energy Storage and Conversion: A Review." *Journal of Power Sources* 110 (1): 1–10. [https://doi.org/10.1016/S0378-7753\(01\)01014-X](https://doi.org/10.1016/S0378-7753(01)01014-X).
- Li, Tao, Meng Huang, Xue Bai, and Yan Xiang Wang. 2023. "Metal–Air Batteries: A Review on Current Status and Future Applications." *Progress in Natural Science: Materials International*. Chinese Materials Research Society. <https://doi.org/10.1016/j.pnsc.2023.05.007>.
- Li, Yanguang, and Hongjie Dai. 2014a. "Recent Advances in Zinc–Air Batteries." *Chemical Society Reviews* 43 (15): 5257–75. <https://doi.org/10.1039/C4CS00015C>.
- Li, Yanguang, and Hongjie Dai. 2014b. "Recent Advances in Zinc-Air Batteries." *Chemical Society Reviews*. Royal Society of Chemistry. <https://doi.org/10.1039/c4cs00015c>.
- Li, Yanguang, Ming Gong, Yongye Liang, Ju Feng, Ji Eun Kim, Hailiang Wang, Guosong Hong, Bo Zhang, and Hongjie Dai. 2013a. "Advanced Zinc-Air Batteries Based on High-Performance Hybrid Electrocatalysts." *Nature Communications* 2013 4:1 4 (1): 1–7. <https://doi.org/10.1038/ncomms2812>.
- Li, Yanguang, Ming Gong, Yongye Liang, Ju Feng, Ji Eun Kim, Hailiang Wang, Guosong Hong, Bo Zhang, and Hongjie Dai. 2013b. "Advanced Zinc-Air Batteries Based on High-Performance Hybrid Electrocatalysts." *Nature Communications* 4. <https://doi.org/10.1038/NCOMMS2812>.
- Li Zhu, Aaron, Haijiang Wang, Wei Qu, Xiaoxia Li, Zoe Jong, and Hui Li. 2010. "Low Temperature Pyrolyzed Cobalt Tetramethoxy Phenylporphyrin Catalyst and Its Applications as an Improved Catalyst for Metal Air Batteries." *Journal of Power Sources* 195 (17): 5587–95. <https://doi.org/10.1016/J.JPOWSOUR.2010.03.015>.
- Lin, Guangyu, and Trung Van Nguyen. 2005. "Effect of Thickness and Hydrophobic Polymer Content of the Gas Diffusion Layer on Electrode Flooding Level in a PEMFC." *Journal of the Electrochemical Society* 152 (10): A1942.

- Linden, David, and Thomas B Reddy. 2002. "Handbook of Batteries 3 Ed. Amerika Serikat: The Mcgraw-Hills Companies." Inc.
- Liu, Chang, Feng Li, Ma Lai-Peng, and Hui Mmg Cheng. 2010. "Advanced Materials for Energy Storage." *Advanced Materials* 22 (8): E28–62. <https://doi.org/10.1002/ADMA.200903328>.
- Liu, Ming-Biann, G. M. Cook, and N. P. Yao. 1981. "Passivation of Zinc Anodes in KOH Electrolytes." *Journal of The Electrochemical Society* 128 (8): 1663–68. <https://doi.org/10.1149/1.2127707/PDF>.
- Liu, Qingqing, Ruiting Liu, Chaohui He, Chenfeng Xia, Wei Guo, Zheng Long Xu, and Bao Yu Xia. 2022. "Advanced Polymer-Based Electrolytes in Zinc–Air Batteries." *EScience* 2 (5): 453–66. <https://doi.org/10.1016/J.ESCI.2022.08.004>.
- Liu, Xiaorui, Xiayue Fan, Bin Liu, Jia Ding, Yida Deng, Xiaopeng Han, Cheng Zhong, and Wenbin Hu. 2021. "Mapping the Design of Electrolyte Materials for Electrically Rechargeable Zinc–Air Batteries." *Advanced Materials*. John Wiley and Sons Inc. <https://doi.org/10.1002/adma.202006461>.
- Liu, Yangyang, Xieyu Xu, Matthew Sadd, Olesya O Kapitanova, Victor A Krivchenko, Jun Ban, Jialin Wang, et al. 2021. "Insight into the Critical Role of Exchange Current Density on Electrodeposition Behavior of Lithium Metal." *Advanced Science* 8 (5): 2003301. <https://doi.org/10.1002/ADVS.202003301>.
- Liu, Yanzhen, Zhanhong Yang, and Jie Yan. 2016. "Zinc Hydroxystannate as High Cycle Performance Negative Electrode Material for Zn/Ni Secondary Battery." *Journal of The Electrochemical Society* 163 (14): A3146–51. <https://doi.org/10.1149/2.1411614JES/XML>.
- Lu, Cian Tong, Zhi Yan Zhu, Sheng Wen Chen, Yu Ling Chang, and Kan Lin Hsueh. 2022. "Effects of Cell Design Parameters on Zinc-Air Battery Performance." *Batteries* 8 (8). <https://doi.org/10.3390/batteries8080092>.
- Lu, Wenjing, Congxin Xie, Huamin Zhang, and Xianfeng Li. 2018. "Inhibition of Zinc Dendrite Growth in Zinc-Based Batteries." *ChemSusChem* 11 (23): 3996–4006. <https://doi.org/10.1002/CSSC.201801657>.
- Lu, Yi Chun, David G. Kwabi, Koffi P.C. Yao, Jonathon R. Harding, Jigang Zhou, Lucia Zuin, and Yang Shao-Horn. 2011. "The Discharge Rate Capability of Rechargeable Li–O₂ Batteries." *Energy & Environmental Science* 4 (8): 2999–3007. <https://doi.org/10.1039/C1EE01500A>.

- Luan, Jingyi, Qi Zhang, Hongyan Yuan, Dan Sun, Zhiguang Peng, Yougen Tang, Xiaobo Ji, et al. 2019. "Plasma-Strengthened Lithiophilicity of Copper Oxide Nanosheet–Decorated Cu Foil for Stable Lithium Metal Anode." *Advanced Science* 6 (20): 1901433. <https://doi.org/10.1002/ADVS.201901433>.
- Mainar, Aroa R., Elena Iruin, Luis C. Colmenares, Andriy Kvasha, Iratxe de Meatza, Miguel Bengoechea, Olatz Leonet, Iker Boyano, Zhengcheng Zhang, and J. Alberto Blazquez. 2018. "An Overview of Progress in Electrolytes for Secondary Zinc-Air Batteries and Other Storage Systems Based on Zinc." *Journal of Energy Storage* 15 (February):304–28. <https://doi.org/10.1016/J.EST.2017.12.004>.
- Maja, Mario, Claudio Orecchia, Morela Strano, Paolo Tosco, and Marco Vanni. 2000. "Effect of Structure of the Electrical Performance of Gas Diffusion Electrodes for Metal Air Batteries." *Electrochimica Acta* 46 (2–3): 423–32. [https://doi.org/10.1016/S0013-4686\(00\)00601-0](https://doi.org/10.1016/S0013-4686(00)00601-0).
- Mao, Z., and R. E. White. 1992. "Mathematical Modeling of a Primary Zinc/Air Battery." *Journal of The Electrochemical Society* 139 (4): 1105–13. <https://doi.org/10.1149/1.2069348>.
- Martha De Souza, Cleusa Cristina Bueno, Denise Corrêa De Oliveira, and Jorge Alberto Soares Tenório. 2001. "Characterization of Used Alkaline Batteries Powder and Analysis of Zinc Recovery by Acid Leaching." *Journal of Power Sources* 103 (1): 120–26. [https://doi.org/10.1016/S0378-7753\(01\)00850-3](https://doi.org/10.1016/S0378-7753(01)00850-3).
- Masri, M. N., and A. A. Mohamad. 2009. "Effect of Adding Potassium Hydroxide to an Agar Binder for Use as the Anode in Zn–Air Batteries." *Corrosion Science* 51 (12): 3025–29. <https://doi.org/10.1016/J.CORSCI.2009.08.027>.
- Masri, Mohamad Najmi, Muhammad Firdaus Mohd Nazeri, Chai Yan Ng, and Ahmad Azmin Mohamad. 2015. "Tapioca Binder for Porous Zinc Anodes Electrode in Zinc–Air Batteries." *Journal of King Saud University - Engineering Sciences* 27 (2): 217–24. <https://doi.org/10.1016/J.JKSUES.2013.06.001>.
- Mauger, A., C. M. Julien, A. Paolella, M. Armand, and K. Zaghib. 2018. "A Comprehensive Review of Lithium Salts and beyond for Rechargeable Batteries: Progress and Perspectives." *Materials Science and Engineering: R: Reports* 134 (December):1–21. <https://doi.org/10.1016/J.MSER.2018.07.001>.
- May, Geoffrey J., Alistair Davidson, and Boris Monahov. 2018. "Lead Batteries for Utility Energy Storage: A Review." *Journal of Energy Storage* 15 (February):145–57. <https://doi.org/10.1016/J.EST.2017.11.008>.

- McCloskey, B. D., A. Speidel, R. Scheffler, D. C. Miller, V. Viswanathan, J. S. Hummelshøj, J. K. Nørskov, and A. C. Luntz. 2012. “Twin Problems of Interfacial Carbonate Formation in Nonaqueous Li-O₂ Batteries.” *Journal of Physical Chemistry Letters* 3 (8): 997–1001. https://doi.org/10.1021/JZ300243R/SUPPL_FILE/JZ300243R_SI_001.PDF.
- McLarnon, Frank R., and Elton J. Cairns. 1991. “The Secondary Alkaline Zinc Electrode.” *Journal of The Electrochemical Society* 138 (2): 645–56. <https://doi.org/10.1149/1.2085653/XML>.
- Mitha, Aly, Alireza Z. Yazdi, Moin Ahmed, and Pu Chen. 2018. “Surface Adsorption of Polyethylene Glycol to Suppress Dendrite Formation on Zinc Anodes in Rechargeable Aqueous Batteries.” *ChemElectroChem* 5 (17): 2409–18. <https://doi.org/10.1002/CELC.201800572>.
- MIT Electric Vehicle Team. 2008. “A Guide to Understanding Battery Specifications.”
- Mohamad, Ahmad. 2006. “Zn/Gelled 6M KOH/O₂ Zinc–Air Battery.” *Journal of Power Sources*, January. https://www.academia.edu/98786987/Zn_gelled_6M_KOH_O2_zinc_air_battery.
- Moukalled, Fadl, Luca Mangani, Marwan Darwish, F. Moukalled, L. Mangani, and M. Darwish. 2016. *The Finite Volume Method*. Springer.
- Müller, S., F. Holzer, and O. Haas. 1998. “Optimized Zinc Electrode for the Rechargeable Zinc-Air Battery.” *Journal of Applied Electrochemistry* 28 (9): 895–98. <https://doi.org/10.1023/A:1003464011815>.
- Nam, Gyutae, Joohyuk Park, Min Choi, Pilgun Oh, Suhyeon Park, Min Gyu Kim, Noejung Park, Jaephil Cho, and Jang Soo Lee. 2015. “Carbon-Coated Core-Shell Fe-Cu Nanoparticles as Highly Active and Durable Electrocatalysts for a Zn-Air Battery.” *ACS Nano* 9 (6): 6493–6501. <https://doi.org/10.1021/ACSNANO.5B02266>.
- Narayanan, S. R., G. K. Surya Prakash, A. Manohar, Bo Yang, S. Malkhandi, and Andrew Kindler. 2012. “Materials Challenges and Technical Approaches for Realizing Inexpensive and Robust Iron-Air Batteries for Large-Scale Energy Storage.” In *Solid State Ionics*, 216:105–9. <https://doi.org/10.1016/j.ssi.2011.12.002>.
- Neburchilov, Vladimir, Haijiang Wang, Jonathan J. Martin, Wei Qu, Vladimir Neburchilov, Haijiang Wang, Jonathan J. Martin, and Wei Qu. 2010. “A Review on Air Cathodes for Zinc-Air Fuel Cells.” *JPS* 195 (5): 1271–91. <https://doi.org/10.1016/J.JPOWSOUR.2009.08.100>.

- Neidhardt, Jonathan P., David N. Fronczek, Thomas Jahnke, Timo Danner, Birger Horstmann, and Wolfgang G. Bessler. 2012. "A Flexible Framework for Modeling Multiple Solid, Liquid and Gaseous Phases in Batteries and Fuel Cells." *Journal of The Electrochemical Society* 159 (9): A1528–42. <https://doi.org/10.1149/2.023209JES>.
- Newman, John, and Nitash P Balsara. 2021. *Electrochemical Systems*. John Wiley & Sons.
- Nguyen, Trung, and Robert F. Savinell. 2010. "Flow Batteries." *Electrochemical Society Interface* 19 (3): 54–56. <https://doi.org/10.1149/2.F06103IF/XML>.
- NHI. 2024a. "National Center for Biotechnology Information (2024). PubChem Compound Summary for CID 23994, Zinc." National Center for Biotechnology Information. June 2024. <https://pubchem.ncbi.nlm.nih.gov/compound/Zinc>.
- NHI. 2024b. "National Center for Biotechnology Information (2024). PubChem Compound Summary for CID 3007857." June 2024. <https://pubchem.ncbi.nlm.nih.gov/compound/Zinc-Oxide>.
- Niu, Yanli, Xue Teng, Shuaiqi Gong, Xuan Liu, Mingze Xu, and Zuofeng Chen. 2021. "Boosting Oxygen Electrocatalysis for Flexible Zinc-Air Batteries by Interfacing Iron Group Metals and Manganese Oxide in Porous Carbon Nanowires." *Energy Storage Materials* 43 (December):42–52. <https://doi.org/10.1016/J.ENSM.2021.08.037>.
- Ohmori, Yasuya, Kiyomichi Nakai, Hiroyuki Ohtsubo, Takahide Yagi, and Toshihiro Matsumoto. 1993. "Crystallographic Analysis of Electrodeposited Zinc Crystals on Fe Substrate." *ISIJ International* 33 (11): 1196–1201. <https://doi.org/10.2355/ISIJINTERNATIONAL.33.1196>.
- Olabi, Abdul Ghani, Enas Taha Sayed, Tabbi Wilberforce, Aisha Jamal, Abdul Hai Alami, Khaled Elsaid, Shek Mohammad Atiqure Rahman, Sheikh Khaleduzzaman Shah, and Mohammad Ali Abdelkareem. 2021. "Metal-Air Batteries—a Review." *Energies*. MDPI. <https://doi.org/10.3390/en14217373>.
- Othman, R., W. J. Basirun, A. H. Yahaya, and A. K. Arof. 2001. "Hydroponics Gel as a New Electrolyte Gelling Agent for Alkaline Zinc–Air Cells." *Journal of Power Sources* 103 (1): 34–41. [https://doi.org/10.1016/S0378-7753\(01\)00823-0](https://doi.org/10.1016/S0378-7753(01)00823-0).
- Pan, Huilin, Yuyan Shao, Pengfei Yan, Yingwen Cheng, Kee Sung Han, Zimin Nie, Chongmin Wang, et al. 2016. "Reversible Aqueous Zinc/Manganese Oxide Energy

- Storage from Conversion Reactions.” *Nature Energy* 2016 1:5 1 (5): 1–7.
<https://doi.org/10.1038/nenergy.2016.39>.
- Pan, Jing, Yang Yang Xu, Huan Yang, Zehua Dong, Hongfang Liu, and Bao Yu Xia. 2018. “Advanced Architectures and Relatives of Air Electrodes in Zn–Air Batteries.” *Advanced Science*. Wiley-VCH Verlag.
<https://doi.org/10.1002/advs.201700691>.
- Pan, Jing, Yang Yang Xu, Huan Yang, Zehua Dong, Hongfang Liu, Bao Yu Xia, J Pan, et al. 2018. “Advanced Architectures and Relatives of Air Electrodes in Zn–Air Batteries.” *Advanced Science* 5 (4): 1700691.
<https://doi.org/10.1002/ADVS.201700691>.
- Panero, S., C. Romoli, M. Achilli, E. Cardarelli, and B. Scrosati. 1995. “Impact of Household Batteries in Landfills.” *Journal of Power Sources* 57 (1–2): 9–12.
[https://doi.org/10.1016/0378-7753\(95\)02230-9](https://doi.org/10.1016/0378-7753(95)02230-9).
- Park, Sung Bum, and Yong il Park. 2012. “Fabrication of Gas Diffusion Layer (GDL) Containing Microporous Layer Using Flourinated Ethylene Propylene (FEP) for Proton Exchange Membrane Fuel Cell (PEMFC).” *International Journal of Precision Engineering and Manufacturing* 13 (7): 1145–51.
<https://doi.org/10.1007/S12541-012-0152-X/METRICS>.
- Pei, Pucheng, Keliang Wang, and Ze Ma. 2014. “Technologies for Extending Zinc–Air Battery’s Cyclelife: A Review.” *Applied Energy* 128 (September):315–24.
<https://doi.org/10.1016/j.apenergy.2014.04.095>.
- Peled, Emanuel, Diana Golodnitsky, Roni Hadar, Hadar Mazor, Meital Goor, and Larisa Burstein. 2013. “Challenges and Obstacles in the Development of Sodium–Air Batteries.” *Journal of Power Sources* 244 (December):771–76.
<https://doi.org/10.1016/J.JPOWSOUR.2013.01.177>.
- Pepper, Darrell W., and Juan C. Heinrich. 2017. “The Finite Element Method: Basic Concepts and Applications with MATLAB®, MAPLE, and COMSOL.” *The Finite Element Method: Basic Concepts and Applications with MATLAB, MAPLE, and COMSOL, Third Edition*, January, 1–628.
<https://doi.org/10.1201/9781315395104/FINITE-ELEMENT-METHOD-DARRELL-PEPPER-JUAN-HEINRICH>.
- Polivka, Barbara J. 2018. “ENVIRONMENTS & HEALTH The Great London Smog of 1952.” Vol. 118.

- Pop, Valer, H Bergveld, Dmitry Danilov, P Regtien, and Peter Notten. 2008. *Battery Management Systems: Accurate State-of-Charge Indication for Battery-Powered Applications*. *Journal of Vacuum Science & Technology B - J VAC SCI TECHNOL B*. Vol. 9. <https://doi.org/10.1007/978-1-4020-6945-1>.
- Prabu, Moni, Prakash Ramakrishnan, and Sangaraju Shanmugam. 2014. "CoMn₂O₄ Nanoparticles Anchored on Nitrogen-Doped Graphene Nanosheets as Bifunctional Electrocatalyst for Rechargeable Zinc–Air Battery." *Electrochemistry Communications* 41:59–63.
- Pu, Shengda D., Bingkun Hu, Zixuan Li, Yi Yuan, Chen Gong, Ziyang Ning, Chloe Chau, et al. 2023. "Decoupling, Quantifying, and Restoring Aging-Induced Zn-Anode Losses in Rechargeable Aqueous Zinc Batteries." *Joule* 7 (2): 366–79. <https://doi.org/10.1016/j.joule.2023.01.010>.
- Radenahmad, Nikdalila, Ramin Khezri, Ahmad Azmin Mohamad, Mai Thanh Nguyen, Tetsu Yonezawa, Anongnat Somwangthanaroj, and Soorathep Kheawhom. 2021. "A Durable Rechargeable Zinc-Air Battery via Self-Supported MnO_x-S Air Electrode." *Journal of Alloys and Compounds* 883 (November). <https://doi.org/10.1016/j.jallcom.2021.160935>.
- Rahman, Md. Arafat, Xiaojian Wang, and Cuie Wen. 2013. "High Energy Density Metal-Air Batteries: A Review." *Journal of The Electrochemical Society* 160 (10): A1759–71. <https://doi.org/10.1149/2.062310JES/XML>.
- Schoenmakere, Mieke De, and Jeroen Gillabel. 2017. *Circular by Design: Products in the Circular Economy*. Publications Office of the European Union.
- Schröder, Daniel, and Ulrike Krewer. 2014. "Model Based Quantification of Air-Composition Impact on Secondary Zinc Air Batteries." *Electrochimica Acta* 117 (January):541–53. <https://doi.org/10.1016/j.electacta.2013.11.116>.
- See, Dawn M., and Ralph E. White. 1997. "Temperature and Concentration Dependence of the Specific Conductivity of Concentrated Solutions of Potassium Hydroxide." *Journal of Chemical & Engineering Data* 42 (6): 1266–68. <https://doi.org/10.1021/JE970140X>.
- Shariffudin, S. S., M. Salina, S. H. Herman, and M. Rusop. 2012. "Effect of Film Thickness on Structural, Electrical, and Optical Properties of Sol-Gel Deposited Layer-by-Layer ZnO Nanoparticles." *Transactions on Electrical and Electronic Materials* 13 (2): 102–5. <https://doi.org/10.4313/TEEM.2012.13.2.102>.

- Shehu, Garba. n.d. “Two Ideas of Redox Reaction: Misconceptions and Their Challenges in Chemistry Education” 5 (1): 15–20. <https://doi.org/10.9790/7388-05111520>.
- Shen, Dongxu, Lifeng Wu, Guoqing Kang, Yong Guan, and Zhen Peng. 2021. “A Novel Online Method for Predicting the Remaining Useful Life of Lithium-Ion Batteries Considering Random Variable Discharge Current.” *Energy* 218 (March). <https://doi.org/10.1016/j.energy.2020.119490>.
- Shen, Yue, Dan Sun, Ling Yu, Wang Zhang, Yuanyuan Shang, Huiru Tang, Junfang Wu, Anyuan Cao, and Yunhui Huang. 2013. “A High-Capacity Lithium–Air Battery with Pd Modified Carbon Nanotube Sponge Cathode Working in Regular Air.” *Carbon* 62 (October):288–95. <https://doi.org/10.1016/J.CARBON.2013.05.066>.
- Shimizu, Youichi, Kenichi Uemura, Haruyuki Matsuda, Norio Miura, and Noboru Yamazoe. 1990. “Bi-Functional Oxygen Electrode Using Large Surface Area $\text{La}_{1-x}\text{Ca}_x\text{CoO}_3$ for Rechargeable Metal-Air Battery.” *Journal of The Electrochemical Society* 137 (11): 3430–33. <https://doi.org/10.1149/1.2086234/XML>.
- Stamenkovic, Vojislav R., Dusan Strmcnik, Pietro P. Lopes, and Nenad M. Markovic. 2016. “Energy and Fuels from Electrochemical Interfaces.” *Nature Materials* 2017 16:1 16 (1): 57–69. <https://doi.org/10.1038/nmat4738>.
- Stamm, Johannes, Alberto Varzi, Arnulf Latz, and Birger Horstmann. 2017. “Modeling Nucleation and Growth of Zinc Oxide during Discharge of Primary Zinc-Air Batteries.” *Journal of Power Sources* 360 (August):136–49. <https://doi.org/10.1016/J.JPOWSOUR.2017.05.073>.
- Strasser, Peter. 2016. “Free Electrons to Molecular Bonds and Back: Closing the Energetic Oxygen Reduction (ORR)-Oxygen Evolution (OER) Cycle Using Core-Shell Nanoelectrocatalysts.” *Accounts of Chemical Research* 49 (11): 2658–68. https://doi.org/10.1021/ACS.ACCOUNTS.6B00346/ASSET/IMAGES/MEDIUM/AR-2016-00346K_0011.GIF.
- Sun, Qian, Yin Yang, and Zheng Wen Fu. 2012. “Electrochemical Properties of Room Temperature Sodium–Air Batteries with Non-Aqueous Electrolyte.” *Electrochemistry Communications* 16 (1): 22–25. <https://doi.org/10.1016/J.ELECOM.2011.12.019>.
- Sunu, W. G., and D. N. Bennion. 1980a. “Transient and Failure Analyses of the Porous Zinc Electrode: I . Theoretical.” *Journal of The Electrochemical Society* 127 (9): 2007–16. <https://doi.org/10.1149/1.2130054/XML>.

- Sunu, W. G., and D. N. Bennion. 1980b. "Transient and Failure Analyses of the Porous Zinc Electrode: II . Experimental." *Journal of The Electrochemical Society* 127 (9): 2017. <https://doi.org/10.1149/1.2130055>.
- Tan, Peng, Wei Kong, Zongping Shao, Meilin Liu, and Meng Ni. 2017. "Advances in Modeling and Simulation of Li–Air Batteries." *Progress in Energy and Combustion Science* 62 (September):155–89. <https://doi.org/10.1016/J.PECS.2017.06.001>.
- Taylor, Peter, Ronan Bolton, Dave Stone, Xiao-Ping Zhang, Chris Martin, and Paul Upham. 2012. "Pathways for Energy Storage in the UK." *Report for the Centre for Low Carbon Futures, York*, 56–56.
- Thomas Goh, F. W., Zhaolin Liu, T. S. Andy Hor, Jie Zhang, Xiaoming Ge, Yun Zong, Aishui Yu, and Weiliang Khoo. 2014. "A Near-Neutral Chloride Electrolyte for Electrically Rechargeable Zinc-Air Batteries." *Journal of The Electrochemical Society* 161 (14): A2080–86. <https://doi.org/10.1149/2.0311414JES/XML>.
- Toussaint, Gwenaëlle, Philippe Stevens, Laurent Akrou, Robert Rouget, and Fabrice Fourgeot. 2010. "Development of a Rechargeable Zinc-Air Battery." *ECS Transactions* 28 (32): 25–34. <https://doi.org/10.1149/1.3507924/XML>.
- Trilochana, Siriyala, and C N Sangeetha. 2021. "A Comparative Study and Recent Research of Battery Technologies."
- Tromans, Desmond. 1998. "Oxygen Solubility Modeling in Inorganic Solutions: Concentration, Temperature and Pressure Effects." *Hydrometallurgy*. Vol. 50.
- Vasile, Nicolò S., Ronan Doherty, Alessandro H.A. Monteverde Videla, and Stefania Specchia. 2016. "3D Multi-Physics Modeling of a Gas Diffusion Electrode for Oxygen Reduction Reaction for Electrochemical Energy Conversion in PEM Fuel Cells." *Applied Energy* 175 (August):435–50. <https://doi.org/10.1016/j.apenergy.2016.04.030>.
- Versteeg, Henk Kaarle. 2007. *An Introduction to Computational Fluid Dynamics the Finite Volume Method, 2/E*. Pearson Education India.
- Viculis, Lisa H., Julia J. Mack, and Richard B. Kaner. 2003. "A Chemical Route to Carbon Nanoscrolls." *Science* 299 (5611): 1361. <https://doi.org/10.1126/SCIENCE.1078842/ASSET/C7248B5B-1323-430C-A375-BE145784BA36/ASSETS/SCIENCE.1078842.FP.PNG>.
- Vidts, Pauline De, and Ralph E White. n.d. "Mathematical Modeling of a Nickel-Cadmium Cell: Proton Diffusion in the Nickel Electrode."

- Vincent, Colin A. 2000. "Lithium Batteries: A 50-Year Perspective, 1959–2009." *Solid State Ionics* 134 (1–2): 159–67. [https://doi.org/10.1016/S0167-2738\(00\)00723-2](https://doi.org/10.1016/S0167-2738(00)00723-2).
- Walker, Shawn W. 2018. "Felicity: A Matlab/C++ Toolbox for Developing Finite Element Methods and Simulation Modeling." *SIAM Journal on Scientific Computing* 40 (2): C234–57. https://doi.org/10.1137/17M1128745/SUPPL_FILE/SUPPLEMENTARY_DEMO_S.PDF.
- Wang, Hao Fan, Cheng Tang, Bin Wang, Bo Quan Li, and Qiang Zhang. 2017. "Bifunctional Transition Metal Hydroxysulfides: Room-Temperature Sulfurization and Their Applications in Zn–Air Batteries." *Advanced Materials* 29 (35): 1702327. <https://doi.org/10.1002/ADMA.201702327>.
- Wang, Keliang, Pucheng Pei, Ze Ma, Huicui Chen, Huachi Xu, Dongfang Chen, and Xizhong Wang. 2015. "Dendrite Growth in the Recharging Process of Zinc-Air Batteries." *Journal of Materials Chemistry A* 3 (45): 22648–55. <https://doi.org/10.1039/c5ta06366c>.
- Wang, Keliang, and Jianrong Yu. 2020. "Lifetime Simulation of Rechargeable Zinc-Air Battery Based on Electrode Aging." *Journal of Energy Storage* 28 (April). <https://doi.org/10.1016/j.est.2019.101191>.
- Wang, Qin, Yejian Xue, Shanshan Sun, Shihua Li, He Miao, and Zhaoping Liu. 2017. "La_{0.8}Sr_{0.2}Co_{1-x}Mn_xO₃ Perovskites as Efficient Bi-Functional Cathode Catalysts for Rechargeable Zinc-Air Batteries." *Electrochimica Acta* 254 (November): 14–24. <https://doi.org/10.1016/J.ELECTACTA.2017.09.034>.
- Wang, Zhuo, Jianhang Huang, Zhaowei Guo, Xiaoli Dong, Yao Liu, Yonggang Wang, and Yongyao Xia. 2019. "A Metal-Organic Framework Host for Highly Reversible Dendrite-Free Zinc Metal Anodes." *Joule* 3 (5): 1289–1300. <https://doi.org/10.1016/j.joule.2019.02.012>.
- Wassei, Jonathan K., and Richard B. Kaner. 2013. "Oh, the Places You'll Go with Graphene." *Accounts of Chemical Research* 46 (10): 2244–53. <https://doi.org/10.1021/AR300184V>.
- Weber, Adam Z., Matthew M. Mench, Jeremy P. Meyers, Philip N. Ross, Jeffrey T. Gostick, and Qinghua Liu. 2011. "Redox Flow Batteries: A Review." *Journal of Applied Electrochemistry* 41 (10): 1137–64. <https://doi.org/10.1007/S10800-011-0348-2/FIGURES/15>.

- Wei, Zidong, Wenzhang Huang, Shengtao Zhang, and Jun Tan. 2000. "Carbon-Based Air Electrodes Carrying MnO₂ in Zinc-Air Batteries." *Journal of Power Sources* 91 (2): 83–85. [https://doi.org/10.1016/S0378-7753\(00\)00417-1](https://doi.org/10.1016/S0378-7753(00)00417-1).
- Wu, G. M., S. J. Lin, and C. C. Yang. 2006. "Alkaline Zn-Air and Al-Air Cells Based on Novel Solid PVA/PAA Polymer Electrolyte Membranes." *Journal of Membrane Science* 280 (1–2): 802–8. <https://doi.org/10.1016/J.MEMSCI.2006.02.037>.
- Wu, Qiang, Lijun Yang, Xizhang Wang, and Zheng Hu. 2017. "From Carbon-Based Nanotubes to Nanocages for Advanced Energy Conversion and Storage." *Accounts of Chemical Research* 50 (2): 435–44. https://doi.org/10.1021/ACS.ACCOUNTS.6B00541/ASSET/IMAGES/MEDIUM/AR-2016-00541D_0008.GIF.
- Wu, Qiumei, Luhua Jiang, Luting Qi, Erdong Wang, and Gongquan Sun. 2014. "Electrocatalytic Performance of Ni Modified MnO_x/C Composites toward Oxygen Reduction Reaction and Their Application in Zn–Air Battery." *International Journal of Hydrogen Energy* 39 (7): 3423–32. <https://doi.org/10.1016/J.IJHYDENE.2013.12.076>.
- Wu, Yutong, Yamin Zhang, Yao Ma, Joshua D. Howe, Haochen Yang, Peng Chen, Sireesha Aluri, and Nian Liu. 2018. "Ion-Sieving Carbon Nanoshells for Deeply Rechargeable Zn-Based Aqueous Batteries." *Advanced Energy Materials* 8 (36). <https://doi.org/10.1002/AENM.201802470>.
- Xia, Zhonghong, Li An, Peikai Chen, and Dingguo Xia. 2016. "Non-Pt Nanostructured Catalysts for Oxygen Reduction Reaction: Synthesis, Catalytic Activity and Its Key Factors." *Advanced Energy Materials* 6 (17): 1600458. <https://doi.org/10.1002/AENM.201600458>.
- Xiao, Jie, Donghai Wang, Wu Xu, Deyu Wang, Ralph E. Williford, Jun Liu, and Ji-Guang Zhang. 2010. "Optimization of Air Electrode for Li/Air Batteries." *Journal of The Electrochemical Society* 157 (4): A487. <https://doi.org/10.1149/1.3314375/XML>.
- Xiong, Ming, Mehdi Alipour, and Douglas G Ivey. 2018. "Current Distribution Investigation and Structure Optimization of Zn-Air Batteries." *ECS Transactions* 85 (13): 769–77. <https://doi.org/10.1149/08513.0769ecst>.
- Xu, M., D. G. Ivey, W. Qu, and Z. Xie. 2015. "Study of the Mechanism for Electrodeposition of Dendrite-Free Zinc in an Alkaline Electrolyte Modified with 1-Ethyl-3-Methylimidazolium Dicyanamide." *Journal of Power Sources* 274 (January):1249–53. <https://doi.org/10.1016/J.JPOWSOUR.2014.10.140>.

- Xue, Kan-Hao, Euan McTurk, Lee Johnson, Peter G. Bruce, and Alejandro A. Franco. 2015. "A Comprehensive Model for Non-Aqueous Lithium Air Batteries Involving Different Reaction Mechanisms." *Journal of The Electrochemical Society* 162 (4): A614–21. <https://doi.org/10.1149/2.0121504jes>.
- Yang, Chun Chen, and Sheng Jen Lin. 2002. "Improvement of High-Rate Capability of Alkaline Zn-MnO₂ Battery." *Journal of Power Sources* 112 (1): 174–83. [https://doi.org/10.1016/S0378-7753\(02\)00354-3](https://doi.org/10.1016/S0378-7753(02)00354-3).
- Yang, Qi, Guojin Liang, Ying Guo, Zhuoxin Liu, Boxun Yan, Donghong Wang, Zhaodong Huang, Xinliang Li, Jun Fan, and Chunyi Zhi. 2019. "Do Zinc Dendrites Exist in Neutral Zinc Batteries: A Developed Electrohealing Strategy to In Situ Rescue In-Service Batteries." *Advanced Materials* 31 (43): 1903778. <https://doi.org/10.1002/ADMA.201903778>.
- Yi, Jin, Pengcheng Liang, Xiaoyu Liu, Kai Wu, Yuyu Liu, Yonggang Wang, Yongyao Xia, and Jiujun Zhang. 2018. "Challenges, Mitigation Strategies and Perspectives in Development of Zinc-Electrode Materials and Fabrication for Rechargeable Zinc–Air Batteries." *Energy & Environmental Science* 11 (11): 3075–95. <https://doi.org/10.1039/C8EE01991F>.
- Zhang, C., J. M. Wang, L. Zhang, J. Q. Zhang, and C. N. Cao. 2001. "Study of the Performance of Secondary Alkaline Pasted Zinc Electrodes." *Journal of Applied Electrochemistry* 31 (9): 1049–54. <https://doi.org/10.1023/A:1017923924121/METRICKS>.
- Zhang, Hanguang, Hannah Osgood, Xiaohong Xie, Yuyan Shao, and Gang Wu. 2017. "Engineering Nanostructures of PGM-Free Oxygen-Reduction Catalysts Using Metal-Organic Frameworks." *Nano Energy* 31 (January):331–50. <https://doi.org/10.1016/J.NANOEN.2016.11.033>.
- Zhang, J W, L Zhang, Y Y Jia, G X Chen, X Wang, Q Kuang, Z X Xie, and L S Zheng. 2009. "Nano Res. 2012, 5, 618; e) BK Lim, MJ Jiang, PHC Camargo, EC Cho, J. Tao, XM Lu, YM Zhu, YN Xia." *Science* 324:1302.
- Zhang, Jie, Qixing Zhou, Yawen Tang, Liang Zhang, and Yanguang Li. 2019. "Zinc-Air Batteries: Are They Ready for Prime Time?" *Chemical Science* 10 (39): 8924–29. <https://doi.org/10.1039/c9sc04221k>.
- Zhang, Qi, Jingyi Luan, Yougen Tang, Xiaobo Ji, and Haiyan Wang. 2020. "Interfacial Design of Dendrite-Free Zinc Anodes for Aqueous Zinc-Ion Batteries." *Angewandte*

- Chemie International Edition* 59 (32): 13180–91.
<https://doi.org/10.1002/ANIE.202000162>.
- Zhang, Rui, Xiao Ru Chen, Xiang Chen, Xin Bing Cheng, Xue Qiang Zhang, Chong Yan, and Qiang Zhang. 2017. “Lithiophilic Sites in Doped Graphene Guide Uniform Lithium Nucleation for Dendrite-Free Lithium Metal Anodes.” *Angewandte Chemie International Edition* 56 (27): 7764–68. <https://doi.org/10.1002/ANIE.201702099>.
- Zhang, Wei, Wenzhen Lai, and Rui Cao. 2017. “Energy-Related Small Molecule Activation Reactions: Oxygen Reduction and Hydrogen and Oxygen Evolution Reactions Catalyzed by Porphyrin- and Corrole-Based Systems.” *Chemical Reviews* 117 (4): 3717–97. <https://doi.org/10.1021/ACS.CHEMREV.6B00299>
- Zhang, X. G. 2009. “SECONDARY BATTERIES – ZINC SYSTEMS | Zinc Electrodes: Overview.” *Encyclopedia of Electrochemical Power Sources*, January, 454–68. <https://doi.org/10.1016/B978-044452745-5.00166-0>.
- Zhang, X. Gregory. 2006. “Fibrous Zinc Anodes for High Power Batteries.” *Journal of Power Sources* 163 (1): 591–97. <https://doi.org/10.1016/J.JPOWSOUR.2006.09.034>.
- Zhang, Yuanbo, Yan Wen Tan, Horst L. Stormer, and Philip Kim. 2005. “Experimental Observation of the Quantum Hall Effect and Berry’s Phase in Graphene.” *Nature* 2005 438:7065 438 (7065): 201–4. <https://doi.org/10.1038/nature04235>.
- Zhao, Chang-Xin, Legeng Yu, Jia-Ning Liu, Juan Wang, Nan Yao, Xi-Yao Li, Xiang Chen, Bo-Quan Li, and Qiang Zhang. 2022. “Working Zinc–Air Batteries at 80 °C.” *Angewandte Chemie* 134 (33): e202208042. <https://doi.org/10.1002/ANGE.202208042>.
- Zhao, Zequan, Xiayue Fan, Jia Ding, Wenbin Hu, Cheng Zhong, and Jun Lu. 2019. “Challenges in Zinc Electrodes for Alkaline Zinc-Air Batteries: Obstacles to Commercialization.” *ACS Energy Letters*. American Chemical Society. <https://doi.org/10.1021/acsenergylett.9b01541>.
- Zhao, Zhiming, Jingwen Zhao, Zhenglin Hu, Jiedong Li, Jiajia Li, Yaojian Zhang, Cheng Wang, and Guanglei Cui. 2019. “Long-Life and Deeply Rechargeable Aqueous Zn Anodes Enabled by a Multifunctional Brightener-Inspired Interphase.” *Energy & Environmental Science* 12 (6): 1938–49. <https://doi.org/10.1039/C9EE00596J>.
- Zhu, Shaomin, Zhu Chen, Bing Li, Drew Higgins, Haijiang Wang, Hui Li, and Zhongwei Chen. 2011. “Nitrogen-Doped Carbon Nanotubes as Air Cathode Catalysts in Zinc-

- Air Battery.” *Electrochimica Acta* 56 (14): 5080–84.
<https://doi.org/10.1016/J.ELECTACTA.2011.03.082>.
- Zienkiewicz, Olek C, Robert L Taylor, and Jian Z Zhu. 2005. *The Finite Element Method: Its Basis and Fundamentals*. Elsevier.
- Zuo, Y., K. Wang, P. Pei, M. Wei, X. Liu, Y. Xiao, and P. Zhang. 2021. “Zinc Dendrite Growth and Inhibition Strategies.” *Materials Today Energy*. Elsevier Ltd.
<https://doi.org/10.1016/j.mtener.2021.100692>.

APPENDIX A

PARAMETERS, VARIABLES AND POST-PROCESSING

In this appendix section, parameters and the variables used within the model are given with their respective references, the parameters assigned to model from the battery of the model are referenced as the Battery of the Model (BoM) in this section. Besides, some of the parameters were arbitrarily assigned within reasonable ranges from the literature.

Table A.1 Parameters used within the model

Parameter	Value	Description	Reference
n_CL	2	Number of electrons transferred in ORR/OER	(Mao and White 1992)
dp_CL	7e-6 [m]	CL catalyst particle diameter	BoM
eps_CL	0.5	Porosity of CL	BoM
sigma_CL	138[S/cm]	Electrical conductivity of Ni-Mesh	(Xiong, Alipour, and Ivey 2018)
T	298.15[K]	Temperature	Ambinet air
i0_CL	1.5e-5[A/cm ²]	Exchange current density, OER/ORR, positive electrode	Arbitrarily assigned
cOH_ref	4.98*10 ⁻³ [mol/cm ³]	Reference concentration of the binary electrolyte	(Schröder and Krewer 2014)
alphaa_CL	1	Anodic transfer coefficient for CL	Arbitrarily assigned
alphac_CL	n_CL-alphaa_CL	Cathodic transfer coefficient for CL	Calculated
Eeq_pos	0.4[V]	Reference electrode potential, ORR/OER	(Amunátegui et al. 2018)

(cont. on next page)

Table A.1 (cont.)

Parameter	Value	Description	Reference
L_neg	0.5[mm]	Negative electrode	BoM
L_pos	0.5[mm]	Positive electrode	BoM
D_O2	8e-8[dm ² /s]	Effective diffusion coefficient, O2 (gas and liquid phase)	(Schröder and Krewer 2014)
cO2_init	0.17 [mol/m ³]	O2 Concentration in electrolyte	(Tromans 1998)
I_cell	i_app*A_cell	Applied Current	BoM
t_plus	0.22	Transport number	(Comsol 2020)
rho	1500[kg/m ³]	Electrolyte solution density	(Comsol 2020)
M_K	39.1[g/mol]	Potassium molar mass	(Comsol 2020)
M_OH	17[g/mol]	Anion molar mass	(Comsol 2020)
M_H2O	18[g/mol]	Solvent molar mass	(Comsol 2020)
D_OH	5.26e-9[m ² /s]	Diffusion coefficient of OH ion	(Comsol 2020)
D_K	1.96e-9[m ² /s]	Diffusion coefficient of Zn ion	(Comsol 2020)
Icell	i_app*A_cell	Applied current	BoM
act_ag	1.01	Activity aging param	Arbitrarily assigned
elec_agng	0.995	Electrolyte loss aging	Arbitrarily assigned
n_Zn	2	Number of electrons transferred in Zn	(Mao and White 1992)
alphaa_Zn	0.5	Anodic transfer coeff Zn	(Mao and White 1992)
alphac_Zn	n_Zn-alphaa_Zn	Cathodic transfer coeff Zn	Calculated
i_app	10 [mA/cm ²]	Applied Current Density	BoM
A_cell	25 [cm ²]	Area of the cell	BoM
L_sep	50e-3[mm]	Separator	BoM
fluxGDL	6.78e-8[mol/(m ² *s)]	10 barrer equivalent	BoM
eps_sep	0.68	Porosity of the separator	BoM
Eeq_pos	0.4 [V]	Equilibrium pot of positive electrode	(Amunátegui et al. 2018)

(cont. on next page)

Table A.1 (cont.)

Parameter	Value	Description	Reference
a_neg	10[cm ² /cm ³]	Specific surface area of negative electrode	(Mao and White 1992)
rho_Zn	7.14[g/cm ³]	Density of Zn	(NHI 2024a)
rho_ZnO	5.606[g/cm ³]	Density of ZnO	(NHI 2024b)
sigma_Zn	2e6[S/dm]	Electronic conductivity of Zn	(NHI 2024a)
sigma_ZnO	1e-9[S/dm]	Electronic conductivity of ZnO	(NHI 2024b)
MW_Zn	65.38[g/mol]	Molecular weight of Zn	(NHI 2024a)
MW_ZnO	81.408[g/mol]	Molecular weight of ZnO	(NHI 2024b)
i0_Zn	30e-3[A/cm ²]	Exchange current density of Zn electrode reaction	(Mao and White 1992)
Eeq_neg	-1.20[V]	Equilibrium pot of negative electrode	(Amunátegui et al. 2018)
mZncap	820 [mA*h/g]	Theoretical capacity of ZAB per g of Zn	(Niu et al. 2021)
VZn	$A_{cell} * L_{neg} * (1 - \epsilon_{Zn}) * f_{ZnZnO}$	Volume of the zinc in zinc electrode	Calculated
wZn	$\rho_{Zn} * VZn$	Weight of Zn in zinc electrode	Calculated
VZnO	$A_{cell} * L_{neg} * (1 - \epsilon_{Zn}) * (1 - f_{ZnZnO})$	Volume of ZnO in zinc electrode	Calculated
wZnO	$\rho_{ZnO} * VZnO$	Weight of the ZnO in zinc electrode	Calculated
theo_cap	$wZn * mZncap$	Theoretical capacity of ZAB	Calculated
eps_Zn	0.3	Electrolyte fraction in zinc electrode	BoM
fZnZnO	0.3	Fraction of Zn/ZnO	BoM
dp_Zn	6e-6[m]	Particle size for zinc electrode	(Kolhekar, Nyce, and Banerjee 2021)
resis_zn	3.63e3 [ohm*cm]	ZnO resistance	(Shariffudin et al. 2012)
x_film	1[nm]	ZnO film length	(Shariffudin et al. 2012)

Table A.2 Variables used in the model

Variables	Value	Description
alphaa_CL_e	$\text{alphaa_CL} * (\text{act_ag})^{(\text{cyclec})}$	GDE aging
cl_e	$\text{cl} * \text{elec_agng}^{(\text{cyclec})}$	Electrolyte loss
CO_O2	$((\text{cO2})/\text{cO2_init})^{1/2}$	Oxidized Species for ORR/OER
CO_Zn	$\text{cZnO}/\text{cZn_init}$	Oxidized Species for Zn Electrode
CR_O2	$(\text{cl_e}/\text{cOH_ref})^2$	Reduced species for ORR/OER
CR_Zn	$(\text{cl_e}/\text{cOH_ref})^2 * (\text{cZn}/\text{cZn_init})$	Reduced species for Zn Electrode
cyclec	cyclec	Cycle counter
cZn	cZn	Concentration of Zn
cZnO	cZnO	Concentration of ZnO
dp_Zn_e	$\text{dp_Zn} * 1.05^{(\text{cyclec})}$	Dendrite growth
mZn	$(\text{cZn} * \text{MW_Zn}) / (\text{cZn} * \text{MW_Zn} + \text{cZnO} * \text{MW_ZnO})$	Mass fraction of Zn

(cont. on next page)

Table A.2 (cont.)

Variables	Value	Description
mZnO	$c_{ZnO} * MW_{ZnO} / (c_{Zn} * MW_{Zn} + c_{ZnO} * MW_{ZnO})$	Mass fraction of ZnO
sigmaleff	$(\epsilon_{sl} * F_{const}^2 / R_{const} / T) * (D_K + D_{OH}) * cl$	Effective electrolyte conductivity
sigmaseff	$\sigma_{Zn} * m_{Zn}^{1.5} + \sigma_{ZnO} * m_{ZnO}^{1.5}$	Effective electrical conductivity Negative
R_film	resistivity * x_film_e	Film resistance
x_film_e	$\text{if}(x_{film_e} < 175e-9[m], x_{film} * 1.08^{cyclec}, 175e-9[m])$	Film thickness

To post-process the model's capacity fade, example code of capacity calculations within respective cycle numbers were computed with the following code:

```
import pandas as pd
import matplotlib.pyplot as plt
file_path = "Mother-of-all-corrected.xlsx"
data = pd.read_excel(file_path)
data = data[data['CycleNo'] < 56]
data['Mode'] = ""
for i in range(1, len(data)):
    if data.loc[i, 'Electric Potential (V)] < data.loc[i - 1, 'Electric Potential (V)']:
        data.loc[i, 'Mode'] = 'Discharge'
    elif data.loc[i, 'Electric Potential (V)] > data.loc[i - 1, 'Electric Potential (V)']:
        data.loc[i, 'Mode'] = 'Charge'
    else:
        data.loc[i, 'Mode'] = data.loc[i - 1, 'Mode']
capacities = []
for cycle_no, group in data.groupby('CycleNo'):
    discharge_group = group[group['Mode'] == 'Discharge']
```

```

discharge_time = discharge_group['Time (s)'].diff().sum()
if pd.notna(discharge_time) and discharge_time > 0:
    capacity = (discharge_time * 250) / 3600
else:
    capacity = 0
capacities.append(capacity)
capacity_df = pd.DataFrame({
    'CycleNo': data['CycleNo'].unique(),
    'Capacity': capacities
})
if 'Capacity' in data.columns:
    data = data.drop(columns=['Capacity'])
data = data.merge(capacity_df, on='CycleNo', how='left')
plt.figure(figsize=(10, 6))
plt.plot(capacity_df['CycleNo'], capacity_df['Capacity'], marker='o')
plt.xlabel('Cycle Number')
plt.ylabel('Capacity (mAh)')
plt.title('Capacity vs Cycle Number')
plt.grid(True)
plt.show()

```

Post processing the model's specific cycle numbers to discretely observe cycling performance and aging of the batteries, following code is executed:

```

import pandas as pd
import matplotlib.pyplot as plt
# Load the data
data = pd.read_excel('data_file.xlsx')
# Filter the data for specific cycle numbers
cycle_numbers = [1, 20, 35, 41]
filtered_data = data[data['CycleNo'].isin(cycle_numbers)]
# Reset the time for each cycle and mode to start from zero
filtered_data['Adjusted Mode Time (s)'] = filtered_data.groupby(['CycleNo',
'Mode'])['Time (s)'].transform(lambda x: x - x.min())
# Colors for cycles
cycle_colors = {1: 'blue', 20: 'green', 35: 'red', 41: 'purple'}

```

```

# Plotting
plt.figure(figsize=(12, 8))
for cycle in cycle_numbers:
    for mode in ['Charge', 'Discharge']:
        mode_data = filtered_data[(filtered_data['CycleNo'] == cycle) &
(filtered_data['Mode'] == mode)]
        plt.plot(mode_data['Adjusted Mode Time (s)'], mode_data['Electric Potential (V)'],
            label=f'Cycle {cycle} {mode}', color=cycle_colors[cycle])
plt.xlabel('Time (s) from Start of Mode in Each Cycle')
plt.ylabel('Electric Potential (V)')
plt.title('Electric Potential vs Time for Different Cycles and Modes')
plt.legend()
plt.grid(True)
plt.savefig('plot_path.png') # Update 'plot_path.png' with desired path

```